Salt Flux, Salinity Intrusion and Estuarine Circulation in the Ota Diversion Channel

(太田川放水路における塩分フラックス，塩水遡上とエスチャリー循環に関する研究)

Department of Civil and Environmental Engineering

Graduate School of Engineering

Hiroshima University

September 2013

MOHAMMAD SOLTANIASL

ABSTRACT

The large salinity variation in estuaries may create a challenging environment for the ecological system. Changes in the balance between freshwater and saltwater can lead to the loss of species. Therefore, investigation of salinity intrusion in estuaries is important, both in terms of understanding the complex balance between the fluvial and tidal processes that affect the salinity intrusion within the estuary, and also in terms of formulating effective policies for sustainable development in coastal regions. Understanding the mechanisms that affect the salinity intrusion has implications for management of estuaries. A clear understanding of the factors affecting the salinity intrusion in estuaries is thus required for the long-time period of hydrological conditions.

The Ota Estuary encompasses the branched section of the Old Ota River and the Ota Diversion Channel about 9 km upstream from the estuary mouth. The present study attempts to identify the salinity intrusion through the Ota Diversion Channel that is a shallow tidally-dominated channel with gates. The existence of the Gion Gates at the upstream border which restricts the freshwater runoff is an important feature of Ota Diversion Channel. This study consists of the field observations and numerical simulations. This thesis addresses the variability of salinity flux, flushing time, salinity intrusion length, stratification and estuarine circulation in the Ota Diversion Channel under the different estuarine forces (freshwater, tides, etc.).

Near the upstream border of the Ota Diversion Channel (Gion Station), the long-term salinity and flow velocity data are collected using an innovative instrument which is called Fluvial Acoustic Tomography System (FATS). FATS data provides novel information about seasonal and annual variability of salinity and flow rate in this region. The long-term salinity and flow rate variations at the Gion Station are analyzed over the period between 2009 and 2013. The salinity variations show a correlation with seasonal variations of the mean sea level, winds and freshwater runoff. Furthermore, spring-neap tidal cycles significantly influence the salinity variations due to differences in tidal mixing. The larger tidal range during the spring tides constricted the saltwater intrusion.

The flushing time in the Ota Diversion Channel is estimated using a practical method based on the FATS data. The average flushing time is estimated about 1.8 days under mean flow conditions. This result indicates that the flushing time is considerably short compared to other estuaries. Moreover, the transition time from highly stratified to partially-mixed is a few days. This study indicates that the flushing time is controlled by the advection process at the Ota Diversion channel. The maximum flushing time in the Ota Diversion Channel is usually occurred when the freshwater discharge is low and the mean sea level is reached the highest levels.

In this study the salinity variations at the two main branches are investigated. The results suggest that the variability of salinity at both branches is significantly different. This difference is mainly caused due to the condition of both gates.

In addition, a three-dimensional numerical model (EFDC) is used to simulate water level, salinity and flow rate in the Ota Diversion Channel. Several field observations through the Ota Diversion Channel were carried out for validation and calibration purposes. The numerical experiments are carried out to: 1) estimate the longitudinal distribution of salinity and velocity at the Ota Diversion Channel. 2) clarify the dominated salinity transport mechanisms and salinity balance in the Ota Diversion Channel during spring-neap tidal cycles and wet and dry seasons. 3) investigate the variability in the estuarine circulation and stratification. 4) examine the response of the salinity intrusion to changes in the freshwater runoff and tides.

The results indicate that the longitudinal salinity gradient is around -1.1 km^{-1} between the channel mouth and about 7 km upstream from the mouth. On the other hand, at the upstream region the salinity gradient is about -5 km^{-1}. This result indicates that the longitudinal salinity gradient is large at the upstream border of Ota Diversion Channel compared with the other estuaries. Higher salinity gradient at the upstream region can generate stronger estuarine circulation.

To investigate the salinity transport mechanisms, the salinity flux is decomposed into three components: steady shear, advection, and tidal dispersion salt fluxes. The steady shear flux is induced by gravitational circulation and the tidal dispersion generated by temporal correlations between the salinity, water level and velocity. The advection flux is mainly induced by river discharge. The results indicate that the salinity balance is not in a steady balance during spring-neap tidal cycles. During spring tides, the total salt flux is directed seaward, and the salt exits from the estuary. In contrast, during neap tides, the total salt flux is directed landward, and the salt enters the estuary. During the spring tides, the tidal dispersion is maximized due to larger correlations between the water level, salinity and velocity. While during the neap tides the steady shear flux is increased due to higher longitudinal salinity gradient and estuarine circulation near the upstream border of Ota Diversion Channel.

The variability of tidal currents and stratification during wet and dry seasons are simulated. The amplitude of tidal velocity varies from 0.5 m/s at the strongest spring to 0.16 m/s at the weakest neap tides, respectively. The estuarine circulation and stratification at the Ota Diversion Channel is significantly varied by the changes in freshwater runoff. During the low freshwater runoff the estuarine circulation is weak, especially at the downstream sections. Then the stratification is low at the downstream sections. Meanwhile, the maximum bottom-surface salinity differences at the upstream regions are established during neap tides by the values around 20, when low vertical mixing persists for several days. During the high freshwater runoff, estuarine circulation is reinforced. The larger freshwater runoff increases the thickness of halocline at the downstream, so that the bottom-top salinity difference increases.

The relation between the salinity intrusion length and freshwater runoff is examined. During the low and moderate freshwater runoff the salinity intrusion length responding to the freshwater discharge generally follows a power law of -0.11 and -0.14 for the neap and spring tides, respectively. The dependence of salinity intrusion on freshwater discharge is weaker from the standard -1/3 power dependence that is derived theoretically for exchange dominated estuaries. The reason for behavior is due to the existence of the Gion gates which restricts the freshwater runoff to the channel significantly. Due to the Gion gate operation the time response of tidally-averaged salinity to changes in freshwater runoff is decreased significantly. Also the result shows that the difference in salt intrusion length between springs and neaps is significant in Ota Diversion Cannel. The reason is related to the influence of tidal amplitude on the salinity and flow velocity variations. The stronger vertical mixing reduces density stratification during spring tides. The higher mixing levels actually inhibit salinity advection, and salinity intrusion is stronger on neap tide.

Contents

List of Figures

List of Tables

List of Notations

Symbols

A	Cross section area (L^2)	
a_0, a_1, k_1	Constants	
A_b	Vertical turbulent diffusivity (L^2T^{-1})	
A_v	Vertical eddy Viscosity (L^2T^{-1})	(Chapter 3)
A_z	Vertical eddy Viscosity (L^2T^{-1})	
C	Mass concentration (ML^{-3})	
c, c_m	Sound speed (LT^{-1})	
C_D	Bottom Drag coefficient (-)	
f	Coriolis parameter (T^{-1})	
F	Salt flux (L^3T^{-1})	
F	Flushing number (-)	
F_E	Steady shear flux (L^2T^{-1})	
F_T	Tidal oscillatory flux (L^2T^{-1})	
f_{vis}	Viscous force ($ML^{-1}T^{-2}$)	
g	Acceleration due to gravity (ML^{-2})	
H	Total water depth (L)	
h	Water depth (L)	
H_m	Mean sea level (L)	
J, J_x, J_y, J_z	Mass flux vector per unit width ($ML^{-1}T^{-1}$)	
K	Diffusion Coefficient (L^2T^{-1})	
K_x	Longitudinal dispersion (L^2T^{-1})	
K_z	Vertical eddy diffusivity (L^2T^{-1})	

L	Ray path Length (L)
L	Salinity intrusion length (L)
L	Tidal compartment (L)
l	Turbulence length scale (L)
p	Water pressure ($ML^{-1}T^{-2}$)
q	Turbulence intensity (LT^{-1})
Q_R	Freshwater discharge (L^3T^{-1})
Q_R	River discharge (L^3T^{-1})
Q_s	Salinity transport source-sink terms (LT^{-1})
Q_T	Temperature transport source-sink terms (C LT^{-1})
Q_u, Q_v	Momentum source-sink terms (L^2T^{-2})
R_i, R_q	Richardson number (LT^{-1})
s	Water salinity (-)
s_0	Reference salinity (-)
T	Tidal period (T)
t	Time (T)
T_f	Flushing Time (T)
t_i (i,1,2)	Travel time (T)
T_m	Temperature along the ray path (C)
T_r	Tidal range (L)
u_*	Shear velocity (LT^{-1})
u, v, w	Instantaneous longitudinal, transverse, and vertical velocities, respectively (LT^{-1})
u_b	Near-bottom velocity (LT^{-1})
u_E	Estuarine Circulation (LT^{-1})
u_m	Velocity along the ray path (LT^{-1})

u_r	River velocity (LT^{-1})
u_t	Tidal velocity (LT^{-1})
V	Estuary volume (L^3)
V_f	Freshwater volume (L^3)
W	Wind speed (LT^{-1})
x	Longitudinal distance (L)
z	Vertical distance (L)
μ	Dynamic viscosity ($M\ L^{-1}T^{-1}$)
τ	Shear stress ($ML^{-1}T^{-2}$)
τ_b	Bottom stress ($M\ L^{-1}T^{-2}$)
β	Coefficient of saline contraction (-)
Δs	Top-to- bottom salinity differences (-)
η	Water surface displacement (L)
v	Diffusive fraction of upstream salt flux (-)
ρ	Density of water (ML^{-3})
ϕ	Stratification ($ML^{-1}\ T^{-2}$)
ϕ_0	Stratification ($ML^{-1}\ T^{-2}$)
ϕ_v, ϕ_b	Stability functions (-)
ψ	Stratification Parameter (-)

Operators

$\bar{(\bullet)}$	Spatially-averaged operator
$\langle\bullet\rangle$	Temporally-averaged operator
$(\bullet)'$	Deviation from time-averaged value

CHAPTER 1

Introduction

1.1. Study Overview

An estuary is defined as a semiclosed coastal waterbody that is freely connected to the open sea and within which seawater is measurably diluted with freshwater derived from land drainage (Pritchard, 1967). They fresh and saline water act as both sink and source for pollutants depending on (i) the geographical source of the contaminants (marine, fluvial, internal and atmospheric), (ii) their biological and chemical nature and (iii) with temporal variations in tidal amplitude, river flow, seasons and wind. Because many cities are located next to estuaries (e.g., Hiroshima City), the variability on estuarine environment is a frequent concern (Dyer 1973). Assessing these impacts require an understanding of the variability of circulation and stratification in the estuary. Tides and river freshwater are generally the major source of energy input into estuaries.

Seasonal cycles occur in temperature, river flows, stratification and nutrients. These seasonal cycles alongside occasional events may be extremely significant for estuarine ecology. Generally, the tidal wave drives the strongest flows in an estuary. River discharge produces a seaward directed flow that usually exhibiting a seasonal variation and shorter term fluctuations due to flood events. Vertical and horizontal shear in tidal currents generate turbulence, which determines the overall rate of mixing. On neap tides, near-bed saline intrusion may enhance stability, while on springs, enhanced near-surface advection of saline water can lead to overturning.

According to vertical structure of the salinity or stratification, estuaries can be classified as salt wedge, strongly stratified, weakly stratified or vertically mixed (Pritchard, 1955). This classification considers the competition between buoyancy forcing from river discharge and mixing from tidal forcing. Mixing from tidal forcing is proportional to the volume of saline water entering the estuary during every tidal cycle, which is also known as the tidal prism. Moderate to large river discharge and weak to moderate tidal forcing result in strongly stratified estuaries. The tidally averaged salinity profiles have a well-developed pycnocline with weak vertical variations above and below the pycnocline. Weakly stratified or partially mixed estuaries result from moderate to strong tidal forcing and weak to moderate river discharge. The mean salinity profile either has a weak pycnocline or continuous stratification from surface to bottom, except near the bottom mixed layer. The mean exchange flow is most vigorous (when compared to other types of estuaries) because of the mixing between freshwater and saline water. Strong tidal forcing and weak river discharge result in vertically mixed estuaries. Downstream part of Ota Estuary exhibits this behavior. Mean salinity profile in mixed estuaries is practically uniform and mean flow is unidirectional with depth.

The circulation and stratification of estuaries are a result of the interactions of the tides, the river outflow, the density difference between the river and the ocean, the coastal sea level fluctuations, the winds and the bathymetry (Dyer 1973; Fischer et al.,

1979). Generally, the tidal wave drives the strongest flows in an estuary (Fischer et al. 1979). Mean circulation and circulation at frequencies lower than the semidiurnal and diurnal tides are called the residual circulation (Lewis and Lewis 1983; Jay and Musiak 1996). The vertical and lateral deviation of the residual circulation from the cross-sectional average are usually defined as the estuarine circulation (Fischer, 1976, Geyer et al., 2001). The stratification in an estuary is a result of shears straining the along-channel salinity gradient and mixing from tides, winds, and waves (Simpson et al. 1990; Dyer 1973).

The velocity and salinity determine the salt transport in an estuary. Generally salinity is flushed from the estuary by two important mechanisms: 1) the estuarine salt transport due to the vertical and lateral variations of tidally-averaged velocity and salinity, 2) the tidal dispersion due to the tidal correlation of velocity and salinity (Fischer 1976). The magnitude of salt transport and the processes that produce it depend on the bathymetry of the estuary and on the strength of the physical forcing (e.g., tides, freshwater flow). In highly-stratified estuaries, salt transport is predominantly due to advection by the net flow and the estuarine salt transport (Hansen and Rattray 1966). In contrast, in well-mixed estuaries, which are weakly stratified, tidal dispersion plays a larger role in the salt balance (Smith 1980). The stratification of partially-stratified (also known as partially-mixed) estuary varies between these extremes and the mechanisms of salt transport should vary consequently.

1.2. Previous Studies

The conceptual model of estuarine circulation, salinity transport and the salt balance of estuaries are based on the work of Hansen and Rattray (1965, 1966). Hansen and Rattray (1965) related the strength of the estuarine salt transport in an estuary to the vertical mixing, along-channel salinity gradient, and depth, based on momentum and salt balances developed by Pritchard (1954, 1956). Although their study provided a useful

way of classifying estuaries (Hansen and Rattray 1966), their analysis did not consider the connection between vertical mixing and the forcing conditions nor the variations of vertical mixing within the tidal cycle. In addition, their study did not provide any insight into the processes of tidal dispersion. Jay (1991) introduced the idea of tidal asymmetry, suggesting that the estuarine circulation is not principally driven by the baroclinic pressure gradient but rather by the imbalance of the magnitude of eddy viscosity between flood and ebb. This imbalance results from the weaker stratification, and more intense turbulence, during floods than ebbs. Jay provided evidence that tidal asymmetry is important in the Columbia River estuary, which has particularly strong tidal currents, but his ideas would appear to be relevant in many estuarine environments due to the tidal straining of the salinity field resulting in tidal variation in stratification (Simpson et al., 1990). Studies since Hansen and Rattray (1965) have shown that the modulation of vertical mixing due to tidal and spring-neap cycles is critical in determining the magnitude of residual circulation and stratification. Observations (e.g., Nunes and Lennon 1987; Geyer et al., 1999), laboratory experiments (Linden and Simpson 1988), and numerical models with more advance parameterizations of vertical mixing (e.g., Blumberg and Mellor, 1987; Hamrick, 1992) demonstrate that variations in vertical mixing within a tidal cycle also play a role in determining the magnitude of the residual circulation. These studies suggest that the variations of vertical mixing over the spring-neap cycle and within a tidal cycle must be included in order to understand the dependence of salt transport mechanisms on the forcing parameters. The salt balance of an estuary is unsteady while adjusting to the spring-neap cycle and changing freshwater flow. Some authors have observed this adjustment process and made qualitative links between variations of forcing, salt transport, and the length of the salinity intrusion (e.g., Jay and Smith 1990; Monismith et al., 2002; Ralston et al., 2010; Gong and Shen, 2011). Analytic approaches have also been used to predict the adjustment of the salt balance for more general bathymetries and variations of forcing. For example, Hansen and Rattray

(1965) solution for the advection-dominated limit, the Chatwin (1976) solution for partially mixed estuaries, and the MacCready (1999) solution for advection-dominated estuaries.

1.3. Objectives and Challenges

The balance between the fresh and salt water in an estuary influence many facets of environment. Changes in salinity have major effects on water density and water stratification. Dynamic behavior of suspended sediment can be controlled by the salinity-driven flow and mixing. Salinity can also alter the water chemistry that impacts marine organisms. In the Ota Estuary (Located in Hiroshima City, Japan) the maximum tidal tide range is about 4m at the river mouth during the spring tide. Variability in tide affects the conditions in the main bifurcation. The main function of Ota Diversion Channel is flood control. However, this channel has extensive tidal flats with habitats for many creatures in the brackish river. In the Ota Diversion Channel due to low freshwater flow which caused by the operation of Gates, the salt water from the Hiroshima Bay propagates upstream and exerts more influence in the upstream sections of the channel. Moreover, the estuarine forces (e.g., freshwater runoff and tide) significantly change the salinity variations in this channel. For this reason, an understanding of the salinity transport throughout the Ota Diversion Channel help us to assess the impact of salinity variations on the ecosystem of this channel.

The general focus of this study is to determine what physical mechanisms influence the salinity intrusion in the Ota Diversion Channel. The major estuarine forces on the salinity intrusion in the Ota Diversion Channel include freshwater runoff, wind, and tidal influence. The influence of major estuarine forces on the salinity variation was determined through long-term data analysis of these variables during period from 2009 to 2013. In addition, to better understanding of the salinity transport in the Ota Diversion Channel, a 3D numerical model is used to examine the longitudinal salinity intrusion

throughout the channel during different freshwater runoff. Investigation of the salinity intrusion under the moderate and high freshwater runoff helps us to precise management of the gates.

1.4. Outline of the Thesis

The thesis can generally be divided into three parts: introduction and overview (Chapters 1 and 2); materials and methods (Chapter 3); results, discussions and conclusions (Chapters 4, 5 and 6). Chapter 1 presents a brief introduction, challenges and objectives of this study. In Chapter 2 the estuarine physical processes (e.g., estuarine circulation, mixing, salt intrusion) are investigated. Chapter 3 gives general information of the study area and main instrumentations which were used for field observations. Also this chapter shows general features of the three-dimensional numerical model (EFDC) which were used in this study. In Chapter 4 the variability of salinity, salt flux and flushing time are investigated. In Chapter 5 the results of numerical simulation are presented. In this section the variability in the estuary are investigated at different time scales. Finally, Chapter 6 presents the conclusions and recommendations of the study.

References

Blumberg, A. F., Mellor, G.L. (1987) A description of a three-dimensional coastal ocean circulation model, *Three-dimensional coastal ocean models,* Editor: N. S. Heaps, American Geophysical Union, 1-16.

Chatwin, P. C. (1976) Some remarks on the maintenance of the salinity distribution in estuaries, *Estuarine and Coastal Marine Science*, 4, 555–566.

Dyer, K. R. (1973) Estuaries: A Physical Introduction, John Wiley and Sons, *Wiley- Interscience*, New York.

Fischer, H. B. (1976) Mixing and dispersion in estuaries. *Annual review of Fluid Mechanics,* 8, 107-133.

Fischer, H. B., E. J. List, R. C., Koh, J., Brooks, N. H. (1979) Mixing in Inland and Coastal Waters. *Academic Press*, New York.

Geyer, W. R., Trowbridge, J., Bowen, M. (1999) The dynamics of a partially mixed estuary, *Journal of Geophysical Research*, 30, 2035-2048.

Geyer, W. R., Woodruff. J. D., Traykovski, P. (2001) Sediment transport and trapping in the Hudson River estuary, *Estuaries* 24, 670–679.

Gong, W., Shen, J. (2011) The response of salt intrusion to changes in river discharge and tidal mixing during the dry season in the Modaomen Estuary, China, *Continental Shelf Research*. 31, 769-788.

Hamrick, J. M. (1992) A Three-dimensional Environmental Fluid Dynamics Computer Code: Theoretical and Computational Aspects, The College of William and Mary, Virginia Institute of Marine Science, Special Report 317, 63 pp.

Hansen, D. V., Rattray, M. Jr. (1965) Gravitational circulation in straits and estuaries, *Journal of Marine Research*, 23, 104-122.

Hansen, D. V., Rattray, M. (1966) New dimensions in estuary classification, *Limnology and Oceanography*, 11(3), 319-325.

Jay, D. A. (1991) Estuarine salt conservation: A Lagrangian approach. *Estuarine Coastal Shelf Science,* 32**,** 547-565.

Jay, D. A., Musiak, J. D. (1996) Internal tidal asymmetry in channel flows: origins and consequences. *Mixing in Estuaries and Coastal Seas,* C. Pattiaratchi, Ed., American Geophysical Union, Washington D.C., 211-249.

Lewis, R. E., Lewis, J. O. (1983) The principal factors contributing to the flux of salt in a narrow, partially stratified estuary. *Estuarine Coastal Marine Science*, 16, 599-626.

Linden, P. F., Simpson, J. E. (1988) Modulated mixing and frontogenesis in shallow seas and estuaries. *Continental Shelf Research,* 8(10), 1107-1127.

MacCready, P. (1999) Estuarine adjustment to change in river flow and tidal mixing, *Journal of Physical Oceanography*, 29, 708-729

Monismith, S., Kimmerer, W., Burau, J.R., Stacey, M.T (2002) Structure and flow-induced variability of the subtidal salinity field in Northern San Francisco Bay, *Journal of Physical Oceanography*, 32, 3003-3016

Nunes, R. A., Lennon, G. W. (1987) Episodic stratification and gravity currents in a marine environment of modulated turbulence. *J. Geophys. Res.,* 92(C5), 5465-5480.

Pritchard, D. W., 1954: A study of teh salt balance in a coastal plain estuary. *Journal of Maine Research*, 13 (1), 133-144.

Pritchard, D.W. (1956) The dynamic structure of a coastal plain estuary, *Journal of Maine Research*, 15(1), 22-42.

Pritchard, D. W. (1967) Observations of circulation in coastal plain estuaries. *Estuaries*, *American Association for the Advancement of Science*, 83, 37-44.

Ralston, D.K., Geyer, W.R., Lerczak, J.A. (2008) Subtidal salinity and velocity in the Hudson River Estuary: Observations and modeling, *Journal of Physical Oceanography*, 38, 753-770.

Simpson, J.H., Brown, J., Matthews, J., and Allen, G. (1990) Tidal straining, density currents, and stirring in the control of estuarine stratification, *Estuaries*, 13,125-132.

Smith, R. (1980) Buoyancy effects upon longitudinal dispersion in wide well-mixed estuaries. *Philosophical Transactions of the Royal Society of London Series A,* 296, 467-496.

CHAPTER 2

Characteristics of the Estuarine System

2.1. Classification of Estuaries

An estuary has characteristics of a river and a sea. The sea and the river exchange their water, substances and sediments. Therefore, the estuary is a unique environment that is mainly influenced by tidal movements of the sea and freshwater discharge of the river. The unique characteristics of estuaries include that (1) tides are a major driving force; (2) salinity and its variations usually play a significant role in hydrodynamic and water quality processes; (3) two directional net flows, seaward in the surface layer and landward in the bottom layer.

The type of an estuary depends on the relative magnitudes of river and tidal flow and on the geometry of the estuarine basin (Dyer, 1997; Savenije, 2005). Changes in any of these factors may alter the mixing and the estuarine circulation. These forces lead to different shapes of estuaries, each with a different aquatic environment. Here we mention

to some main classification schemes of estuaries, according to: a) shape, b) tidal variation, c) vertical structure of salinity.

2.1.1. Classification Based on Shapes

In estuaries, the following characteristic shapes can be distinguished:

Prismatic Estuaries

The banks of the estuary are parallel. This is a type of estuary that only exists in a man-made environment where the banks are artificially fixed. Examples are shipping channels that are regularly dredged and where the banks are stabilized.

Deltas

A near prismatic estuary where the tidal influence is small compared to the amount of river discharge. Deltas occur in seas with a relatively small tidal range and on rivers with a high sedimentation.

Funnel or Trumpet Shapes

This is the natural shape of an alluvial estuary, where the tidal energy is equally spread along the estuary axis.

Fjords

Fjord is a long, narrow inlet with steep sides or cliffs, created in a valley carved by glacial activity.

2.1.2. Classification Based on the Tide Propagation

The range of the tide and the strength of the tidal currents are mainly controlled by the interaction between the tidal wave and the topography of an estuary. Dyer (1997) indicated that in an ideal estuary, the amount of energy lost by friction is balanced by the amount of energy that is gained by the converging of the river banks. Base on the

mentioned characteristic of tide propagation in the estuaries the following categories can be distinguished as:

Ideal Estuaries

An estuary where, as the tidal wave travels upstream, the amount of energy per unit width lost by friction is exactly equal to the amount of energy gained by convergence of the banks. In an ideal estuary, the tidal range is constant along the estuary axis (Savenije and Veling, 2005).

Amplified Estuaries

An estuary where, the tidal range increases in upstream direction because convergence is stronger than friction. Clearly this process cannot continue indefinitely. The process of damping is enhanced by the river discharge, which increases the friction and reduces bank convergence (Savenije and Veling, 2005).

Damped Estuaries

An estuary where friction outweighs bank convergence. Tidal damping occurs in estuaries with a long convergence length or in drowned river values with a narrow opening (Savenije and Veling, 2005).

2.1.3. Classification Based on Stratification

Dyer (1997) classified estuaries by their stratification and the characteristics of their salinity distributions. This probably is the most common classification for estuaries due to its physical characteristics. The advantages of this classification type are to have a better understanding of mixing process and water circulation in the estuaries. Based on this classification four main estuarine types are defined (Figure 2.1).

Highly Stratified or Salt Wedge Estuaries

Highly stratified estuaries are characterized by the presence of a tongue of higher salinity water (or salt wedge) near the bottom and an overlying layer of freshwater. The

salt wedge extends from the estuarine mouth and moves with the tides. River discharges control the circulation and push back the seawater. There is a sharp transition and weak mixing between the two layers. With weak tides and dampened vertical mixing, the salt wedge can penetrate a long distance upstream. A typical example of a salt wedge estuary is the South West Pass of the Mississippi. When the flow is low the salt wedge extends more than 100 miles inland, but with high river discharge the salt wedge only reaches a mile or so above the mouth. (Hardisty, 2007).

Partially Mixed Estuaries

In partially mixed estuaries, the water mass moves seaward and landward with tide-generated mixing between the salt water and the fresh water. Examples of partially mixed estuaries include the Rotterdam waterway in The Netherlands and the Potamac in America (Hardisty, 2007). Weakly stratified or partially mixed estuaries result from moderate to strong tidal forcing and weak to moderate river discharge. The mean salinity profile either has a weak pycnocline or continuous stratification from surface to bottom, except near the bottom mixed layer. The mean exchange flow is most vigorous (when compared to other types of estuaries) because of the mixing between riverine and oceanic waters. (Levinson, 2010).

Well- Mixed Estuaries

Well-mixed estuaries exhibit complete mixing of saltwater and freshwater resulting in a constant fluid density over the depth and a varying density in longitudinal direction from that of seawater (1026 kg/m^3) to that of freshwater (1000 kg/m^3). Examples of well-mixed estuaries include the Severn in England and the Gironde in France, the Western Scheldt in The Netherlands, and the Mersey in England (Hardisty, 2007).

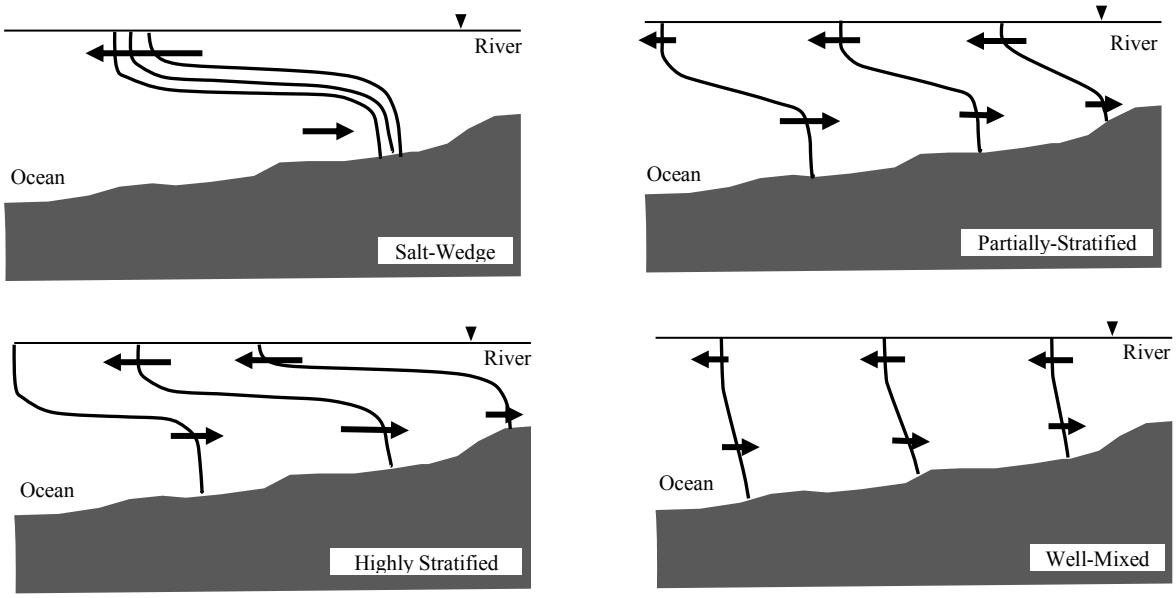

Fig 2.1 Classification of estuaries based on the vertical structure of salinity

2.2. Salinity Variations in Estuaries

Salinity is a measure of salt concentration in water: Higher salinity means more dissolved salts. Salinity originated as an oceanographic term and does not have a precise chemical definition. The major elements that determine salinity are similar worldwide, but the exact proportions of the various ions vary in different waters. Salinity is often expressed in parts per thousand (ppt or ‰), which is approximately grams of salt per liter of water. Salinity ranges from 0 to 33 ppt in estuaries and ~35 ppt in the open oceans. The UNESCO Practical Salinity Scale of 1978 (UNESCO, 1981) redefined salinity in Practical Salinity Unit (psu): the conductivity ratio of a sea water sample. The ratio has no unit. The concentration of dissolved solids in water can be expressed in mass ratio as:

$$\text{Concentration} = \frac{\text{Mass of dissolved solids}}{\text{Mass of water}} \tag{2.1}$$

By weight, seawater by the salinity equal to 35 has only 96.5% of water. The remaining 3.5% is dissolved solids. Since the dissolved solids are much heavier than freshwater, the

density of saltwater is greater than that of freshwater and varies with both salinity and temperature. At a temperature of 20°C, seawater has a density ~ 1026 kg/m^3, whereas freshwater has a density of 1000 kg/m^3. This slight difference in density can significantly affect estuarine circulations. Water density increases with increasing salinity and decreasing temperature. This relationship explains why water of low salinity tends to float above denser water that is colder and of higher salinity. In terms of density variation, increasing 1 unit of salinity is approximately equal to decreasing 4°C of water temperature. Therefore, salinity variation often changes estuarine stratification more effectively than temperature variation. Tides are the major forcing in an estuary and, along with freshwater inflows, control the vertical and horizontal distributions of salinity. Vertically, high tides lead to strong vertical mixing and little stratification, whereas low tides are insufficient to break up the vertical stratification. Horizontally, salinity in small, tidally mixed estuaries can change from completely fresh to saline within a tidal cycle, whereas salinity in larger estuaries is controlled to a greater degree by seasonal freshwater inflows. Wind forcing can also significantly affect vertical mixing in large estuaries.

2.2.1. Salt Balance Equations

The principal factors determining the pollutant concentration are hydrodynamic transport and chemical/biological reactions. Hydrodynamic transport acts to move pollutants from the location at which they are generated, resulting in impacts that can be distant from the pollution source. Hydrodynamic transport includes the following processes: (1) advection, (2) dispersion, and (3) vertical mixing. Material in water systems can be transported by one or all of these processes. These three processes are referred to as hydrodynamic transport.

Advection refers to horizontal transport by flows that move patches of material around, but do not significantly distort or dilute them. In rivers and estuaries, advection

often represents the primary transport process of pollutant in the longitudinal direction. Lateral advection across a river is usually small. In a straight channel the velocity profile indicates that the maximum advection occurs in the middle of the channel and that the minimum advection occurs near the banks. The lateral velocity differences cause the flow at the center of the river moving faster than the flow near the banks. This lateral variation promotes dispersion across the river.

Dispersion is the horizontal spreading and mixing of water mass caused by turbulent mixing and molecular diffusion. Dispersion reduces the gradient of material concentration. Dispersion processes are important to the distributions of temperature, salinity and other hydrodynamic variables in waterbodies.

In order to adequately estimate and predict salt transport characteristics in estuaries, it is important to find a way to quantify the water circulation and the mixing processes. It can be done by considering the budget of salt within sections of an estuary and assuming the conservative property of salt concentration. Fick‟s law states that the dispersive flux of mass movement is proportional to the gradient of mass concentration in that direction. as:

$$J = K\nabla C \tag{2.2}$$

where J ($ML^{-1}T^{-1}$) the dispersive mass flux density per unit width with components (J_x, J_y, J_z). C (ML^{-3}) is the mass concentration in water, K (L^2T^{-1}) is the diffusion coefficient. In one dimension, this equation can be rewritten as:

$$J_x = K_x \frac{\partial C}{\partial x} \tag{2.3}$$

where, x (L) is the longitudinal axis. The total rate of mass transport is the advetctive flux plus the diffusive flux as:

$$J_x = uC + \left(- K_x \frac{\partial C}{\partial x} \right) \tag{2.4}$$

where, $u(LT^{-1})$ is velocity across the longitudinal axis. Based on the principle of conservation of mass it can be written:

$$\frac{\partial C}{\partial x} + \frac{\partial J_x}{\partial x} = 0 \tag{2.5}$$

With combining Eqs. (2.4) and (2.5) can be written as:

$$\frac{\partial C}{\partial t} + \frac{\partial (uC)}{\partial x} - \frac{\partial}{\partial x}(K_x \frac{\partial C}{\partial x}) = 0 \tag{2.6}$$

Equation 2.6 is called the advection-diffusion equation in a one-dimensional transport process for substances. If salt is the considered substance, then it is the salt balance equation.

2.2.2. Types of Salinity Intrusion in Estuaries

In the estuaries, there are different types of salt intrusion, depending on topography, hydrology, and tide. The salt intrusion can be adequately described by the one-dimensional dispersion equation. When this equation is combined with equations describing topography and dispersion, it yields a predictive equation that can be used for both unsteady and steady state, particularly for the tidal average situation, high water slack, and low water slack. In an estuary of the well-mixed type, the variation of the salinity along the longitudinal axis of the estuary is gradual. This implies that if a continuous survey is done along an estuary a smooth curve can be fitted through the observed cross- sectional averaged salinities. The following types are distinguished (Savenije, 2005):

Type 1, Recession Shape

Type 2, Bell shape

Type 3, Dome shape

Type 4, Humpback shape

Type 1 is an intrusion curve with a logarithmic convex shape; the salinity gradient at the estuary mouth is steep (Fig 2.2). Type 3 is completely the opposite: it has a concave shape and the salinity gradient at the mouth is small. This type occurred in estuaries which are all wide channels with a pronounced funnel shape. Type 2 is not a transition from type 1 to 3. It starts concave, but within 50 percent of the salt intrusion length, it changes into a convex shape. These estuaries are close to prismatic upstream, but funnel-shaped near the mouth. Apparently, these three types of intrusion curves are very much linked to the geometry of the estuary. In all estuaries the length of intrusion curve follows the hydrological conditions and may increase or decrease, but the shape type remains unchanged. A humpback shape is entirely the result of a rainfall deficit or an evaporation excess. Evaporation can change a bell-shaped intrusion into a dome-shaped intrusion and eventually into a hyper- saline intrusion. Generally, in well-mixed estuaries, the salinity reduces in upstream direction. Such an estuary is a normal or „positive" estuary (Section 2.1). In a positive estuary, the sum of the fresh water inflow and the direct rainfall on the estuary surface exceeds the evaporation. In contrast, in the hypersaline or „negative" estuaries evaporation exceeds the sum of rainfall and runoff. In a hypersaline estuary, the salinity increases in the upstream direction until it reaches a maximum after which it decreases depending on the amount of fresh water inflow.

2.2.3. Longitudinal salinity Gradient

Estuaries show a great diversity of size, shape, depth, and forcing characteristics, but a general characteristic of estuaries is the presence of a horizontal salinity gradient. Normally the salinity decreases from the ocean toward the head of the estuary due to

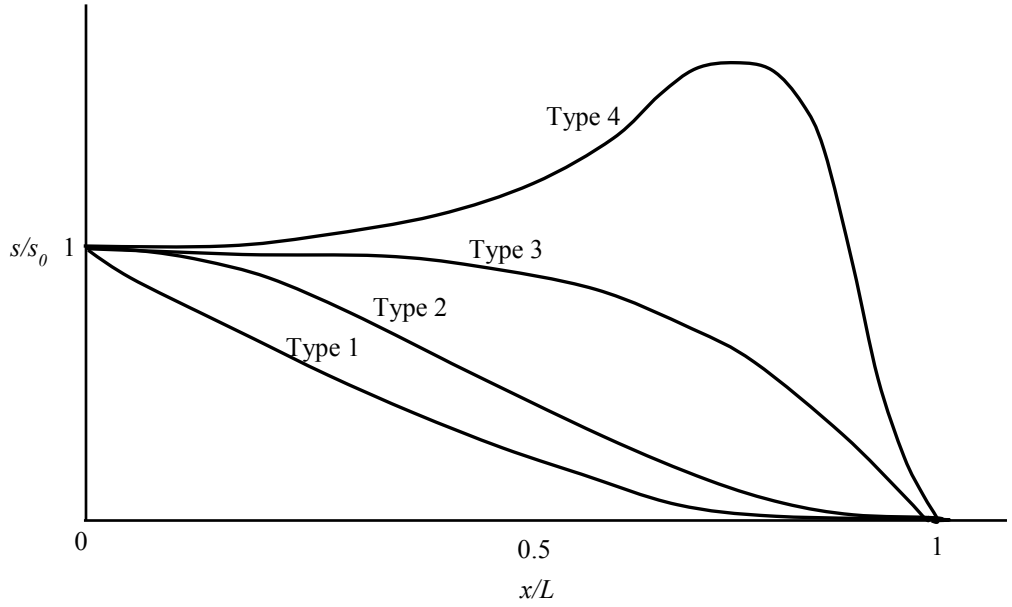

Fig 2.2 Four types of salt intrusion curves (Savenije, 2005), in which L is the salt intrusion length, x is the distance from the mouth, s_0 is the salinity at the mouth and s is the salinity corresponding with the distance x.

freshwater input. This salinity gradient is the key dynamical variable that makes estuaries different from any other marine or lacustrine environment. The horizontal salinity gradient is the key driving force for the estuarine circulation, which in turn plays a key role in maintaining salinity stratification in estuaries. The combined influence of the estuarine circulation and stratification determines the fluxes of salt and freshwater within the estuary, and their intensity varies with the strength of the freshwater inflow. Because of these dynamics, estuaries are often the most strongly stratified aquatic environments, but they also tend to have vigorous water and salt exchange, due to the estuarine circulation.

2.2.4. Estuarine Circulation

One fundamental feature of estuaries is the tidal-averaged circulation of two-layer net flow which is called estuarine circulation. Estuarine circulation is the result of

momentum balance in the estuary. The basic form of estuarine circulation consists of the interaction between the surface freshwater and the bottom saltwater, which gives a baroclinic pressure field that drives vertical and along-estuary motions.

The conservation of momentum can be derived from Newton‟s second law. Hence, the momentum equation can be expressed as:

$$\rho \frac{du}{dt} = \frac{\partial(\rho u)}{\partial t} + \nabla.(\rho u^2) = \rho g - \nabla p + f_{vis} \tag{2.7}$$

where ρ(kg/m^3) is the water density, f_{vis} is viscous force, p(pa) is the water pressure, and ∇ is gradient operator. The negative sign for the pressure gradient is to indicate that the pressure gradient force is directed opposite to the gradient. For an incompressible Newtonian fluid, the viscous force can be expressed as:

$$f_{vis} = \nabla \tau = \mu \nabla^2 u \tag{2.8}$$

where τ is shear stress, μ is absolute (or dynamic) viscosity, assumed to be constant, and ∇^2 is the Laplacian operator. Also the hydrostatic pressure distribution can be expressed as:

$$p(z) = \int_z^{\eta} \rho g dz = \rho g(-z + \eta) \tag{2.9}$$

where, z is the vertical coordinate and η is water surface. The longitudinal pressure gradient can be expressed as:

$$\frac{\partial p}{\partial x} = \rho g \frac{\partial \eta}{\partial x} + (-z + \eta) g \frac{\partial \rho}{\partial x} \tag{2.10}$$

In this equation the third term on the right hand side is negligible. Also the relation

between the longitudinal salinity and density gradient can be expressed as:

$$\frac{1}{\rho}\frac{\partial \rho}{\partial x} = \beta \frac{\partial s}{\partial x} \tag{2.11}$$

where β is the coefficient of saline contraction. By substitution of Eq. (2.11) into the Eq. (2.10) we can write:

$$\frac{\partial p}{\partial x} = \rho g \frac{\partial \eta}{\partial x} + \beta \rho g \frac{\partial s}{\partial x} \tag{2.12}$$

Pritchard represented the vertical shear stress in terms of an eddy viscosity A_z,

$$\tau = \rho A_z \frac{\partial u}{\partial z} \tag{2.13}$$

where τ (pa) is the stress and $\partial u/\partial z$ is the vertical shear of the horizontal flow. Geyer et al. (1999) denoted that the eddy viscosity varies significantly in space and time due to variations in forcing, but the momentum balance can be approximated using a constant value that represents an "effective" tidal average. So the steady-state representation of the horizontal momentum balance regarding Eq. (2.7) can be expressed as:

$$\frac{\partial p}{\partial x} + \frac{\partial \tau}{\partial z} = 0 \tag{2.14}$$

In fact this equation indicates the balance between the longitudinal pressure gradient and vertical shear stress as major external forces in Eq. (2.7). By substitution Eqs. (2.13), (2.12) and (2.11) into the Eq. (2.14) we can write:

$$\rho g \frac{\partial \eta}{\partial x} + g \frac{\partial \rho}{\partial x} z + \frac{\partial \tau}{\partial z} = 0 \tag{2.15}$$

Geyer"s result indicates that the bottom stress can be obtained using a quadratic drag law as:

$$\tau_b \approx \rho C_D |u_b| u_b \tag{2.16}$$

where C_D is the bottom drag coefficient and u_B is a near-bottom velocity. Geyer revealed that there is a slight but significant difference in C_D between springs and neaps. He point out that the difference may reflect a difference in near-bottom stratification between spring and neap tides. Finally he mentioned that tidally averaged bottom stress can be determined based on the magnitude of the tidal velocity and the subtidal velocity (Estuarine Circulation). Based on Geyer‟s approximation Eq. (2.16) can be expressed as:

$$\frac{\partial \tau}{\partial z} \approx \frac{\tau_b}{h} \approx \frac{\rho C_D u_E u_t}{h} \tag{2.17}$$

where, u_t is tidal velocity u_E is the magnitude of estuarine circulation. By substitution Eq. (2.17) into Eq. (2.15) and considering Eq. (2.11) we can write:

$$\beta g \frac{\partial s}{\partial x} h + \frac{1}{a_0} \frac{C_D u_E u_t}{h} = 0 \tag{2.18}$$

where a_0 is a constant related to the vertical variability of stress. Finally the Estuarine Circulation can be expressed as (Figure 2.3):

$$u_E = a_0 \frac{\beta g \frac{\partial s}{\partial x} h^2}{C_D u_t} \tag{2.19}$$

As it can be seen the estuarine circulation is relative to the key estuarine quantities: linearly with $\partial s/\partial x$, inversely with tidal velocity, and quadratically with water depth.

2.2.5. Stratifications of Estuaries

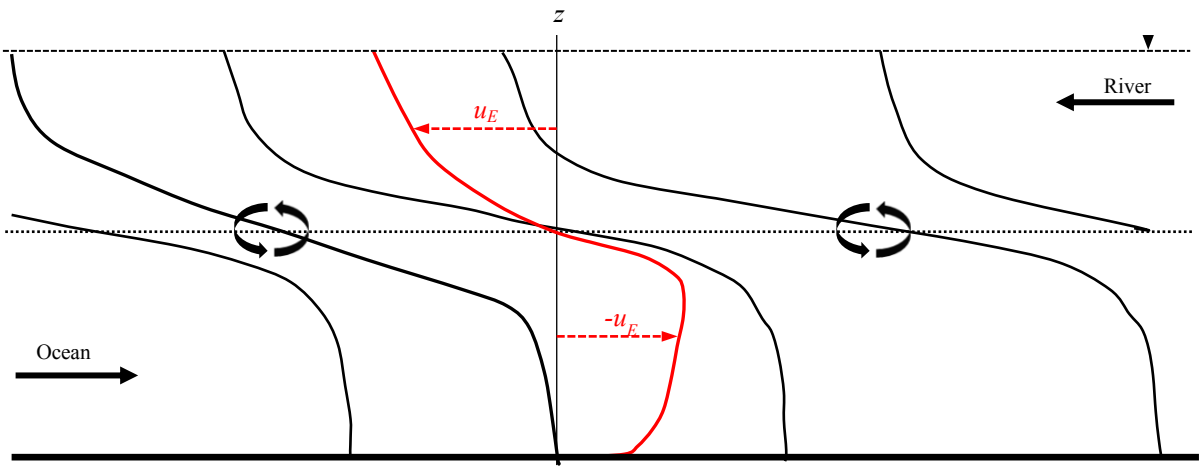

Fig 2.3 Schematic distribution of estuarine circulation and vertical mixing. In this figure the black and red lines are the salinity isohalines and estuarine circulation, respectively. The vertical mixing is controlled by the interaction of horizontal advection process at the upper layer and tidal forces at the under layer.

The stratification in an estuary is a result of shears straining the along-channel salinity gradient and mixing from tides, winds, and waves (Simpson et al., 1990; Dyer 1973). Estuarine stratifications are also affected by spring and neap tides. Estuarine stratification is weaker during spring tides than during neap tides because spring tidal currents are stronger and contribute more energy to mix the water column. As a result, the salinity gradient in the vertical is stronger during a neap tide than during a spring tide. The steady-state form of salt balance equation can be expressed as:

$$u(z)\frac{\partial s}{\partial x} = \frac{\partial}{\partial z}(K_z \frac{\partial s}{\partial z}) \tag{2.20}$$

where *u(z)* is the vertically varying, tidally averaged (steady-state) velocity, and K_z is the eddy diffusivity of salt, with the same dimensions and similar magnitude to A_z. As with the eddy viscosity, the eddy diffusivity can be represented in terms of tidal velocity and depth as:

$$K_z = k_1 C_D u_t h \tag{2.21}$$

here, k_1 is a constant. Also we note that $\partial s/\partial z \approx \Delta s/h$; where Δs is the top-to-bottom salinity difference. By replacing the estuarine circulation velocity as tidally-averaged velocity and the eddy diffusivity in Eq. (2.20) we obtain:

$$\Delta s = a_1 \frac{u_E \frac{\partial s}{\partial x} h}{C_D u_t} \tag{2.22}$$

where a_1 is a constant also depends on the shape of the salinity and velocity profiles. Combining Eqs. (2.22) and (2.19) the stratification can be expressed based on estuarine features as:

$$\Delta s = a_0 a_1 \frac{\beta g (\frac{\partial s}{\partial x})^2 h^3}{(C_D u_t)^2} \tag{2.23}$$

This equation indicates that the stratification depends quadratically on the salinity gradient and inversely on the square of the tidal velocity. As it can be seen the stratification is much more sensitive to changes in these forcing variables than is the estuarine circulation. The estuarine forcing varied mostly depends on the estuarine response to river discharge, wind and tidal mixing over time scales, ranging from days (intratidal) to fortnight (spring-neap tides) and month (seasonal variations). The classic estuarine theory suggests that the dynamics of the estuarine circulation involve a balance between the pressure gradient induced by the out-estuary surface slope, the baroclinic pressure gradient due to the along-estuary salinity gradient, and the stress associated with the estuarine circulation (Hansen and Rattray, 1965). On the other hand, there are some evidences jeopardize the classic estuarine paradigm of previous scholars and suggest that the tidally averaged, estuarine share flow may arise not as a result of the along-estuary salinity gradient but rather as a consequence of tidal process (Geyer et al., 1999).

2.2.6. Length of Salinity Intrusion

Another major change related to river flow variability is the length of the salinity intrusion into the estuary. The salt intrusion length in an estuary is controlled by the tidal amplitude, density differences, vertical eddy viscosity and diffusivity, and channel length (Hansen and Rattray, 1965). The variability of the salt intrusion length in estuaries has been investigated by different investigators using field measurement data or from numerical and empirical modeling. In both approaches the relation between the salt intrusion length and water discharge have been analyzed thoroughly (Monismith et al., 2002; Bowden, 1963) However, in the empirical modeling method the geometry variations have an important role in forecasting model (Nguyen and Savenije, 2006). Based on the Hansen and Rattray (1965) steady-state estuarine model, in an exchange flow dominated estuary, the intrusion length can be expressed as (Monismith et al., 2002):

$$L \propto \left(\frac{A(\beta g)^2 h^8 s_0}{A_z^3} \right)^{1/3} Q_R^{-1/3} \tag{2.24}$$

here, $A(\mathrm{m}^2)$ is the local cross-sectional area and $Q_R(\mathrm{m}^3/\mathrm{s})$ is the river discharge and s_0 is the reference salinity. This equation suggests that salinity intrusion length is proportional to $Q_R^{-1/3}$. Notice that the power dependence coefficient of the salt intrusion length to discharge varies under different estuarine conditions than the theoretical value, -1/3 (Monismith et al., 2002; Gong and Shen, 2011). Assuming A_z is proportional to tidal velocity, the salt intrusion length is inversely proportional to tidal velocity. In many estuaries the length of salt intrusion is varied significantly during the spring-neap tidal cycles. The vertical mixing during spring tides reduces density stratification, allowing higher dissipation throughout the water column. The higher mixing levels actually inhibit salinity advection, and salinity intrusion is stronger on neap throughout much of the

annual flow cycle.

2.3. Mixing in Estuaries

There are several mixing mechanisms that vary in importance depending on the shape of the estuary, the location, the level of stratification, the density, and the strength of the tide. One can distinguish different types of mixing, such as mixing by turbulence, mixing by tidal shear, mixing by residual currents, mixing by trapping, and density-driven mixing. All mixing mechanisms can be grouped as "tidal-driven" and "density-driven" which will be described in the following sections. All these mixing mechanisms together drive horizontal dispersion of salinity, which can be decomposed into many smaller constituting fluxes.

2.3.1. Main Driving Forces for Mixing

We can distinguish three main driving forces for mixing:

The Wind

Wind drives both vertical and horizontal circulation. The vertical circulation is driven by wind shear inducing a surface current of relatively fresh water and a water level slope in the direction of the wind, while the surface slope triggers a relatively saline return flow close to the bottom. Mixing occurs along the interface between these two currents and through upwelling of relatively saline water from the bottom. The wind also can cause horizontal circulation depending on the shape of the estuary. Although in lakes and coastal lagoons wind-driven mixing can be dominant, in small estuaries this mixing mechanism has a minor role.

The River

River discharge provides potential energy. Freshwater drives vertical gravitational circulation. Gravitational circulation is an important mechanism in the part of the estuary where the longitudinal salinity gradient is the largest. In estuaries with a strong funnel shape (and hence a dome-shaped salt intrusion curve), this region is located in the central part of the salt intrusion length. In the downstream part of these estuaries, where the salinity gradient is small, tide-driven mixing is dominant. In narrow estuaries, with a recession-shaped salt intrusion curve and a rather constant salinity gradient, gravitational circulation is the main mixing mechanism throughout the estuary.

The Tide

Tides provide kinetic energy to the estuary that can overcome the potential energy deficit of the river water. There are different types of mixing due to tidal influence which can be grouped into "tidal-pumping" and "tidal-trapping" (Fischer et al., 1979).

2.3.2. Mixing by the tide

The tides in the estuaries generate different types of mixing which we shall describe in somewhat more detail below.

Turbulent Mixing

In a river cross section, there is a balance between the tidal driving force (gravity) and friction. Although gravity works on all water particles, the friction only works along the bottom and banks of the estuary. The friction force is transported to all other particles through a shear stress that is transferred by turbulence. As a result, the flow velocity in a cross section is generally highest at the largest distance from the bottom and the banks. The turbulence that is associated with this shear stress also causes mixing, much as in a regular river. Turbulent mixing has been intensively studied and subsequently described by investigators. Fischer et al. (1979) consider relative importance of this mechanism

with the other tide-driven mechanisms that can be classified as advective-dispersion. Three-dimensional (3D) hydraulic models are able to model the salt fluxes resulting from advective dispersion by the combination of the velocity field with the salinity field. The turbulent dispersion is imposed through the eddy diffusivity of turbulent flow that these models use. Hence a good three-dimensional hydraulic model should be able to simulate tidal mixing adequately.

Tidal Trapping

Tidal trapping results from the phase difference between the main estuary branch and a dead-end tidal branch, bay or tidal flat. In a dead-end branch, slack occurs at HW, whereas the water in the estuary is still flowing upstream at HW. Between HW and HWS the water level drops and the dead-end branch already starts emptying while the estuary still flows upstream with relatively saline water. Hence a tidal flat discharges relatively fresh water into the flood flow. In estuaries with an irregular topography trapping can be an important mechanism. Because trapping occurs only along the sides of the estuary, its relative importance is less in very wide estuaries.

Tidal Pumping

Fischer et al. (1979) defined “tidal pumping” as the energy available in the tide that drives steady circulations similar to what would happen if pumps and pipes were installed to move water about in circuits. Tidal pumping is an important large-scale mixing mechanism for moving pollutants and transporting salinity upstream against a mean outflow of freshwater. There are two types of residual circulation that cause tidal pumping: (i) interaction of the tidal flow with a pronounced flood-ebb channel system; and (ii) interactions of the tidal flow with the irregular bathymetry, which in fact is the tidal trapping mechanism defined earlier.

2.3.3. Gravitational Circulation

In estuaries the hydrostatic pressure on the sea-side and on the river-side does not gain equilibrium. Because sea water is denser than river water, the pressure on the ocean-side would be higher at equal depth than on the river-side. As a result, the water level at the limit of the salt intrusion is slightly higher than at sea. Near the surface, the resultant pressure is directed towards the sea, while near the bottom, it is directed upstream. As a result, there is a residual circulation that carries relatively saline water upstream along the bottom and relatively fresh water downstream along the surface. This phenomenon has been fully studied, both in laboratories and in the field, and analytical equations have been derived to describe this mixing process.

Diffusive fraction Index

Hansen and Rattray (1965) started a discussion on which of the two mechanisms density-driven or tide-driven) is dominant in a certain estuary. Their classic estuarine theory suggests that the dynamics of the circulation and mixing processes involve a balance between the pressure gradient induced by the out-estuary surface slope, the baroclinic pressure gradient due to the along-estuary salinity gradient, and the stress associated with the estuarine circulation. Based on these classic assumptions the salt transport in an estuary is a balance between seaward flux, induced by river flow, and landward flux associated with tides and estuarine exchange flows. Landward salt transport can be separated into two parts: estuarine exchange flow, and tidal dispersion (or tidal oscillatory flux). The one-dimensional, along-estuary salt conservation equation is given by:

$$\mathrm{A}(x)\frac{\partial s}{\partial t} = \frac{\partial}{\partial x}\left[-Qs - A(x)\overline{u's'} + A(x)K_x(x)\frac{\partial s}{\partial x}\right] \tag{2.25}$$

where the prime denotes the spatial fluctuation deviated from the spatial mean and the overbar denotes a tidally averaged component. x is longitudinal distance increasing in the upstream direction and K_x is the along-estuary dispersion rate (m^2/s). Q is positive when it flows toward the ocean. In the steady state form Eq. (2.25) can be written as:

$$\frac{Q}{\mathrm{A}(x)}s = -\overline{v's'} + K_x(x)\frac{\partial s}{\partial x} \tag{2.26}$$

Hansen and Rattray (1965) defined a key estuarine parameter v namely the diffusive fraction of upstream salt flux which is the ratio of the tidal diffusion term to the total upstream flux as:

$$\nu = \frac{K_x(\partial s/\partial x)}{\overline{v's'} + K_x(\partial s/\partial x)} \tag{2.27}$$

This key parameter reflects the relative importance of tide-driven mechanism versus the total dispersion fluxes. when v approaches zero, the estuarine exchange flow dominates the landward salt flux, while when ν approximates unity, the diffusive process dominates the landward salt transport. Banas et al. (2004) demonstrated that stronger salt intrusion occurs during neap tides in an exchange flow dominated estuary while stronger salt intrusion happens during spring tides in a tidal diffusion dominated estuary. Generally, the estuarine exchange flow and its associated salt transport increases when tidal amplitude decreases (e.g., Chatwin, 1976; Bowen and Geyer, 2003), whereas the tidal diffusion is believed to increase with increasing tidal amplitude, particularly under well-mixed conditions (Fisher et al., 1979). However, Bowen and Geyer (2003) suggested that tidal oscillatory flux showed no distinct spring-neap variation at their study site in the Hudson River Estuary. More recently, Lerczak et al. (2006) reported that tidal oscillatory flux could even be seaward (up-gradient) in the Hudson during their study period.

Dispersion by Gravitational Circulation

The physical basis of gravitational circulation is a balance between the baroclinic pressure gradient and the tidally averaged shear stress (Hansen and Rattray, 1965). This topic was discussed in section 2.2.4 by the title of Estuarine Circulation. Also Monismith et al. (2002) dealt this concept which a brief presentation is given here,

$$U_{GC} \propto \frac{\beta g \frac{\partial s}{\partial x} h^3}{A_z} \propto \frac{\beta g \frac{\partial s}{\partial x} h^3}{u_* h} \propto \frac{\beta g \frac{\partial s}{\partial x} h^2}{C_D^{1/2} u_{r.m.s}} \tag{2.28}$$

where U_{GC} is the velocity scale for the vertically sheared gravitational circulation, u_* is friction (shear) velocity and $u_{r.m.s}$ is the r.m.s of tidal velocity. This straining flow acts to tilt isohalines, producing a vertically variable salinity perturbation whose strength is determined by a balance between vertical mixing and straining, i.e.

$$s' \propto \frac{U_{GC} \frac{\partial s}{\partial x} h^2}{K_z} \propto \frac{\beta g \frac{\partial s}{\partial x} h4}{C_D {u_{r.m.s}}^2} \tag{2.29}$$

Thus, the total flux integrated over the depth is

$$F \propto U_{GC} s' h \propto \frac{(\beta g)^2 (\frac{\partial s}{\partial x})^3 h^6}{C_D^{3/2} {u_{r.m.s}}^3} \tag{2.30}$$

implying a diffusion coefficient

$$K_{xGC} \propto \frac{(\beta g)^2 (\frac{\partial s}{\partial x})^2 h^5}{C_D^{3/2} {u_{r.m.s}}^3} \tag{2.31}$$

Simpson et al. (1990) denoted that the degree of stratification in an estuary is established primarily by the interaction of two competing mechanisms: the stratifying effects of tidal straining tending to increases stratification during ebbs, which decreases during floods, and the effects of tidal mixing which always decreases stratification. Monismith et al. (1996) found that this transition is best described by a non-dimensional parameter termed the horizontal Richardson number as:

$$Ri_x = \frac{\beta g \frac{\partial s}{\partial x} h^2}{u_*^2} \tag{2.32}$$

Where, u_* is shear velocity. Dispersion resulting from gravitational circulation is found to increase strongly with increased Ri_x (Monismith, 2002). When the "critical Richardson number" is reached, conditions of periodic stratification transition to persistent stratification, leading to dramatically increased salt transport. Monismith et al. (2002) used a "water column" model to estimate that the dispersion coefficient associated with gravitational circulation varied according to the relationship $K_x / (u_* h) = a\ Ri_x^2$. This finding was consistent with a previous analytical relationship derived by Hansen and Rattray (1965).

2.4. Decomposition of Salt Flux

Total salt flux over a cross-section of estuarine system is typically conducted based on velocity, salinity and cross-section area (or water depth) fluctuations. Many of investigators estimated salt flux using measurement of current and salinity at one or several points of a cross-section at one or more stations in a particular estuary (Bowden, 1963; Fischer, 1972; Kjerfve, 1986; 1998, Simpson et al., 2001). In the other approaches the salt fluxes have decomposed based on vertical measurement of velocity and salinity at one location in a cross-section with effect of lateral variability inferred from more

limited measurements or from numerical modeling (Bowen and Geyer 2003; Lerczak et al., 2006; Gong and Shen, 2011).

In general, the total salt flux can be estimated as:

$$F = \frac{1}{T}\int^{T}\int^{A} u(x,y,z,t)s(x,y,z,t)dAdt \tag{2.33}$$

where, T is the tidal period, u and s are the temporal velocity and salinity components respectively. The temporal velocity and salinity can be decomposed as:

$$u(x,y,z,t) = \bar{u}(x,y,z,t) + u'(x,y,z,t) \tag{2.34.a}$$

$$s(x,y,z,t) = \bar{s}(x,y,z,t) + s'(x,y,z,t) \tag{2.34.b}$$

where the overbar and prime quantities represents cross-sectionally-averaged and deviation from cross-sectionally-averaged variables, respectively. The cross-sectionally-averaged means were decomposed into tidally-averaged and a time varying components as:

$$\bar{u}(x,y,z,t) = <\bar{u}(x,y,z,t)> + u_T(x,y,z,t) \tag{2.35.a}$$

$$\bar{s}(x,y,z,t) = <\bar{s}(x,y,z,t)> + s_T(x,y,z,t) \tag{2.35.b}$$

$$A(x,y,z,t) = <A(x,y,z,t)> + A_T(x,y,z,t) \tag{2.35.c}$$

Finally, after substitution and integrating of Eq. (2.33) over a tidal cycle, the total salt flux can then be decomposed into different components as:

$$F = \overbrace{\langle A\rangle\langle\bar{u}\rangle\langle\bar{s}\rangle}^{1} + \overbrace{\langle Au_Ts_T\rangle}^{2} + \overbrace{\langle\bar{u}\rangle\langle A_Ts_T\rangle}^{3} + \overbrace{\langle\bar{s}\rangle\langle A_Tu_T\rangle}^{4} + \overbrace{\langle A\overline{u's'}\rangle}^{5} \tag{2.36}$$

Each term in the right side of Eq. (2.36) can be related to different physical process in the estuaries. Term (1), the "advective" flux, is driven by the river flow and change in

storage during the tidal cycle. Term (2) is the tidal dispersion via triple correlation between tidal depth change, tidal current, and tidal salinity changes. Term (3) is the cross-correlation between tide and salinity. Term (4), which is the time average of the tidal correlation of the cross-sectional averages (i.e., driven by temporal deviations from the mean), is considered to represent "tidal pumping" and "tidal trapping" mechanisms and is frequently a major dispersive mechanism. Term (5) is the "steady" or "residual" circulation term driven by time-averaged spatial profiles of u and s; this term includes mechanisms such as gravitational circulation. In cases where thorough mixing over the cross-section and minimal shear (e.g. negligible gravitational circulation) may be assumed, then this term may be neglected (Kjerfve, 1986).

Many authors have obtained a number of important salt fluxes for mixing mechanisms from Eq. (2.33), ranging from the most important three mechanisms (i.e. residual flux due to river discharge, residual flux of tidal pumping and residual flux of mean shear effect produced by gravitational circulation) even eleven components. The relative magnitudes of the salt fluxes may vary between estuaries and also temporally for an individual system, depending on variability in freshwater input, tidal range, velocity and salinity fluctuations, geometry, and strength of vertical mixing. Mostly, we can estimate the advective term relatively easily by obtaining some estimate of river discharge and mean salinity. The dispersive terms are more difficult to estimate because they require much more temporally and spatially detailed measurements, usually through the deployment of moored or boat-mounted instrumentation. With sufficient data, the decomposition method is a useful tool to investigate dominant mixing mechanisms in estuaries, at least between the two main mechanisms: tidal pumping and gravitational circulation (tide-driven and density-driven circulation). The development of 2-D and 3-D hydrodynamic models, especially with the 3-D hydrodynamic models, can provide detailed data to investigate the mixing mechanisms. The models, of course, have to be

treated with care in order to reproduce the correct velocity field and salinity field.

2.5. Time Scales of Physical Transport in Estuaries

A variety of time scales, such as "flushing time", "residence time", "transit time", and "water age", are used to describe time scales for transport and removal of materials that enter waterbodies. As first-order descriptions meant to represent the retention of water mass within defined boundaries (Monsen et al., 2002), transport time scales are related to the time required for water and dissolved substances to pass through aquatic systems (Sheldon and Alber, 2002). Time scales for transport can be compared to time scales characterizing inputs or transformations of biological or chemical constituents in order to identify the dominant processes underlying variability in water quality. For example, transport time has been used to explain variability in thermal stratification, dissolved organic carbon, elemental ratios of heavy metals, algal biomass and primary production, dissolved nutrient concentrations, and isotopic composition (Monsen et al., 2002). For reactive water quality constituents, a long transport time is seen as providing more time for biological or geochemical processes to occur, potentially allowing for significant modification of the mass of a constituent (e.g., algal biomass) present in an estuary, or possibly even modifying the dominant form of a constituent (e.g., dissolved vs particulate nitrogen). Many estuarine researchers and resource managers have an intuitive understanding of the concepts of "residence time", "flushing time", and water "age". While these terms have distinct and precise definitions and methods of calculation, they are often confused and loosely and interchangeably used (Zimmerman, 1976; Sheldon and Alber, 2002).

2.5.1. Flushing Time

Flushing time is a useful concept in estuarine management. The harmful effects of a pollutant are usually a function of its concentration. Flushing time (or residence time) is often used to represent time scales for removing materials (especially pollutants) out of estuaries. The shorter the flushing time, the better flushed the estuary. Typical flushing times range from days in small estuaries to months in large estuaries during low flow conditions. Flushing time can be defined in a number of ways in the literatures. Flushing time can be calculated by empirical formulas, numerical and physical models, or by field studies. Dyer (1973) presented several techniques to estimate the flushing time. Alber and Sheldon (1999) used a date-specific method which assumes that the appropriate time period over which to average discharge is equivalent to the flushing time. Wang et al. (2004) used a two-dimensional hydrodynamic eutrophication model (HEM-2D) to calculate the residence time. Huzzy et al. (2005) considered the effect of temporal variability in wind speed and direction to estimate residence and flushing time. Flushing time of estuaries is commonly defined as the time needed to replace the freshwater already in the estuary (freshwater volume) at the rate of freshwater inflow (Dyer, 1973). It represents the average time required to remove a parcel of freshwater (or a conservative tracer) from an upstream location in an estuary to the sea. Since pollutant loadings are often associated with freshwater inflows, the flushing time describes an overall feature of the estuary and is often used in the analysis of pollutant transport in estuaries.

2.5.2. Estimation of the Flushing Time using Freshwater Fraction Method

The flushing time of estuaries is different from the hydraulic residence time of lakes, even though that the two are similar in spirit: both express the ratio of freshwater volume over the freshwater flow rate. The hydraulic residence time of lakes is the average time required to completely empty the lake water with the outflow rate, that is, the ratio of the lake volume to the lake outflow rate. Since estuaries constantly exchange with the sea

and can never be "emptied", the flushing time is focused on the freshwater and its transport in estuaries. The freshwater volume of an estuary, V_f , is calculated using an integration over the estuarine volume:

$$V_f = \int \frac{s_0 - s_m}{s_0} dV = V(1 - \frac{s_m}{s_0}) \tag{2.37}$$

where s_0 is seawater salinity (or reference salinity outside the estuary), s is temporal salinity, s_m is the mean salinity in the estuary, and V is the estuary volume. It should be noted that the term f is the freshwater content or the freshwater fraction. The mean salinity in the estuary is calculated as:

$$s_m = \frac{1}{V} \int s dV \tag{2.38}$$

From Eq. (2.38) , it can be shown that:

1. When $s_m = s_0$, the freshwater volume is zero, and the estuary has no freshwater.

2. When $s_m = s_0 / 2$, the freshwater volume is one - half of the estuary volume.

3. When $s_m = 0$, the freshwater volume is equal to the estuary volume, and the entire estuary has only freshwater.

Therefore, by its definition, the flushing time of an estuary, T_f, can be calculated as:

$$T_f = \frac{V_f}{Q_R} = \frac{V}{Q_R}(1 - \frac{s_m}{s_0}) \tag{2.39}$$

where Q_R is the rate of total freshwater inflow. Note that in Eq. (2.39), the flushing time is not inversely proportional to the freshwater inflow, since the freshwater inflow also changes the mean salinity, s_m, which is determined by the complex hydrodynamic process in the estuary. Flushing time affects a wide range of hydrodynamic, sediment, toxic, and water quality processes that respond to external loadings. Flushing time

indicates the minimum duration for simulations of dissolved, nonreactive pollutants in an estuary and is often used to determine how much of a potentially harmful substance an estuary can tolerate before its ecosystem is significantly affected.

The flushing is a more complicated process in estuaries. Factors controlling flushing in estuaries include freshwater inflow, tidal range, and wind forcing. All these factors are time variable. Therefore, flushing times vary over a range of time scales. Flushing time averaged over a long-term (a season or a year) is often more useful in representing the estuarine characteristics. Estuarine flushing is largely controlled by two processes: advection by freshwater inflow and longitudinal dispersion by tidal forcing. Large freshwater inflow and strong tides lead to short flushing time. Flushing time also varies over the spring-neap tide cycle. Wind may also influence estuarine circulation and flushing time. Large and shallow estuaries are more susceptible to wind forcing. The wind – induced surface current may cause a vertical circulation in the estuary and affect flushing. However, wind-induced circulation and flushing are generally secondary, compared with the ones induced by freshwater inflow and tidal forcing.

2.5.3. Estimation of the Flushing Time using Knudsen's Method

Another estimate of the flushing time can be obtained from the salt balance equations (Knudsen‟s hydrographic theorem). If Q_R denotes the river discharge and Q_b and Q_s are the volume transports of the water entering and leaving the estuary at its mouth with respective salinities s_b and s_s, the continuity of volume and the continuity of mass (salt) give (Fig. 2.4),

$$Q_s - Q_b = Q_R \tag{2.40.a}$$

$$Q_s s_s = Q_b s_b \tag{2.40.b}$$

Solving for Q_s and noting that the flushing time is given by the volume of the estuary, V divided by Q_s, it follows that

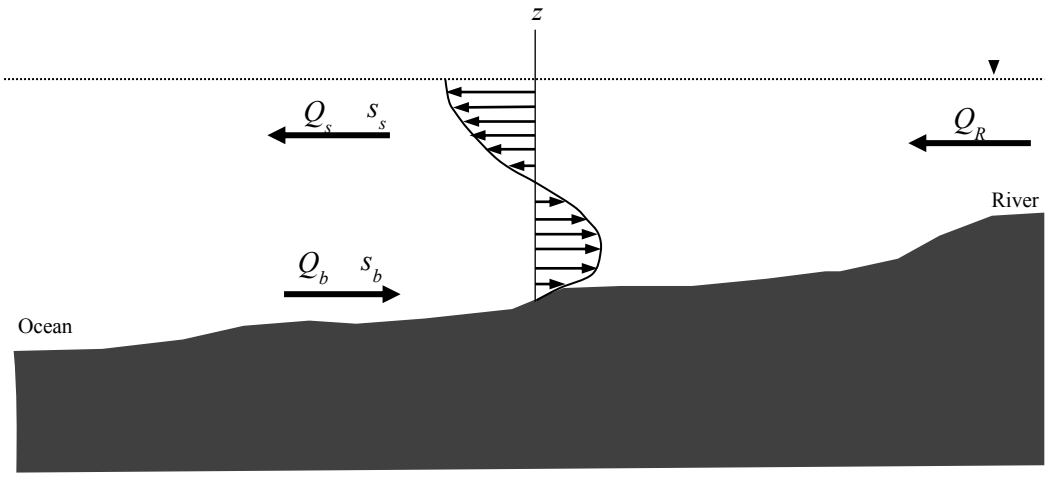

Fig 2.4 Schematic cross-section of an estuarine basin to illustrate Knudsen"s relation for the salt balance.

$$T_f = \frac{V(s_b - s_s)}{Q_R s_b} = \frac{V}{Q_R}(1 - \frac{s_s}{s_b}) \tag{2.41}$$

For estimation of flushing time given by Eq. (2.33), the key element of calculating is to estimate the mean salinity in the estuary. Under the assumption of completely mixing in the estuary, the Knudsen formula, Eq. (2.35) can be derived by considering the continuity of the water column and the continuity of salt. However, more direct assumptions in deriving the Knudsen formula can be stated as the following:

1. There is a strong two- layer circulation in the estuary (Fig. 2.4).
2. Due to this strong circulation, the bottom salinity at the mouth of the estuary (s_b) is equal to the reference salinity outside the estuary (s_0), that is, $s_b = s_0$.
3. The surface salinity at the mouth of the estuary (s_s) is equal to the mean salinity in the estuary (s_m), that is, $s_s = s_m$.

In real estuaries, however, the bottom salinity at the mouth is generally less than the reference salinity outside the estuary (i.e., $s_b < s_0$) and the surface salinity at the mouth is generally larger than the mean salinity inside the estuary (i.e., $s_s > s_m$). The consequence is that, similar to the tidal prism formula, the Knudsen formula in Eq. (2.35) may also consistently underestimate flushing times in a similar manner as the tidal prism method,

since it also assumes complete mixing of fresh water and oceanic water. In practice, the Knudsen formula appears more appropriate for highly stratified and salt wedge estuaries, whereas the freshwater fraction method is more suitable for partially mixed and well-mixed estuaries.

2.5.4. Variability of the Estuarine Salt Balance and Circulation

In Eq. (2.34a), If $Q_b \gg Q_R$ (which is generally the case for partially mixed and well-mixed estuaries), then $s_b \approx s_s \approx s_0$; and Knudsen‟s relation can be rewritten using estuarine circulation, U_e:

$$u_r s_0 = a_2 u_E \Delta s \tag{2.42}$$

where $u_r = Q_R/A_{R.cs}$ (the outflow velocity associated with the river discharge, $A_{R.cs}$ being the local cross-sectional area of the estuary), and a_2 is a constant. Equation (2.36) indicates that the tendency for salt to be carried out of the estuary by the freshwater outflow is balanced by the net input of salt due to the estuarine circulation. The stronger the estuarine circulation, and the larger the vertical salinity difference, the more salt is transported into the estuary. Eq. (2.36) represents the steady-state balance, and it only considers the influence of the estuarine circulation on the salt balance. The salt content of estuaries is not actually constant in time, because a number of factors cause the left-hand and right-hand sides of equation (2.34) to change. Eq. (2.36) also leaves out another contributor to the horizontal salt flux: the horizontal dispersion of salt (tidal dispersion), which is due mainly to tidal stirring. Tidal dispersion is particularly important in short estuaries, in which the length of the salt intrusion is comparable to the tidal excursion, distance, and also in regions of sharp changes in estuarine cross-section. But in large estuaries, and away from major changes in cross-sectional geometry, the salt transport induced by estuarine circulation generally dominates over tidal dispersion, and equation (2.36) is a good representation of the time-averaged salt balance.

References

Alber, M., Sheldon, J. (1999) Use of a date specific method to examine variability in the flushing times of Georgia estuaries, *Estuarine, Coastal and Shelf Science*, 49, 469-482.

Banas, S., Hickey, B. M., MacCready, P., Newton, J.A. (2004) Dynamics of Willapa Bay, Washington: A highly unsteady partially mixed estuary, *Journal of Physical Oceanography*, 34, 2413-2427

Bowden, K.F. (1963) The mixing processes in a tidal estuary, *International Journal of Air and Water Pollution*, 7, 343-356.

Bowen, M., Geyer, W.R. (2003) Salt transport and the time-dependent salt balance of a partially stratified estuary, *Journal of Geophysical Research*, 108 (C5), 185, doi: 10. 1029/2001 JC001231.

Chatwin, P. C. (1976), Some remarks on the maintenance of the salinity distribution in estuaries, *Estuarine and Coastal Marine Science*, 4, 555–566.

Dyer, K. R. (1973) Estuaries: A Physical Introduction, John Wiley and Sons, *Wiley- Interscience*, New York.

Dyer, K.R. (1997) Estuaries: a physical introduction (new revised issue), *John Wiley & Sons*, Aberdeen, UK.

Fischer, H. B. (1972) Mass transport mechanisms in partially stratified estuaries, *Journal of Fluid Mech*. 53, 671-687

Fischer, H. B., E. J. List, R. C., Koh, J., Brooks, N. H. (1979) Mixing in Inland and Coastal Waters. *Academic Press*, New York.

Geyer, W. R., Trowbridge, J., Bowen, M. (1999) The dynamics of a partially mixed estuary, *Journal of Geophysical Research*, 30, 2035-2048.

Gong, W., Shen, J. (2011) The response of salt intrusion to changes in river discharge and tidal mixing during the dry season in the Modaomen Estuary, China, *Continental Shelf Research*. 31, 769-788

Hansen, D. V., Rattray, M. Jr. (1965) Gravitational circulation in straits and estuaries, *Journal of Marine Research*, 23, 104-122.

Hardisty, J. (2007) Estuaries: monitoring and modeling the physical system, *Blackwell*, Malden, USA.

Huzzey, L.M., Christopher, D. N. (2005) Residence Time of Smith Cove, Thames River Estuary, USA *U.S. Coast Guard Academy Center For Advanced Studies Report* 07-05,2005.

Kjerfve, B. (1986) Circulation and salt flux in a well- mixed estuary. In: Van de Kreeke, J. (Ed.). *Physics of Shallow Estuaries and Bays*. Springer, Berlin 280, 22-29

Lerczak, J.A., Geyer, W.R., Chant, R.J. (2006) Mechanisms driving the time-dependent salt flux in a partially stratified estuary, *Journal of Physical Oceanography* 36, 2296–2311.

Levinson, A.V. (2010) Contemporary Issues in Estuarine Physics, *Cambridge University*, UK.

Monismith. **S.** G., J. Burau., Stacey, M. (1996) Stratification dynamics and gravitational circulation in northern San Francisco Bay. *San Francisco Bay: The Ecosystem,* T. Hollibaugh, Ed., American Association for the Advancement of Science, 123-153.

Monismith, S., Kimmerer, W., Burau, J.R., Stacey. (2002) Structure and flow-induced variability of the subtidal salinity field in Northern San Francisco Bay, *Journal of Physical Oceanography*, 32, 3003-3016

Nguyen, A.D., Savenije, H.H.G. (2006) Salt intrusion in multi-channel estuaries: A case study in the Mekong Delta, *Hydrology and Earth System Sciences*., 10, 734-754.

Savenije, H.H.G, Veling, E.J.M. (2005) Relation between tidal damping and wave celerity in estuaries, *Journal of Geophysical Research 110. doi: 10.1029/2004JC002278.*

Savenije, H.H.G. (2005) Salinity and tides in alluvial estuaries, *Elsevier*, Amsterdam

Sheldon, J.E., Alber, M. (2002) A comparison of residence time calculations using simple compartment models of the Altamaha River Estuary, Georgia, *Estuaries*, 25, 1304-1317.

Simpson, J.H., Brown, J., Matthews, J., Allen, G. (1990) Tidal straining, density currents, and stirring in the control of estuarine stratification, *Estuaries*, 13, 125-132.

Simpson, J.H., Vennell, R., Matthews, J., Souza, A. J. (2001) The salt fluxes in a tidally-energetic estuary, *Estuarine, Coastal and Shelf Science*, 52**,** 131–142

Wang, C.F., Hsu, R., Matthews, M.H., and Kuo, A. Y. (2007) Residence time of the Danshuei River Estuary, Taiwan, *Estuarine, Coastal and Shelf Science*, 60**,** 381–396

Zimmerman, J.T.F. (1986) The tidal whirlpool: A review of horizontal dispersion by tidal and residual currents, *Neth. J. Sea Res.*, 20, 133-154.

CHAPTER 3

Study Area and Methods

3.1. Study Area

The Ota River estuary encompasses the branched section of the old Ota River and the Ota River diversion channel about 9 km upstream (Fig 3.1). The designed flood discharge in the Ota river floodway and the old Ota River are 4500 and 3500 m^3/s, respectively (Gotoh et al. 2010). In addition, the Oshiba-floodgate, located in the old Ota River, consists of a fixed weir and a movable weir with three gates. The Gion floodgate, located near the bifurcation in the diversion channel, consists of three movable sluice gates, of which usually only one sluice gate is opened slightly in order to make a stream cross-section of 32 m×0.3 m for spilling water. The inflow discharge is about 10-20% of the total flow rate of the Ota River on normal days (Kawanisi et al., 2010). The Yaguchi Gauging Station, which is located 14 km upstream from the mouth, is not tidally modulated, so the Ota River discharge before the bifurcation can be estimated by using

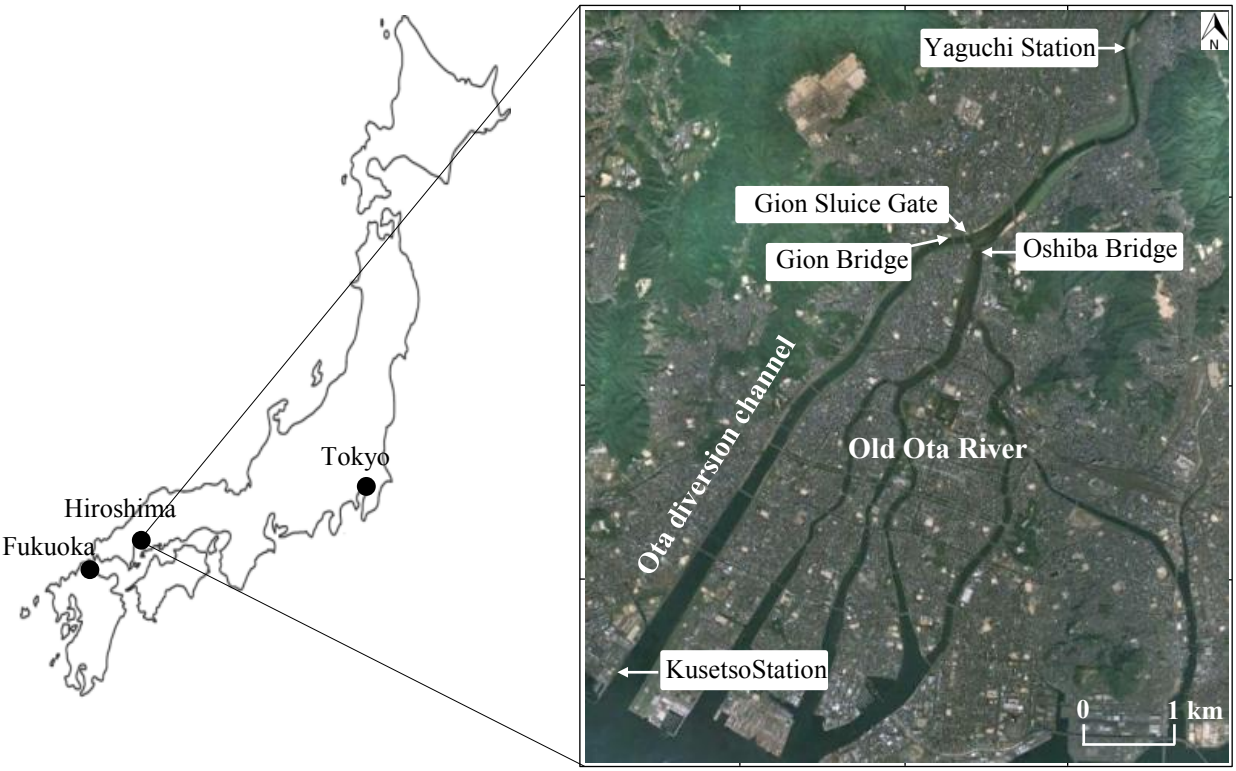

Fig.3.1 General view of study area (Ota Estuary)

the rating curves. During flood events, for discharge over 400 m^3/s, all sluice gates of Gion are completely opened. A large scale flood occurred in September 2005, with a discharge about of 7200 m^3/s observed at this station (Gotoh et al. 2010).

The water level fluctuations were measured at two stations in the estuary. At the Kusatsu and the Gion Stations which are located in the mouth and near the Gion Bridge, respectively (Fig 3.1). The upstream border of the tidal compartment which shows the influenced distance of the tides, in the Ota River estuary is located about 13 km upstream far from the mouth. River flow in this tidal compartment is characterized by the periodic intrusion of salt wedges. The tides are primarily semidiurnal, but mixed with a diurnal component. This study mostly focuses on the salinity variations at the Ota Diversion Channel.

Table.3.1 Characteristic of Ota Diversion Channel compared with the other estuaries in the world

Estuaries	Characteristics			
	River discharge Q (m^3/s)	Mean depth h (m)	Longitudinal length L (km)	Tidal range Tr (m)
Columbia	2000-20000	16	50	1.8-3.6
Hudson	1000-2500	15	75	1.2-1.6
Modaomen	1000-8000	5	40	0.5-2
Chesapeak	280-11000	12	150	< 1
Merrimack	20-1500	5	15	0.5-4
Ota Diversion Channel	25-4000	3	11	0.3-4
Tidal creek, San Francisco Bay	0.05-0.4	1	2	2

Ota Diversion channel is shallow and small estuary. It is about 9 km from the estuary mouth to the Gion Gates at the upstream region. It gradually widens from 110 m near the Gion Gate to 450 m at its river mouth. The average depth in the channel is about 3 m. The maximum and minimum tidal range at the mouth is varied between 0.3 m and 4 m during the neap and spring tides, respectively. Therefore, it can be classified as a tidally-dominated estuary. The stratification in the Ota diversion channel changes significantly with time. The downstream part of the Ota Diversion Channel is well-mixed during the flood and the first half of ebb and partially- mixed during the last half of ebb tides. This change of the stratification results from tidal straining (Kawanisi, 2004).

3.2. Instrumentation

There are three important methods for considering the hydrodynamic issues in the estuaries which are (1) field observations, (2) theoretical analysis, and (3) numerical modeling. Observations are the only way for understanding the real characteristics of the study area and make the basis for theoretical analysis and numerical modeling. In this study the key parameters used to represent the hydrodynamic and water quality conditions of site area include: velocity, water temperature, and salinity.

Water temperature is an important parameter representing the conditions of a waterbody. Changes in temperature can affect local ecosystem significantly. In estuaries, the salinity is a key parameter representing the environmental conditions. Water velocity plays a key role in transporting and mixing water quality variables.

For this study different measuring instruments were deployed to measure the key variables of site are. In this section we shall consider the properties of these instruments.

3.2.1. Fluvial Acoustic Tomography System (FATS)

3.2.1.1. Overview of the System

The measurement of river discharge is required for river management purposes including water resources planning, pollution prevention, and, flood control. Flow measurement technologies have developed rapidly in recent decades. Recently a new method for measuring the cross-sectional averaged velocity and salinity which is called Fluvial Acoustic Tomography System (FATS) has been developed in Hiroshima University (Kawanisi et al., 2010; Kawanisi et al., 2012).

The measurement principle of the FATS is the same as that used in an Acoustic Velocity Meter (AVM) which the range averaged velocity along the transmission line is calculated by using the „„traveltime method" (Sloat and Gain, 1995). However, the FAT system can estimate the mean cross-sectional velocity using multi-ray paths which cover throughout the cross-section. Kawanisi et al. 2012 considered the advantages of this method comparing with the current measuring systems thoroughly (Table 3.2). Hereafter, the abbreviated term "FATS" denotes the name of this self-recorder instrument. The present studies of using FATS have indicated the noticeable reliability and accuracy of this innovative method for the long-term measurement of the velocity and salinity in both freshwater and tidal rivers (Kawanisi et al., 2010; Kawanisi et al., 2012).

3.2.1.2. Measuring principles of FATS

Table.3.2 Significant limitations of current methods of flow rate measurement (Kawanisi et al., 2012)

Methods	Limitations
Rating Curve	-Variation in Rating Curve relation due to changes in bathymetry and roughness -Application of this method in the tidal rivers is complex
Cross- sectional Models	-Variation in the ratio of v_{max} to v_{mean} - Insufficient samples for modeling
H-ADCP	-Attenuated acoustic signal in flood events and turbid waters - Several hydraulic parameters is needed
AVM	-Refreaction of acoustic path under the stratified condition - Low signal-to noise ratio (SNR)

As presented in Fig 3.2, a couple of FATS‟ transducers with central frequency of 30 kHz were installed diagonally on the both sides of the Ota diversion channel near the Gion Bridge to continuously measure the cross-sectional averaged velocity and salinity. The width of the observation site is 120m with a bed slope of about 0.04%, and the tidal ranged from 0.3 m to 3 m during neap and spring tides, respectively. The travels times t_1 and t_2 along the reciprocal ray path between a couple of transducers can be estimated as:

$$t_1 = \frac{L}{c_m + u_m} \tag{3.1.a}$$

$$t_2 = \frac{L}{c_m - u_m} \tag{3.1.b}$$

where c_m and u_m are the sound speed and water velocity along the ray paths. These variables can be calculated using the travel times and raypath length as:

$$c_m = \frac{L}{2}\left(\frac{1}{t_1} + \frac{1}{t_2}\right) \tag{3.2}$$

and

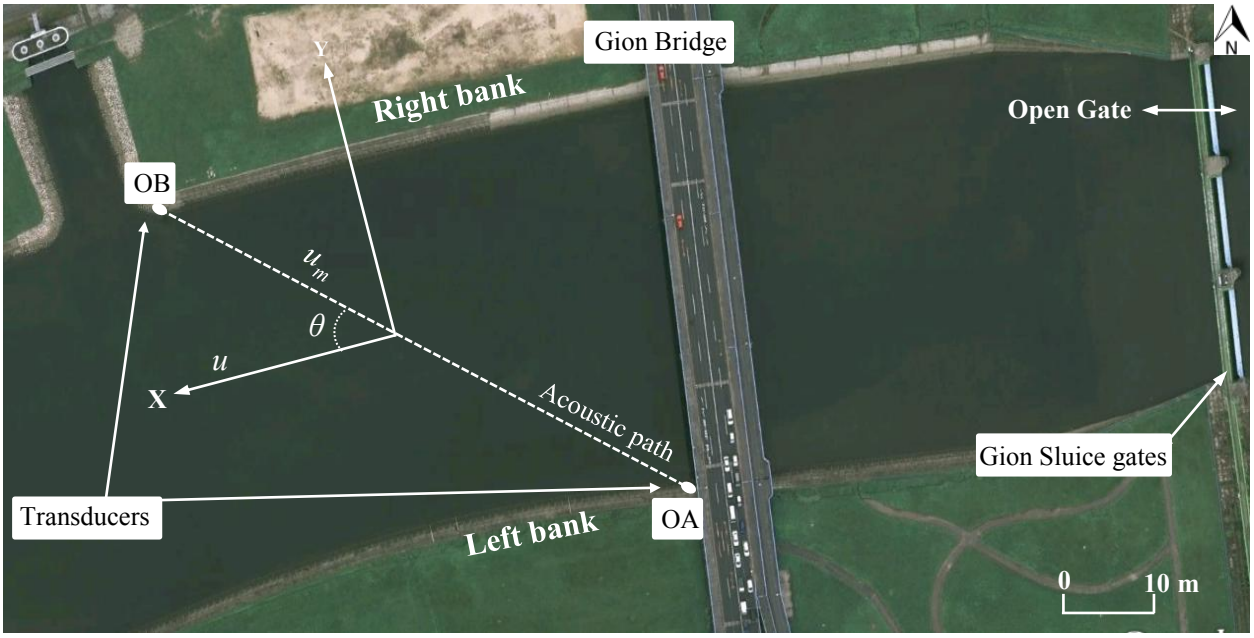

Fig 3.2 Details of FATS measurement at the Gion Station

$$u_m = \frac{L}{2}\left(\frac{1}{t_1} - \frac{1}{t_2}\right) \tag{3.3}$$

The cross-sectional average velocity in the direction of stream flow is estimated by the following formula (see Fig 3.2):

$$u = \frac{u_m}{\cos\theta} \tag{3.4}$$

where, θ is the angle between the ray path and the stream direction. The flow rate is calculated as the product of the mean velocity and the oblique cross-sectional area as:

$$Q = A(h)u\sin(\theta) \tag{3.5}$$

where, h is the water depth. The cross-sectional averaged salinity can be estimated from the sound speed measured by FATS, temperature and water level variations (Medwin, 1975) as:

$$s = 35 + \frac{1449.2 + 4.6T_m - 0.055{T_m}^2 + 2.9\times10^{-4}{T_m}^3 + 0.016h - c_m}{(0.01T_m - 1.34)} \tag{3.6}$$

where, s is the salinity, T (°C) is the temperature, and c (m/s) is the sound speed. Notice here that as mentioned we do not need to notify [*psu*] as a salinity unit, i.e. the practical salinity adopted by the UNESCO/ICES/SCOR/IAPSO Joint Panel on Oceanographic Tables and Standards does not have dimension.

3.2.1.3. Ray Tracing

Sound speed in the water body varies with depth due to changes in density and temperature. Ray tracing technique can be used to calculate the sound path rays of FATS. If the sound speed has an inhomogeneous distribution in the section, sound rays draw curves obeying Snell‟s law of refraction. In this study, ray simulation is carried out by solving the following couple of differential equations (Dushaw and Colosi, 1998):

$$\frac{d\varphi}{dx} = \frac{1}{c(x,z)}\frac{\partial c(x,z)}{\partial x}\tan\varphi - \frac{1}{c(x,z)}\frac{\partial c(x,z)}{\partial z} \tag{3.7.a}$$

$$\frac{dz}{dx} = \tan\varphi \tag{3.7.b}$$

$$\frac{dt}{dx} = \frac{\sec\varphi}{c(x,z)} \tag{3.7.c}$$

where φ is the angle of ray measured from the horizontal axis x, z is the vertical coordinate, and t the time. $c(x,z)$ is the sound speed which can be estimated form Medwin‟s formula. Figure 3.3 indicates typical examples of salinity distribution and ray simulation at the Gion Station. The sound speed was calculated by Medwin‟s formula, using the Compact CTD results which were casted along the raypath. Most of the time, the sound paths cover the cross-section as shown in Fig 3.3 (b).

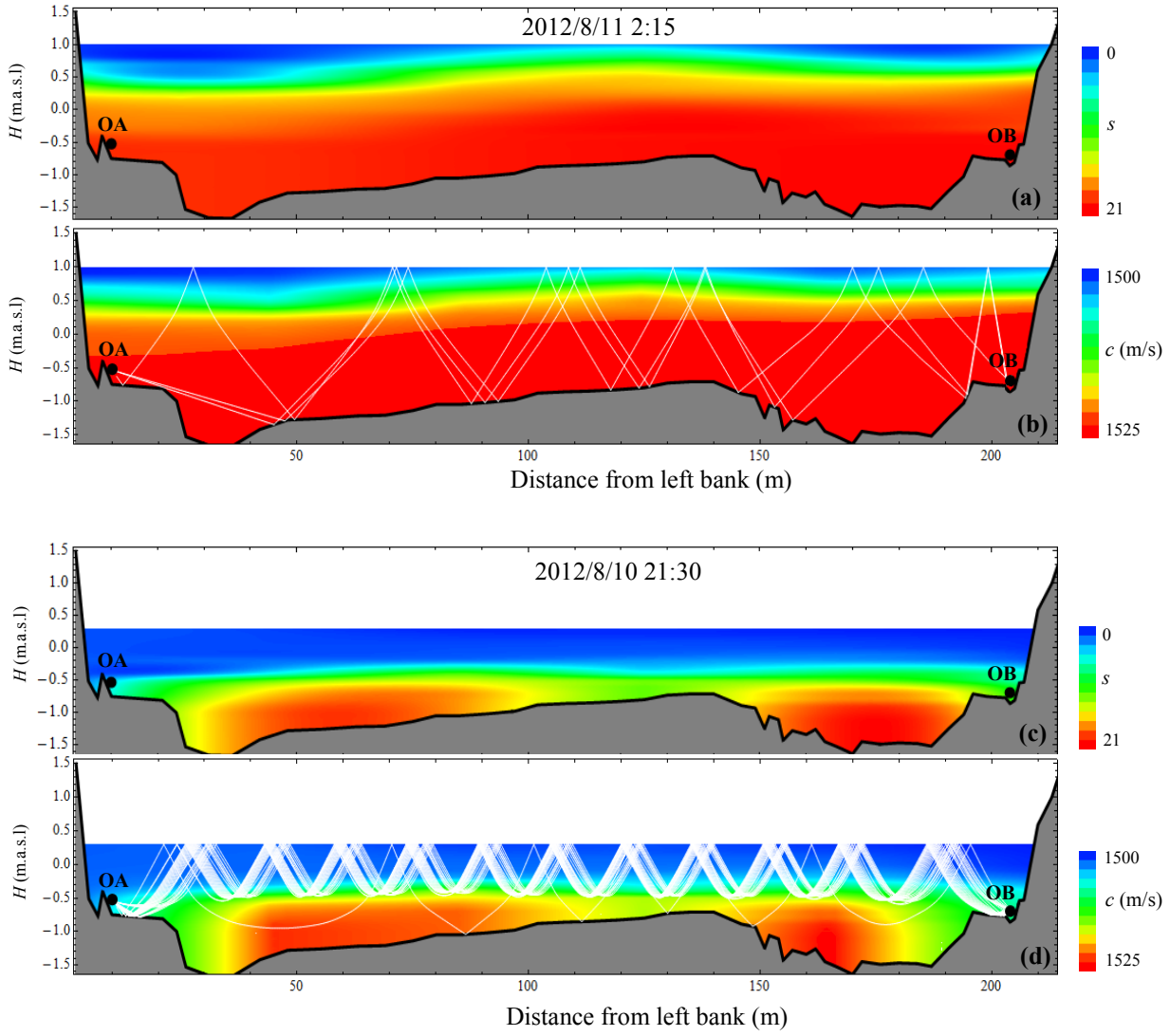

Fig 3.3 Examples of salinity distribution and ray simulations. The cases for the transducer put inside and above the salt wedge are shown in the upper and lower panels, respectively.

The results indicate existence of a salt wedge condition, especially during the first portion of flooding and last portion of ebb tides (e.g., Fig 3.3(d)). In this situation a two-layer system was happened in the observation site and the sound speed varied from 1525 m/s in the lower layers to 1500 m/s in the upper layers. As it can be seen during this period the sound rays in the upper layer are reflected at the underlying interface and could not penetrate into the lower layers. In this case, the cross-sectional average velocity is significantly overestimated by the FAT system since it cannot cover all the cross

sections (Kawanisi et al., 2010). The results of ray tracing suggests that the correction is required when the salinity difference between the upper and lower layers exceeds eight in the configuration with the transducer above the density interface (Kawanisi et al., 2010).

3.2.2. Acoustic Doppler Current Profilers (ADCPs)

Generally, ADCPs are hydro-acoustic instruments for measuring the water current velocities over a depth range using the Doppler effect of sound waves scattered back from particles within the water column. The measurement of vertical profiles of the velocity is the main achievement developed by ADCP. In the last few decades, the applications of ADCPs have been increased in riverine and coastal environments with the primary goal to estimate stream discharges.

For this purpose, ADCPs are attached to boats that transverse the river along a straight paths called transects. Consequently, conventional ADCP post-processing software can provide graphical user interfaces for visualization of selected flow features, estimation of stream discharges, and exporting data into various formats. More recently, attempts have been made to use the ADCP measurements for documenting additional river hydrodynamic characteristics (e.g., estimation of turbulence characteristics and suspended sediment). In this study we employed a moving boat, 1.2-MHz WorkHorse Rio Grande (WH-ADCP) and three AquaDopp ADCPs which are developed by Teledyne RDI and Nortek Co, respectively. The general characteristics of these instruments will be reviewed briefly in next sections.

WH-ADCP:

Teledyne RD Instruments has developed different types of ADCPs for stream flow measurement in oceanography, estuary, and rivers. The WorkHorse Rio Grande ADCP (Acoustic Doppler Current Profiler) is an accurate, rapid-sampling current profiling

Table 3.3 Technical features of WHADCP and Aquadopp ADCPs

Parameters		WHADCP	AquaDopp
Acoustic Frequency		1.2 MHz	2MHz
Water Velocity Measurement	Range	±5 m/s	±10 m/s
	Accuracy	0.25% of measured velocity ±0.2mm/s	1% of measured velocity ±5mm/s
	Cell number	1-128	1-128
	Cell size	0.05-2m	0.1-2m
	Minimum Blank distance	0.05m	0.1m
Software		WinRiverII	AquaPro
Power	Voltage	10.5-18V	9-16V
	Consumption	1.5W	0.2-1W

system designed to operate from a moving boat. The result is the fastest, safest, and most flexible method for measuring discharge. The Rio Grande can be used for a wide range of river conditions, from shallow 0.5 m deep streams to rushing rivers and tidal estuaries.

AquaDopp:

The Aquadopp is a cost-effective, robust with a wide range of applications. The system electronics integrates accurate Doppler velocity measurements with standard sensors such as temperature, pressure, tilt, and compass. The Aquadopp current meter is designed for any body of water, whether ocean, lake or river. The Aquadopp current meter is small in size but an extremely powerful sampling system that allows it to be used in a variety of applications. The instrument usually is used in real-time applications but also includes all parts required for a self-contained deployment with data stored to an internal data logger. In Table 3.3 some of the technical specifications of WHADCP and Aquadopp ADCPs are presented.

Table.3.4 Technical features of CTDs

Parameters		Alec Compact CTD	Diver CTD
Conductivity	Range	0-60mS/cm	0-80mS/cm
	Accuracy	±0.02mS/cm	1% of measured value
	Resolution	0.001 mS/cm	0.1% of measured value
Temperature	Range	-5 - 40 °C	0 - 40 °C
	Accuracy	±0.02°C	0.1°C
	Resolution	0.001°C	0.01°C
Depth	Range	0-600m	0-150m
	Accuracy	0.3% FS	0.1% FS
	Resolution	0.01m	0.02m

3.2.3. CTDs

A CTD is abbreviation for Conductivity, Temperature, and Depth is the primary instrument for determining three main physical properties of saltwater. It gives scientists a precise and comprehensive charting of the distribution and variation of water temperature, salinity, and density. In this study three kinds of CTDs were deployed. The technical specifications of these instruments are summarized in Table 3.4.

3.3. Numerical Model of the Water Level, Salinity and Velocity

Numerical models have a variety of applications in scientific and engineering fields. Numerical models are widely used for the simulations of physical processes in ocean and have many applications in the coastal regions and estuaries. To simulate tidal circulation, sedimentation, salinity distribution etc. in an estuary, various modeling techniques such as physical modeling, analytical models are used. Though physical modeling techniques are useful for the predictions of the estuarine processes, this approach is expensive and has limitations in scaling some physical parameters. Analytical modeling is another tool

to study the estuarine systems and many basic studies were carried out in estuaries using analytical models (e.g., Ippen and Harleman, 1961; Hansen and Rattray, 1965).

Simulation of estuarine processes requires proper representation of bottom topography, irregular coastline and hydrodynamic data. The limitation of analytical modeling is that it assumes a regular geometry of systems. The geometry of an estuarine system has an important role on estuarine circulation and mixing process. Unlike analytical models, which cannot deal with complex problems, numerical models are capable of realistically simulating complex water systems. Since the 1990s, 3D hydrodynamic and water quality modeling has been maturing from being a research subject to a practical analysis technology. The rapid progress of computer technologies provides powerful computers for numerical simulation. Computational requirements for realistic 3D modeling have changed from super computers and high-end workstations to desktop personal computers in the past two decades. Measured data through laboratory and field studies are used to provide insight into hydrodynamic and water quality processes. However, the spatial and temporal resolutions of measured data are often inadequate to fully characterize a waterbody. Numerical models can play a key role in understanding and extrapolating measured data. If a numerical model can accurately simulate the measured data from the waterbody, then the model may be used for further applications with confidence. A numerical model can be used to interpolate between observed data and to guide future data sampling efforts. By incorporating measured data in a numerical simulation, such as via data assimilation, even more reliable results can be produced from the numerical model. Data assimilation is becoming a powerful method in hydrodynamic and water quality modeling. Therefore, numerical models are essential tools not only for understanding the hydrodynamic and water quality processes, but also for developing plans for water resources and environmental management. Numerical models are always

a more or less schematized version of real systems, based on some hypotheses and descriptions of processes.

3.3.1. Description of the Numerical Model Setup (EFDC)

The first step in modeling application is Model selection. Although a variety of models are available to consider hydraulic issues, the best selection of model is still a complex task. The goal of model selection is to choose a model which is capable to simulate the most of study objectives. In all models some assumptions are used to simplify the real system and can impose limitations on the model application. Therefore, it is essential to be familiar with model assumptions before selecting a model. Selection of an appropriate model requires consideration of (1) objectives of the study and (2) time and resources needed, including availability of data, technical expertise and model availability and familiarity.

The Environmental Fluid Dynamics Code (EFDC) is a public-domain modeling package for simulating three-dimensional (3D) flow, transport, and biogeochemical processes in water systems, including rivers, lakes, estuaries, reservoirs and coastal regions (Hamrick, 1992). The EFDC model was originally developed at the Virginia Institute of Marine Science and is currently supported by the U. S. Environmental Protection Agency (EPA). The EFDC model has been extensively tested and documented in more than 100 modeling studies. The model is presently being used by universities, research organizations, governmental agencies, and consulting firms. The EFDC model is an advanced 3D, time-variable model that provides the capability of internally linking hydrodynamic, water quality and eutrophication, sediment transport, and toxic chemical transport and fate submodels in a single source code framework. It includes four major modules:

1. Hydrodynamic model.

2. Water quality model.
3. Sediment transport model.
4. Toxics model.

The full integration of the four components is unique and eliminates the need for complex interfacing of multiple models to address the different processes. A module to represent the submerged aquatic vegetation (SAV) was recently added to the EFDC model (AEE, 2005). The hydrodynamics of the EFDC model and many aspects of the computational scheme are equivalent to the widely used Blumberg-Mellor model (Blumberg and Mellor, 1987). The hydrodynamic model component is based on the 3D shallow water equations and includes dynamically coupled salinity and temperature transport. Notable extensions to the EFDC hydrodynamic model include representation of hydraulic structures for controlled flow systems, vegetation resistance for wetland systems (Moustafa and Hamrick, 2000), and wetting and drying process (Ji et al., 2001). The EFDC model solves the vertically hydrostatic, free-surface, turbulent-averaged equations of motions for a variable-density fluid. Dynamically coupled transport equations for turbulent kinetic energy, turbulent length scale, salinity, and temperature are also solved. The two turbulence parameter transport equations implement the Mellor -Yamada level 2.5 turbulence closure schemes (Mellor and Yamada, 1982; Galperin et al., 1988).

The EFDC model is designed to represent a finite difference computational grid as either a simple Cartesian grid or an orthogonal, curvilinear coordinate system for irregular coastlines. In the vertical domain, EFDC uses a sigma-stretched grid to represent complex bathymetry. As a fully 3D model, EFDC can be applied to all types of surface waterbodies. Originally constructed as a 3D model, the EFDC model can also be readily applied to 1D or 2D studies by using a 1D or 2D model grid and without any modification to the code. The model uses stretched (or sigma) vertical coordinates and curvilinear, orthogonal horizontal coordinates. It simulates density and topographically

induced circulation as well as tidal and wind-driven flows, and spatial and temporal distributions of salinity, temperature, and conservative/non-conservative tracers. The model has a flexible grid network structure, which is capable of linking multiple tributaries to the main channel through grid linkage between upstream and downstream grid cells, including dam structures. Theoretical and computational aspects of the model are described for hydrodynamics (Hamrick, 1992). The model user‟s manual (Hamrick, 1996) also provides details on setup of the EFDC input files. The original user interface is based on text input file templates. This choice was selected in the interest of maintaining model portability across a range of computing platforms and readily allows the user to modify input files using most text-editing software. The text interface also allows modification of model files on remote computing systems and in heterogeneous network environments. Several versions of windows-based user interfaces have also been developed in recent years. The preprocessor has a grid generator (GEFDC), an input data checker, and an initial condition generator. The postprocessor converts output data for use by other third- party visualization applications, often without need for intermediate processing. Some Graphics and visualization software which can be used used with EFDC output include AVS, Tecplot, SiteView, Voxelview, and EFDC_Explorer.

3.3.2. Governing Equations

The formulation of the governing equations for ambient environmental flows characterized by horizontal length scales which are orders of magnitude greater than their vertical length scales begins with the vertically hydrostatic, boundary layer form of the turbulent equations of motion for an incompressible, variable density fluid. To accommodate realistic horizontal boundaries, it is convenient to formulate the equations such that the horizontal coordinates, x and y, are curvilinear and orthogonal. To provide uniform resolution in the vertical, a time variable mapping or stretching transformation is desirable. The stretching is given by:

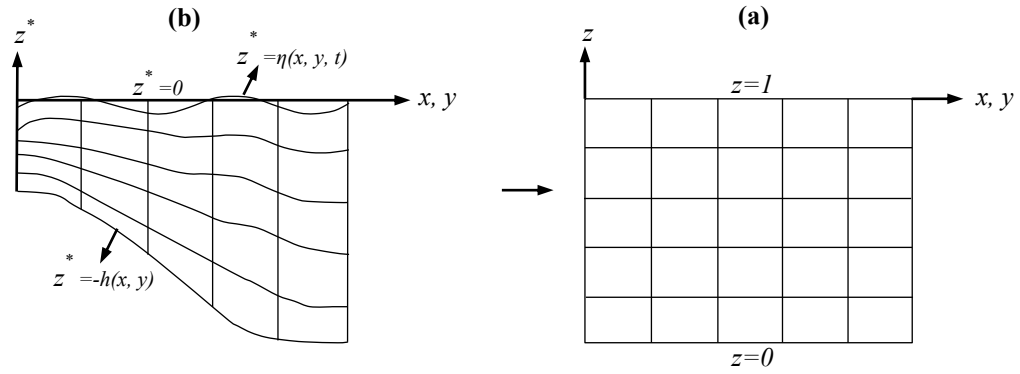

Fig 3.4 Vertical discretization types (a) Cartesian coordinate and (b) sigma-coordinate

$$z = \frac{z^* + h}{\eta + h} \tag{3.8}$$

where z the stretched, dimensionless which called sigma coordinate and z^* is the physical vertical coordinate, or the Cartesian coordinate. h and η are the physical vertical coordinates of the bottom topography and the free surface, respectively. As shown in Fig 3.4, the sigma coordinate allows smooth representation. Transforming the vertically hydrostatic boundary layer form of the turbulent equations of motion and utilizing the Boussinesq approximation for variable density results in the momentum and continuity equations and the transport equations for salinity and temperature, the 3D equations in sigma coordinate are in the following form (Hamrick, 1992):

a) Continuity

$$\frac{\partial H}{\partial t} + \frac{\partial Hu}{\partial x} + \frac{\partial Hv}{\partial y} + \frac{\partial w}{\partial z} = Q_H \tag{3.9}$$

$$\frac{\partial (H)}{\partial t} + \frac{\partial}{\partial x}(H\int_0^1 u dz) + \frac{\partial}{\partial y}(H\int_0^1 v dz) = Q_D \tag{3.10}$$

b) Hydrostatic

$$\frac{\partial p}{\partial z} = -gH\frac{(\rho - \rho_0)}{\rho_0} = -gHb \tag{3.11}$$

c) Momentum

$$\frac{\partial(Hu)}{\partial t}+\frac{\partial(Huu)}{\partial x}+\frac{\partial(Huv)}{\partial y}+\frac{\partial(uw)}{\partial z}-fHv=-H\frac{\partial(p+g\eta)}{\partial x}+(-\frac{\partial h}{\partial x}+z\frac{\partial H}{\partial x})\frac{\partial p}{\partial z}+\frac{\partial}{\partial z}(\frac{A_v}{H}\frac{\partial u}{\partial z})+Q_u \quad (3.12)$$

$$\frac{\partial(Hv)}{\partial t}+\frac{\partial(Huv)}{\partial x}+\frac{\partial(Hvv)}{\partial y}+\frac{\partial(vw)}{\partial z}+fHu=-H\frac{\partial(p+g\eta)}{\partial y}+(-\frac{\partial h}{\partial y}+z\frac{\partial H}{\partial y})\frac{\partial p}{\partial z}+\frac{\partial}{\partial z}(\frac{A_v}{H}\frac{\partial v}{\partial z})+Q_v \quad (3.13)$$

d) Transport

$$\frac{\partial(Hs)}{\partial t}+\frac{\partial(Hus)}{\partial x}+\frac{\partial(Hvs)}{\partial y}+\frac{\partial(ws)}{\partial z}=\frac{\partial}{\partial z}(\frac{A_b}{H}\frac{\partial s}{\partial z})+Q_s \quad (3.14)$$

$$\frac{\partial(HT)}{\partial t}+\frac{\partial(HuT)}{\partial x}+\frac{\partial(HvT)}{\partial y}+\frac{\partial(wT)}{\partial z}=\frac{\partial}{\partial z}(\frac{A_b}{H}\frac{\partial T}{\partial z})+Q_T \quad (3.15)$$

e) State

$$\rho=f(\rho_0,T,s) \quad (3.16)$$

f) Vertical velocity

$$w=w^*-z(\frac{\partial\eta}{\partial t}+u\frac{\partial\eta}{\partial x}+v\frac{\partial\eta}{\partial y})+(1-z)(u\frac{\partial h}{\partial x}+v\frac{\partial h}{\partial y}) \quad (3.17)$$

where $H=h+\eta$ is total water depth, h is the equilibrium water depth η is surface displacement from the equilibrium. In continuity equations u, v and w are water velocity in the x, y and z directions, respectively; and Q_H *and* Q_D are water inflow/outflow from the external sources. In the hydrostatic equation, p and ρ are the physical pressure and density and ρ_o is the reference density. In momentum equations f is the Coriolis parameter. A_v is the vertical turbulent or eddy viscosity Q_u and Q_v are momentum source-sink terms. In transport equations, s and T are the salinity and temperature, respectively; Q_s and Q_T are the source and sink terms and A_b is the vertical turbulent diffusivity. The system of eight equations [Eqs. (3.9)- (3.16)] provides a closed system for the variables u, v, w, p, η, ρ, s, and T, provided that the vertical turbulent viscosity and diffusivity and

the source and sink terms are specified. To provide the vertical turbulent viscosity and diffusivity, the second moment turbulence closure model developed by Mellor and Yamada (1982) and modified by Galperin et al. (1988) is used.

3.3.3. Turbulence Closure

Turbulence processes play a critical role in vertical mixing. Vertical transport by turbulent diffusion can be sufficient to completely mix the water column. To accurately calculate the vertical turbulent mixing coefficients A_v and A_b, in the equations of momentum and mass transport, it is necessary to have turbulence models that can represent the vertical mixing. Here the basic concepts and theories that are commonly used in EFDC mode are presented. In numerical models, turbulent transport and mixing with spatial scales smaller than model grid resolution are represented by vertical and horizontal turbulent dispersion. Treatment of vertical mixing in mathematical models is generally achieved through the vertical eddy viscosity. The simplest approach is to represent turbulent mixing using empirical relationships to specify a constant mixing coefficient. Advanced hydrodynamic models employ closure methods to provide internal calculations of vertical eddy diffusivity. The closure models provide the vertical turbulent diffusion coefficients necessary to represent vertical diffusive mass transport. The turbulence model described here was developed by Mellor and Yamada (1982) and modified by Galperin et al. (1988) and Blumberg et al. (1992). The model relates A_v and A_b to vertical turbulence intensity q, turbulence length scale l, and the Richardson number R_q by:

$$A_v = \phi_v ql = 0.4\frac{(1+8R_q)ql}{(1+36R_q)(1+6R_q)} \tag{3.18}$$

$$A_b = \phi_b ql = 0.4\frac{0.5ql}{(1+36R_q)} \tag{3.19}$$

$$R_q = -\frac{gH\dfrac{\partial b}{\partial z}}{q^2}\left(\frac{l^2}{H^2}\right) \tag{3.20}$$

where the stability functions ϕ_v and ϕ_b (Galperin et al., 1988) account for reduced and enhanced vertical mixing in stable and unstable vertically density-stratified environments, respectively. Turbulence intensity and the turbulence length scale are determined by solving transport equations for q^2 and $q^2 l$:

$$\frac{\partial(Hq^2)}{\partial t}+\frac{\partial(Huq^2)}{\partial x}+\frac{\partial(Hvq^2)}{\partial y}+\frac{\partial(wq^2)}{\partial z}=\frac{\partial}{\partial z}\left(\frac{A_q}{H}\frac{\partial q^2}{\partial z}\right)+2\frac{A_v}{H}\left[\left(\frac{\partial u}{\partial z}\right)^2+\left(\frac{\partial v}{\partial z}\right)^2\right]+ 2gA_b\frac{\partial b}{\partial z}-2\frac{Hq^3}{B_1 l}+Q_q \tag{3.21}$$

$$\frac{\partial(Hq^2 l)}{\partial t}+\frac{\partial(Huq^2 l)}{\partial x}+\frac{\partial(Hvq^2 l)}{\partial y}+\frac{\partial(wq^2 l)}{\partial z}=\frac{\partial}{\partial z}\left(\frac{A_q}{H}\frac{\partial(q^2 l)}{\partial z}\right)+E_1 l\frac{A_v}{H}\left[\left(\frac{\partial u}{\partial z}\right)^2+\left(\frac{\partial v}{\partial z}\right)^2\right]+ 2gE_1E_3 lA_b\frac{\partial b}{\partial z}-\frac{Hq^3}{B_1}\left(1+E_2\left(\frac{l}{\kappa L}\right)^2\right)+Q_l \tag{3.22}$$

$$L^{-1}=H^{-1}(z^{-1}+(1+z)^{-1}) \tag{3.23}$$

where B_1, E_1, E_2, and E_3 are empirical constants and Q_q and Ql are additional source-sink term such as subgrid scale horizontal diffusion. The vertical diffusivity, A_q, is in general taken equal to the vertical turbulent viscosity, A_v.

3.3.4. Initial and Boundary Conditions

Initial conditions and boundary conditions are needed to solve hydrodynamic equations. In a modeling study, the equations of the mathematical model describe the physical, chemical, and biological processes within the water body. In order to solve these equations numerically, initial and boundary conditions are needed for the modeling. Initial conditions specify the state of the water body at the beginning of the simulation.

The value of the boundary conditions cannot be obtained from the equations used to describe the physical phenomena, but must be inserted on the basis of other information. Boundary conditions and external forces to the study area are driving forces for model simulations. A model does not calculate boundary conditions for itself, but are affected by them. The number and type of initial and boundary conditions depend strongly on the nature of the particular water body, on the specific problem of interest, and on the type of the model used.

3.3.5. Model Calibration and Verification

The comparison of model results to measured data is an essential step in modeling. The objective is to calibrate the model to the observed data, utilizing parameter values that are consistent with the observed data within the acceptable ranges. Successful evaluation is essential for developing a credible model for applications. Model calibration is the first stage for comparing the model results with a set of field data not used in the model setup. Model calibration is also the process of determining model parameters. When measured data are available, model parameters can be estimated using curve-fitting procedures. The model parameters may also be obtained through a series of test runs. Comparisons are made between model results and measured data graphically and statistically to assess model performance. Numerous skill metrics exist to comparison between model and measured results. Here we explain the model skill score (SS) which depends on the root-mean-square error between the model and observations normalized by the standard deviation of the observations (Allen et al., 2007; Ralston et al., 2010):

$$SS = 1 - \frac{\sum_{i=1}^{N} (X_{\mathrm{mod}} - X_{obs})^2}{\sum_{i=1}^{N} (X_{\mathrm{mod}} - \overline{X}_{obs})^2} = 1 - \frac{1}{\sigma_{obs}^2} \frac{1}{N} \sum_{i=1}^{N} (X_{\mathrm{mod}} - X_{obs})^2 \tag{3.23}$$

where X is the variable of interest and overbar denotes the time mean value. The maximum SS is 1 when the model exactly agrees with the observations; an SS of 0 means that the model provides equal predictive skill as the mean of the observations, and a negative SS represents that the model is less predictive than the mean of the observations. For reference, Allen et.al, (2007) categorized a SS > 0.65 as excellent, 0.5-0.65 as very good, 0.2-0.5 as good, and SS < 0.2 as poor, respectively.

Model verification uses an independent data set (the second data set that is not used in model setup). Model verification helps establish greater confidence in the model"s capability of predicting future conditions of the system. Values of model parameters obtained from model calibration are not adjusted in the verification step, and the model results are evaluated graphically and statistically in the same manner used for model calibration, but with a different data set. An acceptable verification demonstrates that the model is capable for simulating the waterbody under different external conditions.

3.3.6. General structure of Model Input

The primary component of the EFDC modeling system is the FORTRAN 77 source code *efdc.for* which is universal for all model applications or configurations. Model configuration and environmental data for a particular application are provided in different input files which can be classified in five groups as follows which will be discussed briefly in next sections.

Horizontal Grid Generation Files (cell.inp, depth.inp, dxdy.inp)

The first step in the setup or configuration of the EFDC modeling system is defining the horizontal plane domain of the region being modeled. The terminology grid or grid lines refers to the lines defining the faces of the quadrilateral cells. (Triangular cells are defined by one of four possible regions resulting from diagonal division of a quadrilateral cell.) The horizontal grid of cells is defined by a cell type array which is specified by the

file *cell.inp*. Also to specify the horizontal geometric and topographic properties and other related characteristics of the region, the files *dxdy.inp* and *lxly.inp* are used. The file *dxdy.inp* provides the physical *x* and *y* dimensions of a cell, *dx* and *dy*, the initial water depth, the bottom elevation, and the roughness height.

General Data and Run Control Files (efdc.inp, show.inp)

efdc.inp is the master input file which controls the overall execution of a model simulation. The information in *efdc.inp* provides run control parameters, output control and physical information describing the model domain and external forcing functions. The file is internally documented, in essence providing a template or menu for setting up a simulation. The file consists of card image sections, with each section having header lines which define the relevant input parameter in that section. The file *show.inp*, is used to control screen writing of information during simulation runs.

Initialization and Restart Files (salt.inp)

The input file *salt.inp* is used as initial condition for the salinity fields.

Time Series of Forcing and Boundary Condition (pser.inp, qser.inp, sser.inp)

The input files *pser.inp*, *qser.inp* and *sser.inp* are open boundary water surface elevation, volumetric source-sink and salinity time series which are used for boundary conditions, respectively.

3.3.7. Pre/Post –Processing of Model Data

A variety of graphic and visualization software is available for presenting and analyzing 3D model results. Several versions of the windows-based Graphic User Interface (GUI) have been developed for the EFDC model in recent years. In this study, the graphics from the model results are made using EFDC_Explorer (http: //www. efdc-explorer.com). EFDC_Explorer is a Microsoft Windows based and provides pre-processor and post-processor capability for the EFDC input and output files.

References

Allen, J., Somerfield, P., Gilbert, F. (2007) Quantifying uncertainty in high-resolution coupled hydrodynamic-ecosystem models, *Journal of Marine Systems*, 64(1), 3-14.

Blumberg, A. F., Mellor, G.L. (1987) A description of a three-dimensional coastal ocean circulation model, *Three-dimensional coastal ocean models,* Editor: N. S. Heaps, American Geophysical Union, 1-16.

Blumberg , A. F., Galperin , B., Connor, D. J. (1992) Modeling vertical structure of open - channel flow, *J. Hydraulic Eng* , 118, 1119 – 1134.

Dushaw, B.D., Colosi, J.A. (1998) Ray tracing for ocean acoustic tomography, Technical memorandum, Applied Physics Laboratory, University of Washington (TM 3-98), 31 pp.

Galperin , B., Kantha, L. H., Hassid, S., Rosati, A. (1988) A quasi-equilibrium turbulent energy model for geophysical flows, *J. Atmos. Sci*, 45, 55- 62.

Gotoh, T., Fukuoka, S., Abe, T. (2010) Evaluating Flood Discharge and Bed Variation in The Ota River Floodway, *Proceedings of 9th International ICHE conference,* http://c-faculty.chuo-u.ac.jp/~sfuku/sfuku/03_paper/paper/ICHE2010-goto.pdf

Hamrick, J. M. (1992) A Three-dimensional Environmental Fluid Dynamics Computer Code: Theoretical and Computational Aspects, The College of William and Mary, Virginia Institute of Marine Science, Special Report 317, 63 pp.

Hamrick, J. M. (1996) Users Manual for the Environmental Fluid Dynamic Computer Code . The College of William and Mary, Virginia Institute of Marine Science, Special Report 328, 224 pp.

Hansen, D. V., Rattray, M. Jr. (1965) Gravitational circulation in straits and estuaries, *Journal of Marine Research*, 23, 104-122.

Ippen, A. T. and D. R. F. Harleman (1966) Tidal dynamics in estuaries. In A. P. Ippen (ed.), Estuary and Coastline Hydrodynamics. McGraw-Hill, New York, pp. 493–545.

Ji, Z. G., Morton, M. R., Hamrick, J. M. (2001) Wetting and drying simulation of estuarine processes, *Estuarine, Coastal Shelf Science*, 53, 683-700.

Kawanisi, K. (2004) Structure of Turbulent Flow in a Shallow Tidal Estuary, *J. of Hydraulic Engineering.,* ASCE, 130(4), 360-370.

Kawanisi, K., Razaz, M., Kaneko, A. and Watanabe, S. (2010) Long-term measurement of stream flow and salinity in a tidal river by the use of the fluvial acoustic tomography system, *Journal of Hydrology*, 380, 74-81

Kawanisi, K., Razaz, M., Ishikawa, K., Yano, J and Soltaniasl, M. (2012) Continuous measurements of flow rate in a shallow gravel-bed river by a new acoustic system, *Water Resour. Res*. doi:10.1029/2012WR012064

Medwin, H. (1975) Speed of sound in water: a simple equation for realistic parameters, *Journal Acoustical Society of America* 58, 1318.

Mellor, G. L., Yamada, T. (1982) Development of a turbulence closure model for geophysical fluid problems, *Rev. Geophys. Space Phys*, 20, 851- 875.

Moustafa, M. Z., Hamrick, J. M. (2000) Calibration of the wetland hydrodynamic model to the Everglades nutrient removal project. *Water Quality Ecosystem Modeling*, 1, 141-167.

Ralston, D.K., Geyer, W.R., Lerczak, J.A. (2008) Subtidal salinity and velocity in the Hudson River Estuary: Observations and modeling, *Journal of Physical Oceanography*, 38, 753-770.

Sloat, J.V., Gain, W.S. (1995) Application of acoustic velocity meters for gaging discharge of three low-velocity tidal streams in the St. John River Basin, Northeast Florida. US Geological Survey, Water-Resources Investigations Report, 95-4230, 26 pp.

CHAPTER 4

Variability in Salinity and Flushing Time

4.1. Introduction

Physical, chemical, and biological processes in the estuaries vary over the time and space. Spatial variations largely depend on the topography of the estuary. Temporal variations can be distributed over time scales ranging from minute to annual components. Table 4.1 show different time scales versus the main forces and relative mechanisms in the estuaries. Generally, the estuarine mechanisms can be described into intratidal and subtidal timescales. The temporal variation in the stratification among the diurnal and semi-diurnal tidal constituents is the dominated mechanism at the most shallow to moderate-depth estuaries. The stratification is controlled by the competing mechanisms of longitudinal advection and tidal mixing. As mentioned earlier, for tidal averaged flow, this is the estuarine circulation. The baroclinic circulation promotes stratification by

Table 4.1 Time scales and mechanisms in the estuaries

Estuarine Forces	Time scales			
	Intratidal	Subtidal		
	Minutes- Hours	Days-weeks	Months	Years
Freshwater	Tidal mixing	Daily variability (estuarine circulation, stratification, mean flow and salinity, etc)		
	Temporal variation in stratification	Spring-neap variability (tidal range, flushing time, salt flux, etc)		
Tide	Tidal straining	Seasonal variation (freshwater flow, sea level, temperature, wind, etc)		
	Vertical mixing	Annual variations (flood events, hydroclimatological, etc)		
Wind	Tidal asymmetry			

carrying lighter river water over the saline water. As stratification increases, vertical mixing of momentum is inhabited, and the sheared circulation is reinforced. Alternatively, as turbulent mixing increases, the stratification reduced directly by the mixing. Thus mixing diminishes the estuarine circulation. This concept called tidal straining (Simpson et al., 1990).

The subtidal salinity and flow rate in an estuary mostly depends on the estuarine response to river discharge, wind and tidal mixing over time scales ranging from days (freshwater and wind) to fortnight (spring-neap tides) and months (seasonal river discharge change and mean sea level). As it mentioned earlier the estuarine circulation and stratification are the key characteristics resulted from steady-state balance in the estuaries. Combining equations (2.19), (2.23) and (2.42) and solving $\partial s/\partial x$ we can write:

$$\frac{\partial s}{\partial x} = \frac{C_D}{(a_0^2 a_1 a_2)^{1/3}} \frac{u_t u_r^{1/3} s_0^{1/3}}{(\beta g)^{2/3} h^{5/3}} \tag{4.1}$$

This equation indicates that for steady-state conditions, the horizontal salinity gradient depends on the one-third power of the river flow and the first power of the tidal velocity. The response of the estuarine salt intrusion to changes in river flow is of fundamental interest to many researchers. Based on estuarine classical approach salt intrusion length L,

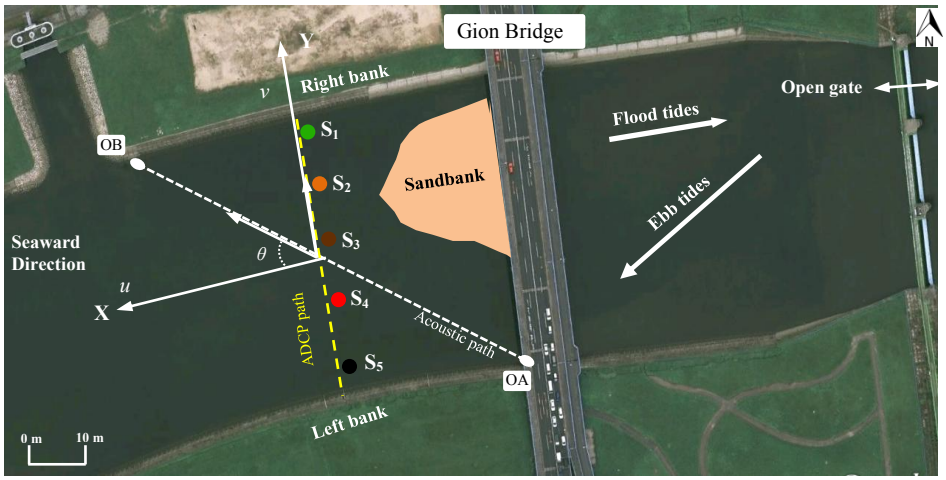

Fig 4.1 General view of observation site

is related to the river discharge Q_R in a power law form ($L \propto Q_R^n$) which discussed in section 2.2.6. Tidal range is another major contributor which fortnightly influences salinity intrusion length. In many estuaries the stronger vertical mixing during spring tides reduces density stratification, allowing higher dissipation throughout the water column. The higher mixing levels actually inhibit salinity advection, and salinity intrusion is stronger on neap throughout much of the annual flow cycle. In the next section we shall consider the intratidal and subtidal variations in tides, salinity, temperature and flow rate at the Gion Station.

4.2. Variability in Tides, Salinity and Discharge at the Gion Station

4.2.1. Intratidal Variations in Salinity and Flow Velocity

As presented in Fig. 4.1 a couple of FATS' transducers with central frequency of 30 kHz have been installed in the upstream section of the Ota Diversion Channel near the Gion Bridge to continuously measure the cross-sectional averaged velocity and salinity since 2008 till now. To evaluate FATS results, section-averaged velocity and salinity, with those acquired from an ADCP and a conductivity sensor, a field observation was conducted on January 25-26. In this observation the velocity were measured using a

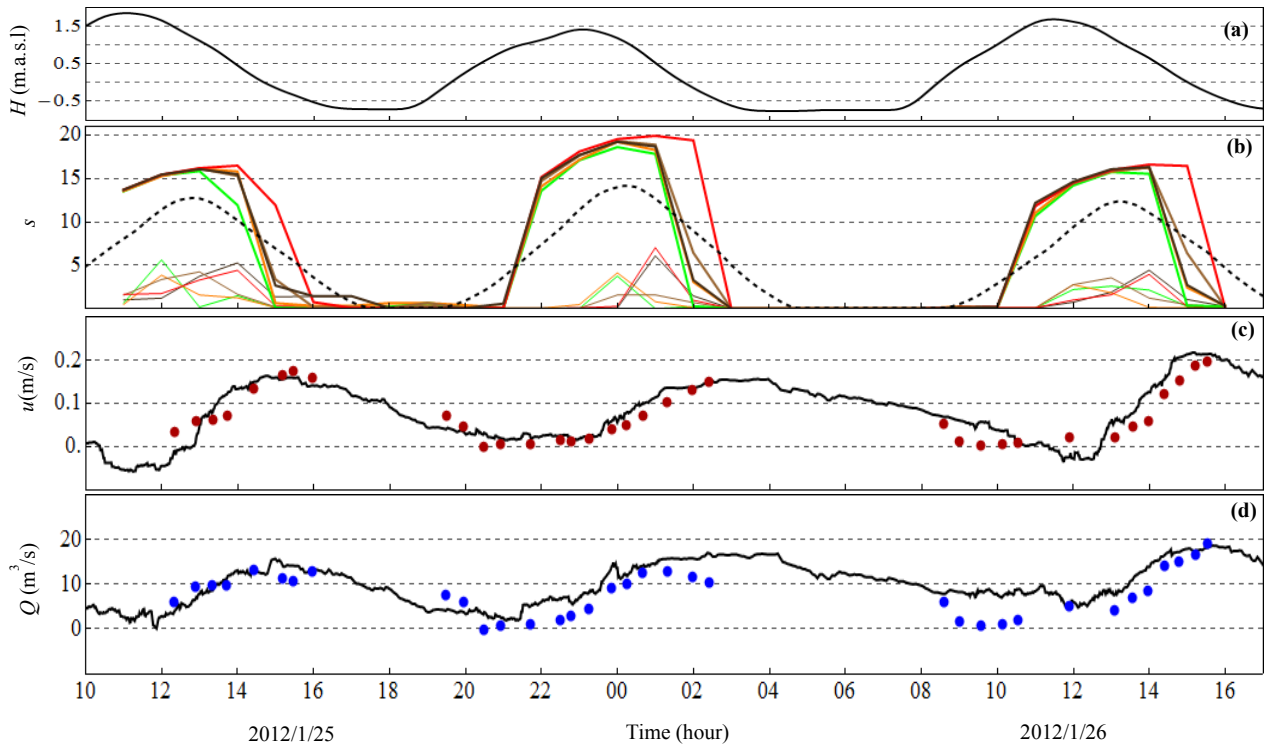

Fig 4.2 Time series of: (a) water level at Gion Station, (b) bottom (thick lines), surface (thin lines) salinity at the stations which casted by Compact CTD, S1 (green line), S2 (orange line), S3 (brown line), S4 (red line) and S5 (black line), the cross-sectional averaged salinity (black dashed line) estimated by FATS, (c) mean velocity (circles) estimated by WHADCP, (thick line) estimated by FATS and (d) mean discharge (circles) estimated by WHADCP, (thick line) estimated by FATS

moving boat, 1.2-MHz Teledyne RDI WorkHorse Acoustic Doppler Current Profiler (WH-ADCP). For removing the trajectory error, the WH-ADCP was connected to a cable which was mounted between the right and the left bank of the field site.

For this study all velocity vectors, which were estimated by the FATS and WH-ADCP, were rotated into river coordinate (X, Y) in which the seaward direction was positive (Fig 4.1). The salinity profiles were measured using Alec Electronic Compact-CTD (conductivity-temperature-depth profiler) at the five stations so the cross-sectional distribution of the salinity as well as temporal variability of the salinity can be analyzed. The stations are shown by circles (Fig 4.1). WinRiver II software computes total volume discharge for each ADCP ensemble. The uncertainty in the discharge estimation arises from random errors, biases, and missed data (near the surface, bottom, and the sides of a

channel). The algorithm for estimating discharge is adopted from (Simpson and Oltmann, 1990). Total discharge is the summation of discharge in the top, measured, bottom, left, and right layers. In this observation, the highest contributions of the bottom, near bank, and top discharge in the total discharge were 7.5%, 2.2% and 1.1%, respectively, which did not significantly bias the ADCP results. In order to compare the salinity estimates of FATS and the Compact CTD, we assumed that the cross-sectional averaged salinity using the compact CTD data can be estimated by:

$$s_{CTD} = \frac{1}{A}\sum_{i}^{n} s_i A_i \tag{4.2}$$

where s_{CTD} and n are the mean salinity of the cross-section and the number of salinity samples which were collected by the Compact CTD, respectively. Figure 4.2 shows the temporal variations in salinity, velocity and discharge according to FATS, CTD and ADCP. Also the relations between the results and the error variations are presented in Figure 4.3.The linear regressions can be presented as:

$$s_{CTD} = 0.99 s_{FAT} - 0.06 \qquad R^2 = 0.96 \tag{4.3.a}$$

$$u_{ADCP} = 0.69 u_{FAT} + .01 \qquad R^2 = 0.73 \tag{4.3.b}$$

$$Q_{ADCP} = 0.68 Q_{FAT} + 2.9 \qquad R^2 = 0.78 \tag{4.3.c}$$

The relative error between FATS and CTD results are within ±10% (Fig 4.3). The relative error of velocity during the flood tides exceeds 20%. However, the relative error of discharge for the noticeable range of variations is ±15%. The results indicate that the relative differences between FATS and ADCP increase during the flood tide. This difference may be caused by two important reasons. The first reason is the variability in flow direction during flood and ebb tides at the Gion Station (Soltaniasl et al. 2012a). The sandbar has been formed upstream of the observation site due to sediments deposition during the floods (Fig 4.1). Then due to the river morphology near the

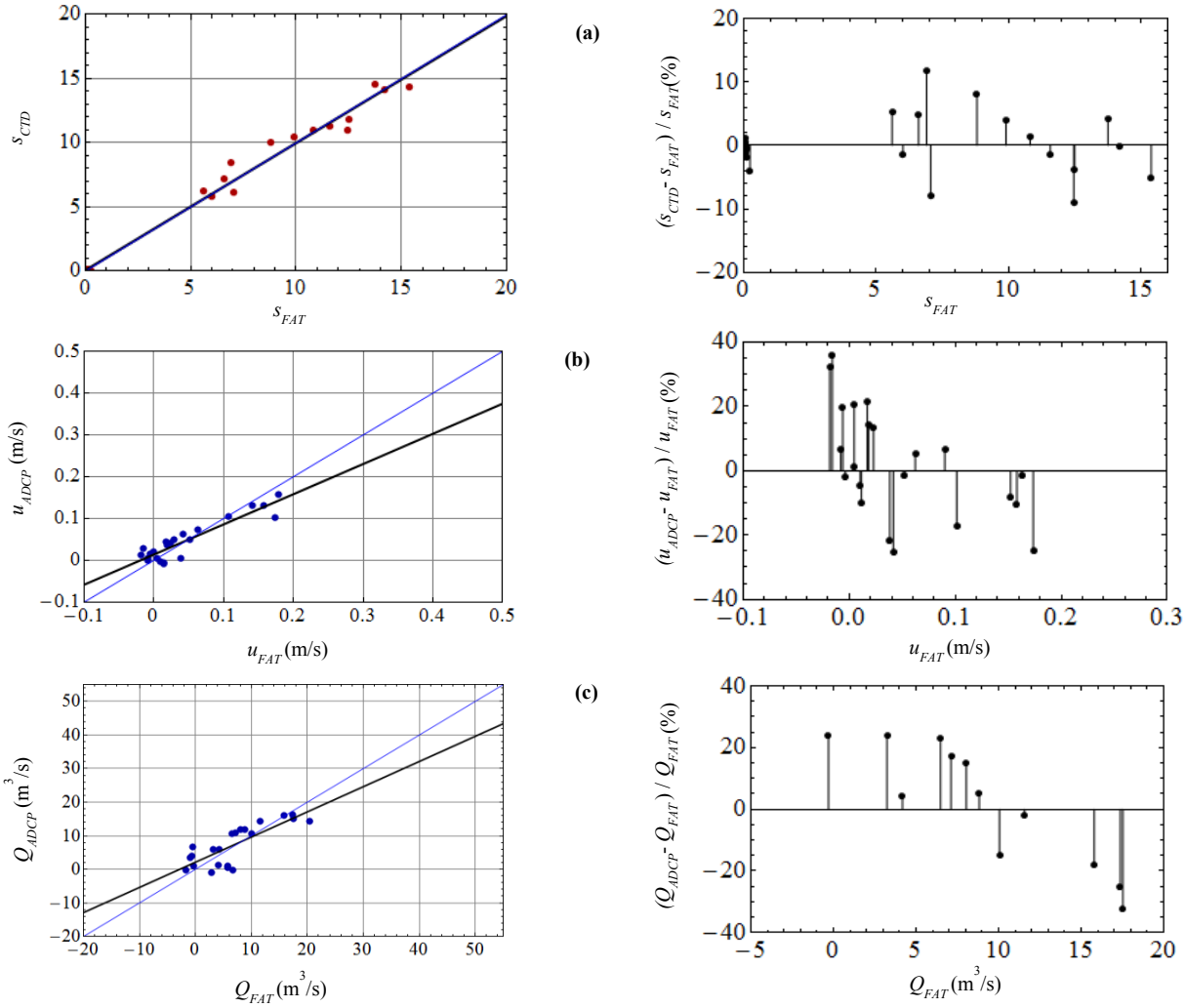

Fig 4.3 Relation between the cross-sectional averaged values and relative errors variations of: (a) salinity of FATS and compact CTD, (b) velocity of FATS and WHADCP and (c) discharge of FATS and WHADCP

observation site, the flow pattern varies with tidal phase (Figure 4.1). The second reason is the effect of the transversal circulation which is discussed in the next sections.

4.2.1.1. Surface and Bottom Salinity Variations

Figure 4.2.b indicates the temporal variations in surface, bottom and cross-sectional averaged salinity during the observation period. Stations 1 and 2 are located in front of the open sluice gate near the right bank, and Station 4 is located at the deepest region of

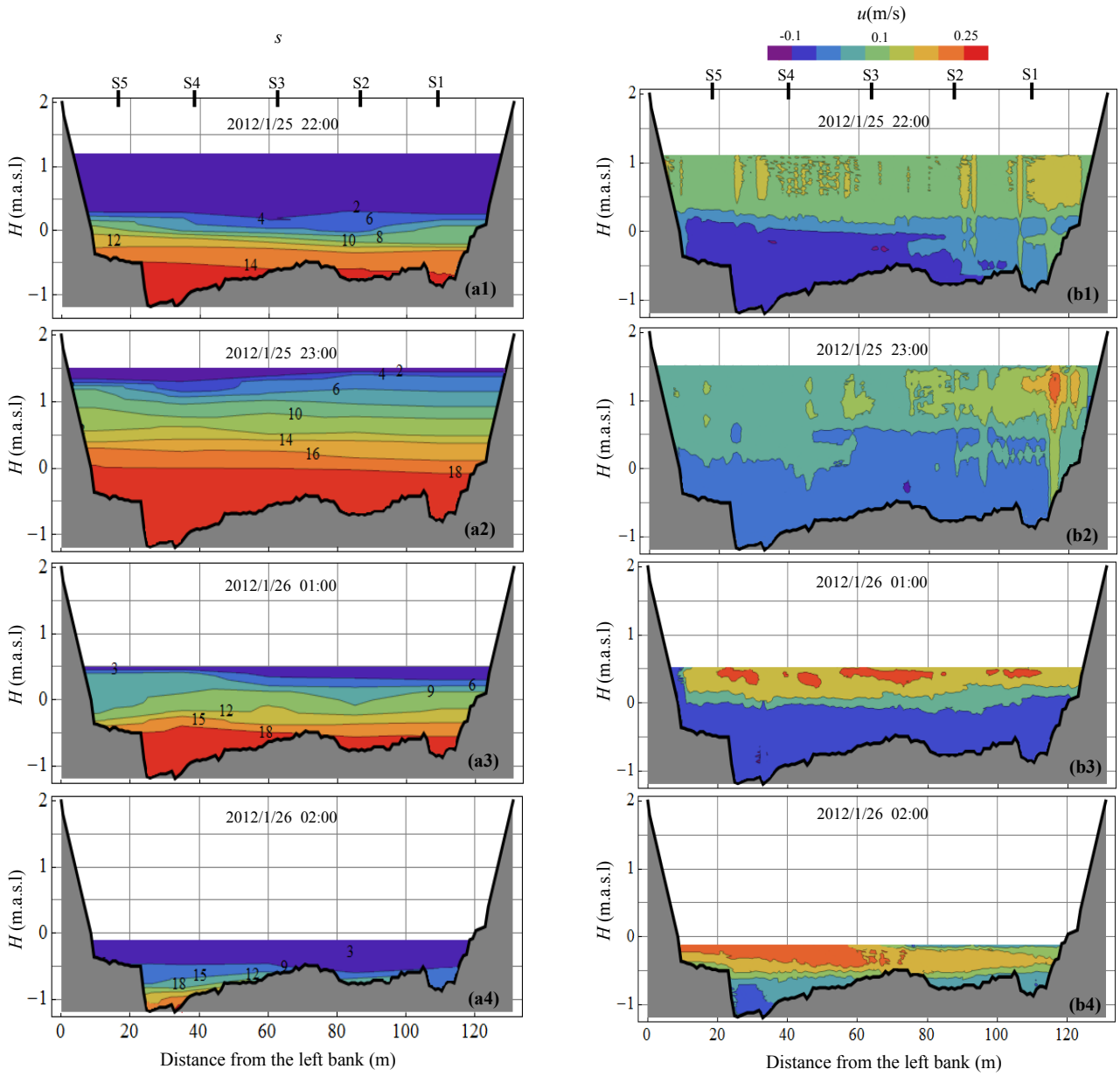

Fig 4.4 The cross-sectional counter plot of, (a) salinity and (b) velocity (m/s) during the second tide

the cross-section close to the left bank, respectively (Fig 4.1). In the Ota Diversion Channel, as in other tidal channels and estuaries, there are phase lags between the water level, velocity, and salinity. It is observed that at all stations the maximum bottom and surface salinities occurred after high water level. The increasing patterns of bottom

salinity at the stations were similar during the whole flood tides. However, during the ebb tides the saline water at the deepest region (S4) left from the cross-section around 30 min later than in shallower sections. The pattern of surface salinity variations at stations indicate an asymmetry and phase lag. The variability of surface salinities at S1 and S2 have similar pattern and there are similar conditions for S4 and S5.

The contour plots of the salinity and velocity at the cross-section of the ADCP path during the second tide are plotted in Figure 4.4. At hour 22, the current at the upper layers (0.25 m.a.s.l < z) was directed seaward by the highest velocity (0.11 m/s at the right bank). In contrast, in the lower layers, saline water was directed landward gradually at a velocity of around -0.15 m/s. At the high water (hour 23), the salinity distribution in the cross-section indicates a highly stratified condition. In this situation the velocity near the surface region of the right bank progressively developed to the left bank (Fig 4.4.b2). At hour 1, salinity had been developed throughout the cross-section, and a strong two-layer flow is seen. The bottom-top velocity difference (Δv) is larger than 0.29 m/s. Finally, at the end of ebb tide (hour 2), the core of the velocity contours moved to the left bank, and saltwater was limited at the deepest region of the cross-section.

4.2.1.2. Vertical Distribution of Salinity and Velocity

Simpson et al. (1990) proposed that the strength of stratification in an estuary is established primarily by the interaction of two competing mechanisms: the stratifying effects of tidal straining tending to increase stratification during ebbs, which decreases during floods, and the effects of tidal mixing that always decreases stratification. The gradient Richardson number is defined as:

$$R_i = -\frac{g}{\rho}\frac{\partial\rho/\partial z}{(\partial u/\partial z)^2} \tag{4.4}$$

where ρ is the density, g is the acceleration of gravity, u is the velocity, and z denotes the vertical coordinate. To characterize the stratification variations during a tidal cycle, a

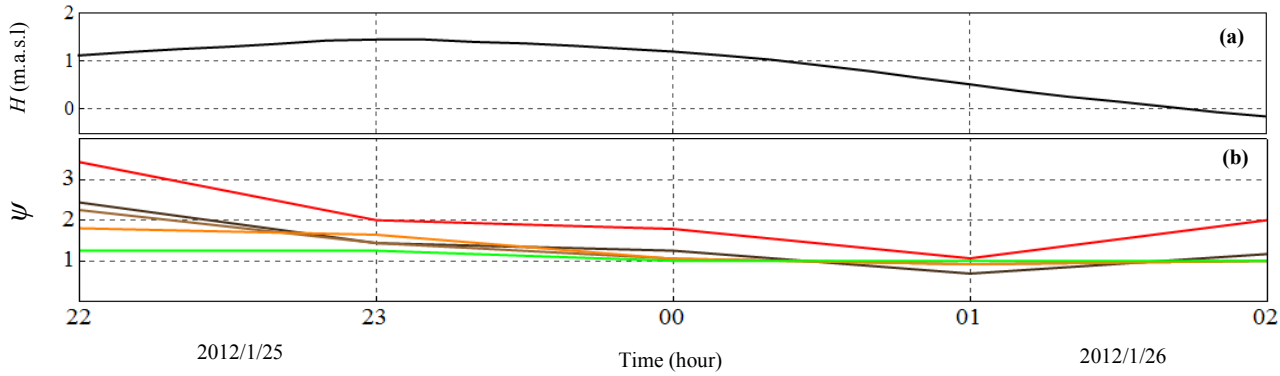

Fig4.5 Variations of: (a) water level and (b) stratification parameter at the station during the second tide, in this figure, S1 (green line), S2 (orang line), S3 (brown line), S4 (red line) and S5 (black line)

dimensionless representation of mixed layer thickness (MacDonald et al., 2008) was used as:

$$\psi = \frac{1}{2}\frac{h}{L_{50}}, \qquad L_{50} = h_{75} - h_{25} \tag{4.5}$$

where h represents the local water depth, and L_{50} is the vertical distance between the 75th (h_{75}) and 25th (h_{25}) percentiles of the cross-section depth (i.e., where salinities typically range from 0 to 30, and L_{50} at any location is the vertical distance between the 7 and 21 isohalines). The stratification parameter ψ, can be interpreted as a continuum from well-mixed conditions at ψ <1 to highly stratified conditions at ψ >1. The temporal change in the dimensionless stratification parameter can be related to the sum of the straining and mixing terms (MacDonald et al., 2008). The variation of ψ through the second tidal cycle at stations is presented in Figure 4.5.

The high stratification parameter of the all stations at the end of flood tides (hour 22) indicates highly stratified situation during the end of flood tide. Meanwhile, throughout the ebb tide, the stratification parameter ψ is gradually reducing and limit to a value of 1, indicating partially mixed situation at hour 1. At the deepest part of the cross-section (S4), this parameter is noticeably greater than the shallower section during the whole tide. The variations of ψ at the stations suggest that during the later portions of the flooding (after hour 22) the tidal mixing contributes both to decrease the stratification at the whole

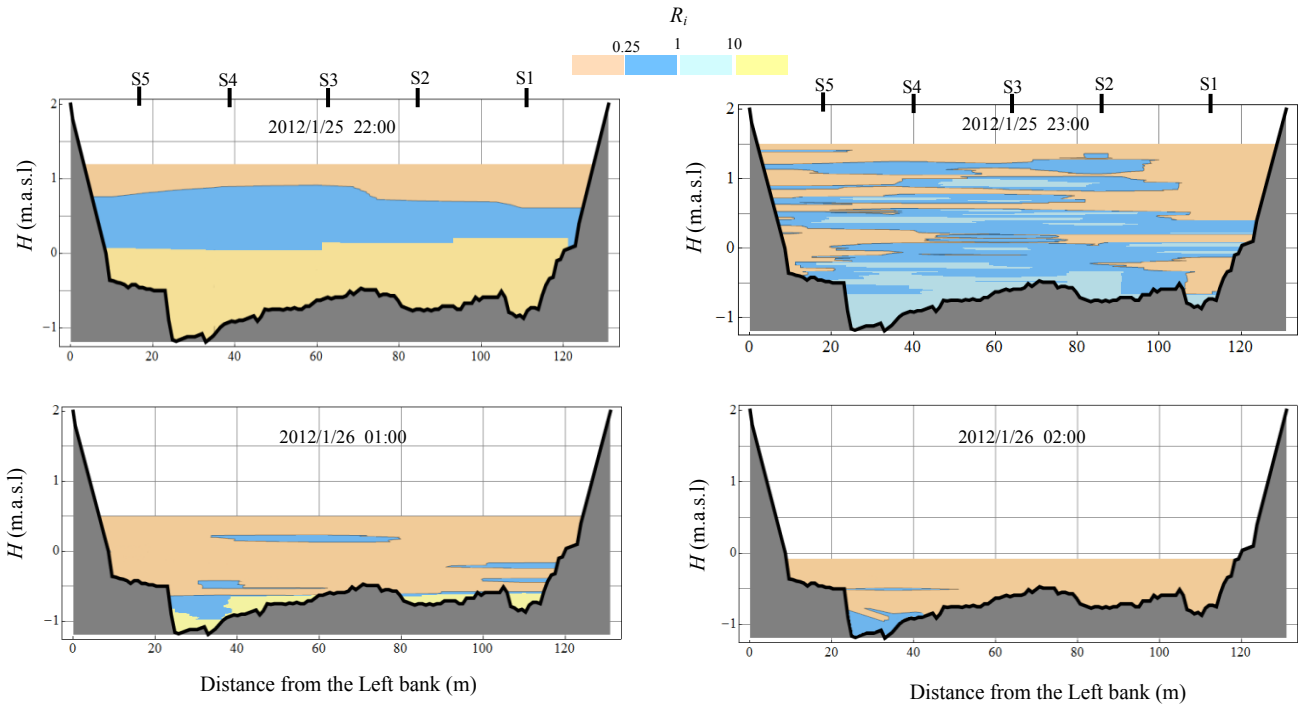

Fig 4.6 Cross-sectional distribution of Richardson number during the second tide

cross-section, and to depressing the stratification parameter to the minimum level at hour 1. Eventually, during the later portion of the ebb tide (after hour 1), the stratification was enhanced by the straining process.

The variation of Richardson number through the second tidal cycle is presented in Figure 4.6. At hour 22, there is a thick layer of freshwater sliding over the saline water. Then, $ds/dz < 0.5$ in the upper layer (Fig 4.4.a1). In the mid-depth of the channel ($z \approx 0$) the Richardson number is small. R_i tends to have large values at the lower layer due to increase in density and depression in velocity gradient. During the high water situation (hour 23), the low R_i region near the surface of the right bank is caused by the greater velocity gradients in this section. However, at the left side, the R_i is large. The temporal variation in the vertical salinity gradient at the whole cross-section is approximately equal, and so the variation in the structure of the velocity distribution at the cross-section has an important role in variation of the Richardson number. During the hours 1 and 2, the magnitude of R_i near the boundary layer of the upper seaward and the lower landward

flow (the depth ≈ 0.5h) vary around by 0.25. While in the near-bottom layer R_i significantly increases due to higher density and shows lower values of velocity gradient.

4.2.1.3. Variations in the Transversal Velocities and Vertical Shear flux

There are two methods for analyzing a series of salt flux measurements. In the first method it is assumed that the primary variations are in the transverse direction, and the transverse deviations are evaluated before the vertical ones. In the second method the vertical deviations are the primary variations (Fischer, 1972; Hughs and Rattray 1980; Uncles et al., 1990; Dyer et al., 1992). Based on this aspect, the partitioning of the shear effect can be considered as transverse and vertical component. Moreover the transverse contributions to the shear dispersion of salt are small in a highly-stratified estuary, whereas in partially-mixed estuaries the transverse and vertical shear contribution is comparable.

In this study, to consider the relative importance of the vertical and transversal shear components similar to that derived in equations (2.33) and (2.34), the instantaneous velocity and salinity are decomposed to a depth-averaged mean, and the vertical and transversal deviation component as:

$$u = \bar{u} + u' + u_t \tag{4.6.a}$$

$$s = \bar{s} + s' + s_t \tag{4.6.b}$$

where the overbar and prime denote are the depth-averaged mean and vertical deviation component, respectively; and index t for the velocity and the salinity shows transversal deviation component. The intratidal salinity transport flux can be estimated as:

$$F = \int_0^T \int_0^h usdz = \int_0^T \int_0^h (\bar{u} + u' + u_t)(\bar{s} + s' + s_t)dz \cong \bar{u}\bar{s}\bar{h} + \overline{u's'}\bar{h} + \overline{u_t s_t}\bar{h} \tag{4.7}$$

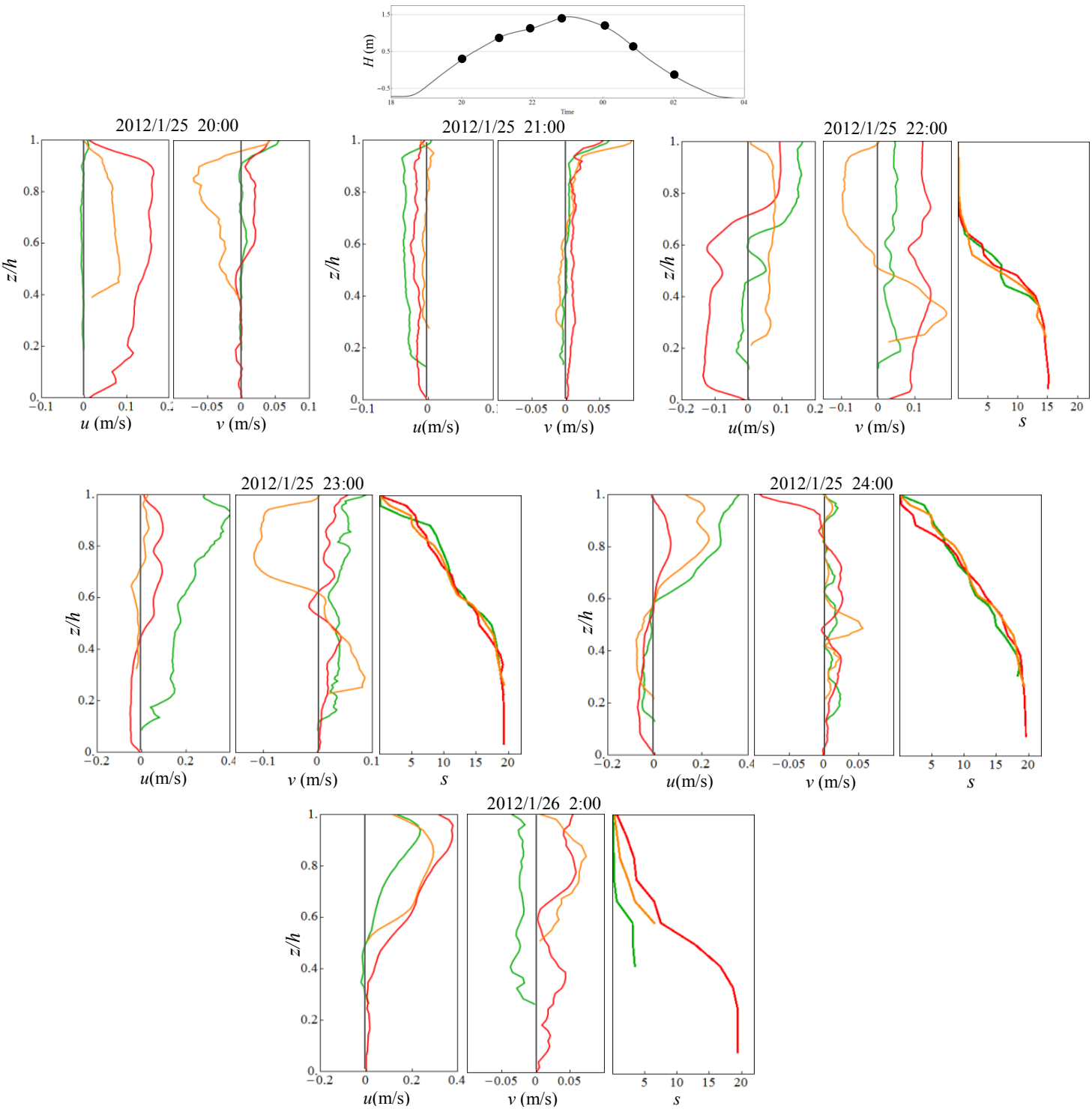

Fig 4.7 Vertical profile of the longitudinal and transversal velocities, and salinity at the cross-section estimated by CTD profiler and WHADCP results, S1 (green line), S3 (orange line), S4 (red line)

The data series was only for three tides. Therefore the salt flux was estimated for an

hourly period (T=1 hour). Figure 4.7 shows the vertical profiles of the velocities and the salinity at S1, S3, and S4 during the second tidal cycle. In this figure the longitudinal (u) and transversal (v) components of the velocities at all the stations were estimated based on the X-Y coordinates in Fig 4.1. At hour 20, the profile of the longitudinal velocity at the deepest region (S4) shows the seaward movement of water throughout the water column, having a maximum value at near the surface of 0.17 m/s at the near surface. Meanwhile, at the shallowest part (S1) the velocity is almost zero. At hour 21, the velocity is completely directed landward at the whole of the cross-section, and the flood current is enhanced in the deepest region during the last portion of flood tides (hour 22). The contribution of the transversal components of the velocity is noticeably increased during the last portion of the flood tide (hours 22 and 23). As can be seen, the transversal component of the velocity at the center area of the cross-section (S3) reaches to the highest variations near the surface and the bottom region of the water column. This result suggests that the upward flow has a tendency to deviate towards the right side of the channel (the front of the open sluice gate), especially in the deepest region of the study site (S4). Finally, at the high water situation (hour 23) the seaward flow is reinforced at the shallowest region. After that, the seaward flow at the upper layer of the water column is moved into the deepest section. At the end portion of the ebb tide the seaward flow reaches to the maximum level at this part. However, at the lower layer of the water column the velocity are significantly diminished. These sequences suggest that the transversal variation in the velocity is significantly important at the study site which is caused by the effect of the local bathymetry condition and the vertical shear term due to the gravitational circulation.

The variations in the salinity profiles indicate that the vertical salinity gradient $\partial s/\partial z$ is noticeably greater than the transversal salinity gradient $\partial s/\partial y$. These results suggest that the transversal shear components are likely negligible, and the vertical deviations are the primary variations for both salinity and velocity variations. Rattray and Doworski (1980)

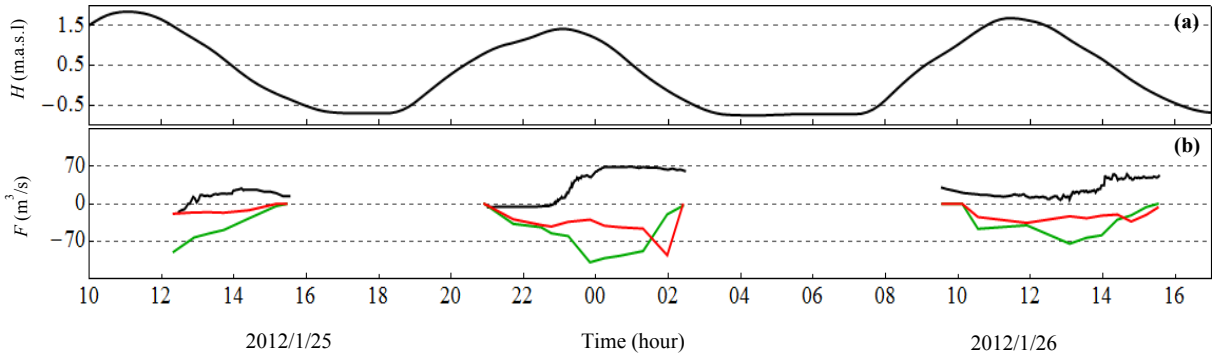

Fig 4.8 Time series of: (a) water level at the Gion; (b) salt fluxes estimated by CTD profiler and WHADCP results, advective term, (black line), vertical shear flux at S1 (green line) and shear flux at S4 (red line).

found that the transverse shear dispersion was very small in the narrow section near the head (width less than 200 m), but was comparable with the vertical shear fluxes at the widest section (width about 800 m). Uncles et al. (1985) reported that the contribution of the transversal shear components was negligible at the upstream region of their site study. The present results indicate that the correlation between velocity and salinity variations along the vertical coordinate is noticeably greater than their transverse correlations at the Gion Station.

In Figure 4.8, the variation of advection and the vertical shear flux which are estimated based on Eq. (4.7) are presented. The advection and shear terms are estimated using the ADCP and the Compact CTD data. The results indicate that the vertical shear flux at both stations directed landward during the observation period, and the contribution of this component is noticeable, compared with the advection term. In addition there was a significant difference between the variation in vertical shear components at the deepest and shallowest sections. As discussed before (Figs 4.4 and 4.7), during the first half of flooding tide, there was upstream directed flow only in the right part of the channel. Then the maximum vertical shear term was occurred at the S1 (Fig 4.7. b, green line) due to larger bottom-top velocity difference at this section. As can be seen, this term reached to the highest level at S1 with the value of -0.74 m^2/s around hour 24. However, in the last portion of ebb tides, the bottom-top velocity and salinity

differences were reinforced at the deepest section (Figs 4.4 and 4.7). Therefore, the highest shear term in this section was occurred during the last portion of ebb tides.

4.2.2. Subtidal Variations

The time series of freshwater discharge at the Yaguchi station, the water level variation at the Kusatsu Station, the salinity and temperature at the Gion and Asahi Bridges are plotted in Figure 4.9. The salinity at the Asahi Bridge was measured using 5 CT sensors at different levels. As mentioned earlier the cross-sectional averaged salinity at the Gion Bridge has been measured using FATS. Annual cycles in estuaries are driven by cyclic variations in energy sources such as freshwater discharge, tides and winds.

Freshwater inflow plays a major role in the salinity and net flushing of estuaries. Increasing in freshwater inflow can change the characteristics of an estuary from well-mixed to partially mixed or stratified. Freshwater inflow varies primarily on seasonal scales, but floods can increase the freshwater discharge into an estuary within a short period of time. Large river flow or weak tidal mixing can lead to vertical stratification. The effect of freshwater runoff on the salinity variation in Ota Estuary is a consequence of two features that may be partly specific to this estuary. First feature is the effect of the seasonal flood event during June and July (e.g., Jun 2009, July 2011). As mentioned for discharge over 400 m^3/s at the Yaguchi Station, all sluice gates of Gion are completely opened. For example during the flood events in June and July 2010 the estuary flushed out much of its salinity (Fig 4.9.e). The results indicated after 1.5 months (45 days) the observed salinity at the Gion Bridge returned to the levels observed in June 2010. Second feature, is the relatively wet and dry seasons. During the dry season the discharge of Yaguchi Station is less than 50 m3/s (e.g., autumn 2009 and 2010). However, during the wet season the freshwater discharge at Yaguchi Station is gradually increased (Fig 4.9.b). Consequently the average discharge exceeded 80 m3/s (e.g., March and April 2009 and 2012).

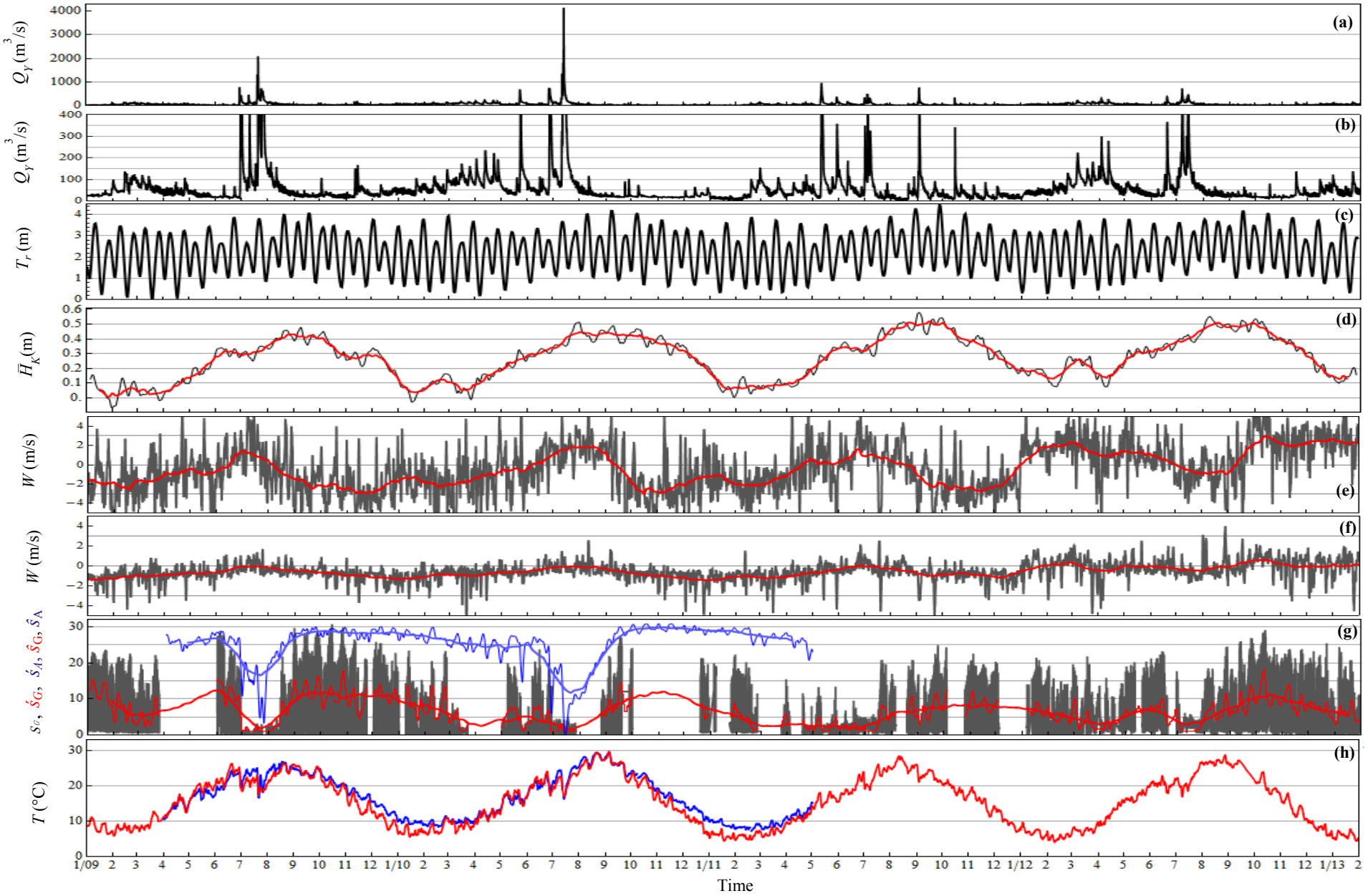

Fig 4.9 Time series of: (a) and (b) Freshwater discharge at the Yaguchi Station; (c) Tidal range at the mouth (Kusetso Station); (d) Sea level, fortnightly averaged (black line) and seasonal variations (red line); (e) and (f) Wind speed along and across the major axis of estuary (SW-NE),respectively, in this figures, daily averaged (gray line) and seasonal averaged (red line); (g) Cross-sectional averaged salinity variations at the Gion Bridge, temporal fluctuations (black line, s_ϕ), daily averaged (red thin line, $\acute{s}_G$), seasonal averaged (red thick line, $\hat{s}_G$), also the thin and thick blue line denotes the daily, $\acute{s}_A$ and seasonal $\hat{s}_A$ averaged salinity variations at the Asahi Bridge; (h) Daily averaged water temperature at the Gion (red line) and Asahi Bridges (blue line). The cross-sectional averaged salinity at the Gion was estimated by the FATS and the depth-averaged salinity at the Asahi was estimated from CTs

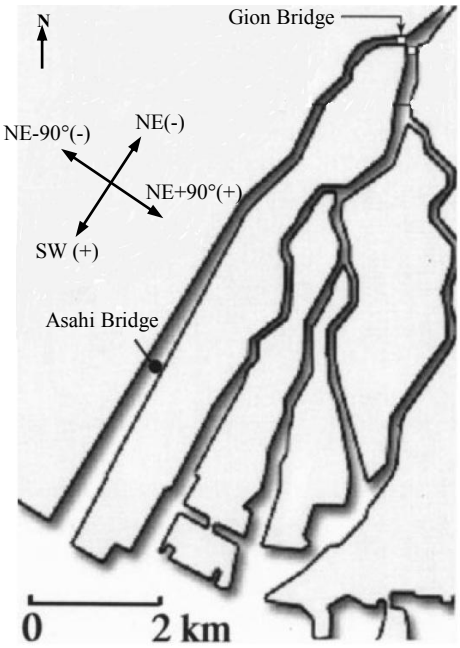

Fig 4.10 The major wind components at the Ota Estuary

Table 4.2 Standardized partial multiple regression coefficients for salinity variations at the Gion and Asahi Bridges

Subtidal salinity components	Coefficients of Regression					
	α	β	γ	θ	ε	R^2
s_{G3}	-0.42	-0.06	0.24	-0.18	-	0.54
s_{G45}	-0.61	-	0.26	-0.21	-	0.76
s_{A3}	-0.35	-0.04	0.49	-0.46	-	0.54
s_{A45}	-0.41	-0.01	0.63	-0.60	-	0.54

Variability of tides is another major source for the tidal-driven mechanisms (e.g., tidal pumping) in the estuaries. The tidal range at the mouth of estuary is mostly ranged from

0.3 to 4 m (Fig.4.9.c). The highest mean sea-levels occur in September and October while lowest levels occur in January and February (Fig.4.9.d). The spring-neap tidal cycles and seasonal variations significantly influence the tidal velocity and vertical mixing. In addition to the tides and freshwater inflow, transport and mixing processes in an estuary can also be affected significantly by wind. Wind-induced circulation is transient and interacts with estuarine geometry to produce various circulation patterns. In shallow estuaries, wind stress can dominate transport and produce energy to vertically mix the water column. In contrast to tidally induced vertical mixing that is produced by bottom friction and propagates upward, wind-induced vertical mixing is produced on the water interface and propagates downward. Figures 4.9. (e, f) show the daily averaged and seasonal component of the wind speed along (SW-NE) and across the Ota Diversion Channel. The sign of the wind components are shown in Figurer 4.10. The variation of the daily mean water temperate at the Gion and Asahi Bridges are plotted in Figure 4.9.h. The results indicate an annual cycle in temperature, with maximum temperatures in summer (September and October) and minimum temperatures in winter, respectively. The difference between the water temperature at the Asahi and Gion Bridges increases during the winter. The reason for this issue can be related to the larger difference between the temperature of freshwater and saltwater during the winter.

To quantify the relative effect of main forces on the salinity variations at the Asahi and Gion Bridge multiple-regression analysis is employed. The regression equation is:

$$\bar{s} = \alpha Q_Y + \beta T_r + \gamma H_m + \theta W + \varepsilon \tag{4.8}$$

where, $\bar{s}$ is fluctuations of salinity, Q_Y is the freshwater discharge at the Yaguchi station, T_r is tidal range at the mouth of the estuary (Kusetso Satation), H_m is mean sea level and W is wind speed. The wind in the SW directions is associated with positive signs (Fig 4.10). In Table 4.2 the coefficients of standardized partial correlation are presented. The index 3 and 45 denote 3 days averaged and 45 days averaged salinity variations,

respectively (The time scales was selected based on the spectral analysis of salinity variation at the Gion Station). It is found that the freshwater discharge of Yaguchi Station, tidal range and wind all depress the salinity in both Stations (Gion and Asahi). Meanwhile, increasing the mean see level enhances the salinity intrusion in the estuary. The influence of changes in freshwater discharge is greater than the other variables at the upstream section (Gion) of the estuary. However, the effect of the mean sea level and wind on the seasonal variability of the salinity is noticeably important at the Asahi Bridge.

Comparing with other forces, the effect of the wind on the salinity variation especially at the Asahi Bridge is noticeable and also the wind speed along the Ota Diversion Channel is significantly larger than the across-shore component (Fig 4.9.e, f). These results suggest that the freshwater plays an important role in the subtidal variations of the salinity at the upstream sections of the estuary. However, the variations in mean sea level and wind primarily control salinity variations and the mixing process at the downstream sections (Soltaniasl et al. 2012b); Kawanisi et al. 2011).

4.3. Estimation of the Flushing Time and Salt Flux using FATS

4.3.1. Determining the Flushing Time in the Ota Diversion Channel using Freshwater Fraction Method

As discussed in section 2.51 the flushing time of an estuary is defined as the time required to replace the existing freshwater in the whole or a segment of the estuary at a rate equal to river discharge. In this study the flushing time in the Ota Diversion Channel is estimated using an empirical formula based on Dyer's method to evaluate the dependence of flushing times on both river discharge and the variation of salinity concentration. Therefore, the flushing time of the estuary can be calculated as:

$$T_f = \frac{V_f}{Q_R} = \frac{V}{Q_R}\left(1 - \frac{s_m}{s_0}\right) \tag{4.9}$$

where, s_0 is the seawater salinity or reference salinity, V is the estuary volume, V_f is the fr eshwater volume, and s_m is the spatial mean salinity in the estuary. The spatial mean salinity of the estuary and the rate of freshwater can be estimated as:

$$s_m = \frac{1}{V}\int sdV \tag{4.10}$$

and

$$Q_R = Q(\frac{s_0 - s}{s_0}) \tag{4.11}$$

here, $Q(\mathrm{m}^3/\mathrm{s})$ and s are the observed discharge and salinity in the Gion Station (FATS results), respectively. The mean salinity in the estuaries depends on the salinity distribution over the estuary. In this study a method based on spatial variation of salinity, featuring the flushing number technique suggested by (Arnos et al., 1951) is used to estimate the spatial salinity distribution throughout the Ota Diversion Channel, specifically:

$$s(x) = s_0 \exp\left[F\left(1 - \frac{L}{x}\right)\right] \tag{4.12}$$

where, F is the flushing number (dimensional less), L (m) is the length of the tidal compartment, and x is the longitudinal distance. F is the function of the river discharge, the mean depth, the eddy diffusivity, and the tidal range (Arnos et al, 1951). Because these parameters are not available, instead of using direct estimation, we calibrated the amount of F using observed salinities in the Gion station as:

$$F = \frac{\ln s - \ln s_0}{1 - L/x_G} \tag{4.13}$$

where, x_G is the position of Gion Bridge. Therefore, based on Eqs. (4.10), (4.12) and (4.13), the mean salinity along the Ota Diversion Channel is calculated as:

$$s_m = \frac{1}{L}\int_{x_G}^{L} s_0 \exp(F(t)(1-\frac{L}{x}))dx \tag{4.14}$$

Finally, Eq. (4.9) and Eq. (4.14) result in a new form of Eq. (11) as:

$$T_f = \frac{V_f}{Q_R} = \frac{V}{Q(1-\frac{s}{s_0})}\left(1-\frac{\frac{1}{L}\int_{x_G}^{L} s_0 \exp(L(t)(1-\frac{L}{x}))dx}{s_0}\right) \tag{4.15}$$

For estuarine flushing time analyses in unsteady flow and tidal conditions, researchers usually use weekly or monthly averaging techniques. In this study, the flushing times for the Ota Diversion Channel were calculated using the tidally averaged salinity and discharge over 14 tidal cycles (7 days).

4.3.2. Variability of the Longitudinal Salt fluxes at the Gion Station

The advective and dispersive salt fluxes were estimated using Eq. (2.36) at the Gion Station. In this study, to investigate the long-time variability in salinity transport the variations of the salt fluxes and flushing time during dry (August 15 to November 15, 2009) and wet (December 5, 2009 to March 15, 2010) seasons were investigated. The results during the first periods are presented in Fig 4.11. In these periods, the freshwater discharge at the Yaguchi Station is mostly less than 50 m^3/s and the salinity vary between 0 and 25 at the Gion Station. The temporal salinity fluctuations at the Gion Station were noticeably followed the spring-neap tidal cycles (Figs 4.11. c), but also the salinity was decreased during the high freshwater discharge at the Yaguchi Station (e.g., between

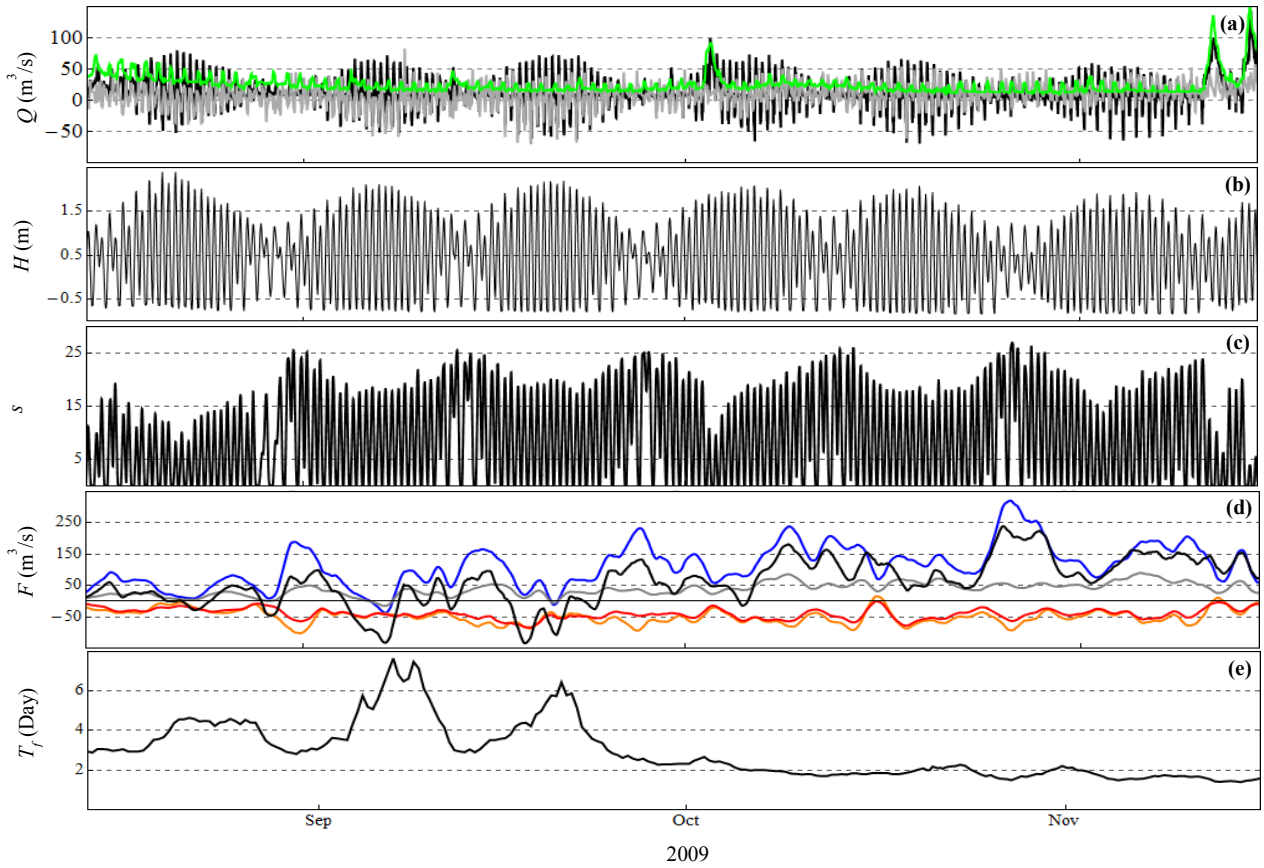

Fig 4.11 Variations of (a) temporal discharge in the Yaguchi Station (green line), Oshiba Gate (black line) and in the Gion Station (gray line); (b) temporal water level at the Gion Station; (c) temporal salinity variation at the Gion Station; (d) salt fluxes, advective term (blue line), tidal trapping term (gray line), tidal pumping term (orange line), sloshing term (red line); total salt flux, $F_1+F_2+F_3+F_4$ (black line); (e) flushing time

October 2 and November 13). The salinity values during the neap tides are larger than that for spring tides. It results from the difference of tidal mixing, namely stronger tidal mixing (larger vertical eddy viscosity) for spring tide damps down the salt intrusion.

In the first period the advection term (F_1) is mostly seaward. It generally follows the characteristics of the spring-neap tides and reaches the peak value during the neap tides. However, it is also modulated by the variation of the freshwater runoff. Tidal sloshing flux (F_2), which has the significant contribution between the dispersive terms always act to bring salt into the estuary. This flux directed landward among first period. However, it was depressed by the flood events. This flux followed the fluctuations of the tidal range

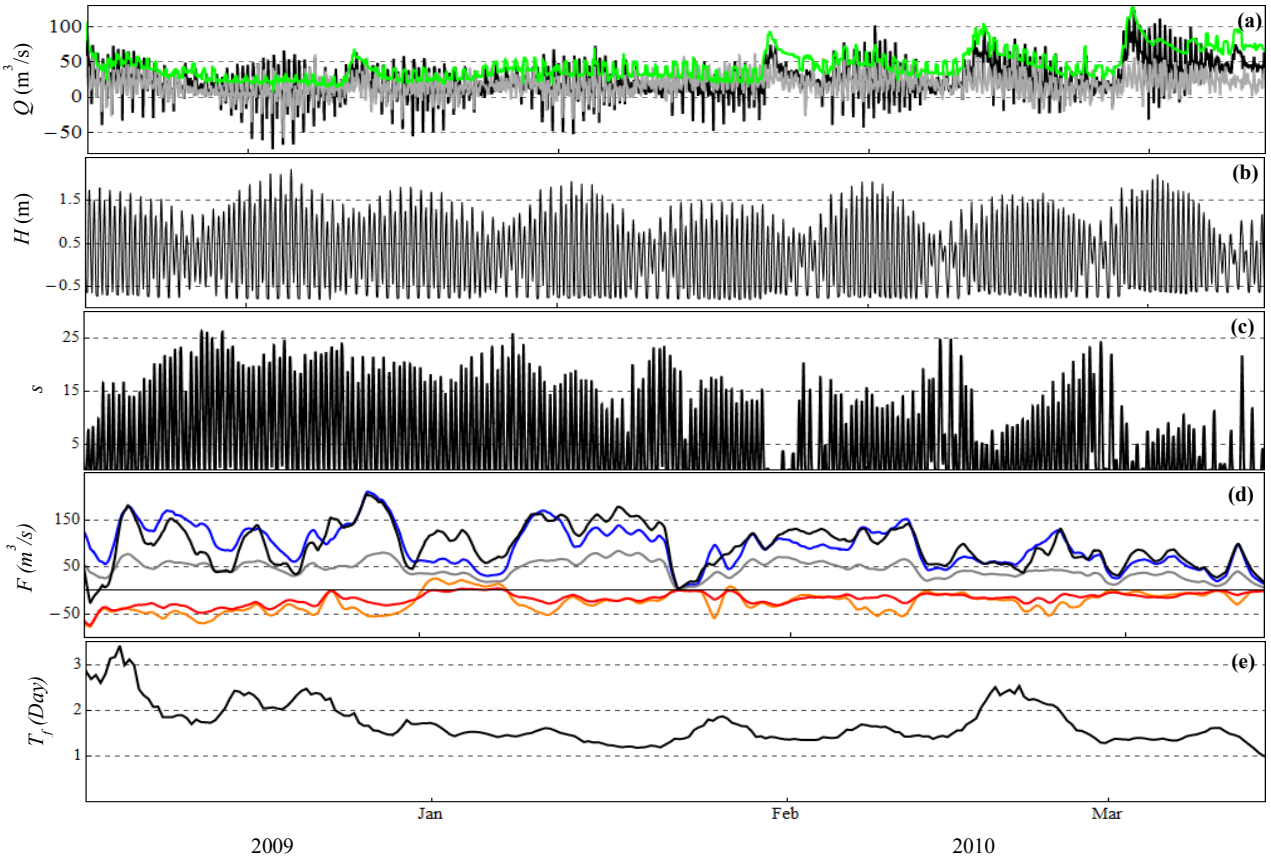

Fig 4.12 Variations of (a) temporal discharge in the Yaguchi Station (green line), Oshiba Gate (black line) and in the Gion Station (gray line); (b) temporal water level at the Gion Station; (c) temporal salinity variation at the Gion Station; (d) salt fluxes, advective term (blue line), tidal trapping term (gray line), tidal pumping term (orange line), sloshing term (red line); total salt flux, $F_1+F_2+F_3+F_4$, (black line); (e) flushing time

(spring-neap cycle) and reaches the highest level during the neap tides (e.g. September 1). Flux 3 (tidal trapping) could be significant due to topographic and bathymetric features. This flux is always directed seaward following the same trend of the advective component.

The Stokes' drift dispersion flux (F_4) is directed upstream, thus pushing water into the estuary. Thus the fluxes 1 and 3 are the substantial seaward salt fluxes, whereas, flux 2 and 4 are the most significant mechanisms of upstream salt transport during the first period. The results during the second period are presented in Fig 4.12. In this period, the

freshwater discharge at Yaguchi Station gradually increases. The average discharge is around 50 m^3/s during December 2011 and January 2012 while it exceeds 80 m^3/s over February and March 2012. The salinity variations follow the characteristics of the spring-neap tides. However, it is depressed during freshwater discharge rising periods (March 2012). The advection flux (F_1) is the dominant flux between December 2011 and January 2012, whereas this term is depressed due to the salinity decreasing during February and March 2012. Tidal sloshing fluxe (F_2) follows the spring-neap cycle and reaches to the highest level during neap tides. The tidal pumping flux (F_4) was decreased gradually among the period and is the smallest contributor during the last portion of the second period.

4.3.3. Variability of Flushing Time in the Ota Diversion Channel

Estimated flushing time based on Eq. (4.15) is plotted in (Figs 4.11.e and 4.12.e). In general, flushing time decreases with the increase in freshwater inputs. The maximum flushing time is about 8 days while the minimum is less than 1 day during the peak event (July 2009). We can divide the flushing time variations into three periods. The first period, is during the flood events (July 2009). In this situation, the salinity at the observation site is flushed out for about 1.5 months (Soltaniasl et al, 2011). The second period starts from the middle of August and lasted until the October. As mentioned before, during this period the salinity was in the highest level due to low freshwater discharge and an increase in the mean sea levels. Finally, in the rest of months the flushing time follows the variability of mean salinity fluctuations.

The fluctuations of the flushing time are plotted versus the daily averaged freshwater discharge at the Yaguchi Station, tidal range and wind speed in Fig 4.13. As it can be seen, the flushing time of the Ota Diversion Channel is quite sensitive to the freshwater discharge variations. Statistically, the best fit to the data is obtained with a power-law

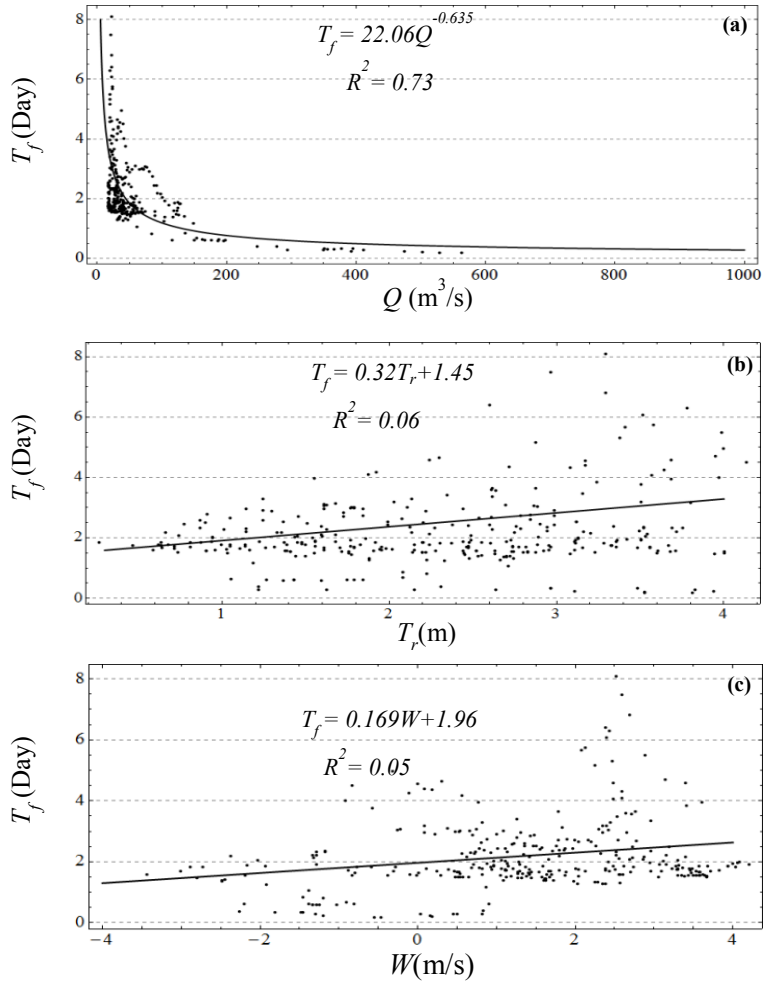

Fig.4.13 Power-law function between flushing time and freshwater discharge of the Yaguchi Station, (b) linear function between flushing time and tidal range fluctuations, and (c) linear function between flushing time and wind speed and directions

function. The noticeable correlation between the flushing time and wind, and tidal range are not found (Soltaniasl et al. 2012c).

4.3.4. Relation between the Flushing Time and Salt Flux

The results indicate that the flushing time is relatively short at the Ota Diversion Channel, ranging from about 8 days at low freshwater discharge at the Yaguchi Station to less than one day at the high flood events. Generally, in the tidally-dominated estuaries such as Ota Diversion Channel, tide exerts great influence on the salinity transport

process. The maximum flushing time in the Ota Diversion Channel occurred in September 2009, when the upstream freshwater discharge was low and the mean sea level reached the highest levels. In this condition, the advective flux was directed landward due to higher correlation between the water level, salinity, and velocity. So the flushing time was dramatically increased. This result suggests that the variation in the flushing time at the Ota Diversion Channel is largely controlled by the advection mechanism contributed by freshwater discharge and the longitudinal dispersion process as a result of tidal forcing.

4.4. Variability of the Salinity and Discharge at the Ota Bifurcation and Main Branches

The Ota estuary is a multi-channel estuary with two main branches (Old Ota River and Ota Diversion Channel). Due to different adjustments at the Gion and Oshiba Gates, the inflow discharge to these two branches is different. As well the difference in the water discharge and topographical features can cause different salt intrusion mechanism in the Ota main branches. We will consider this issue using the data measured at these two branches.

Data sources:

Three sets of data are used in our analysis: 1) Discharge estimation at the Oshiba Gate for the period from June 2009 to April 2010 using three acoustic Doppler current profilers (ADCPs) which was installed at the Oshiba Gate; 2) Discharge estimates at the Gion Bridge and upstream section of the bifurcation. The measurements were conducted using two couples of FATS from November 2011 to December 2012; and 3) Salinity, temperature and water level fluctuation were observed every 10 minutes at the Oshiba Flood-Gate using CTD Diver logger from November 2011 to February 2012.

Figure 4.14 shows the details of the observation site. The time series of discharge variations at Oshiba Gate, Gion Station and Yaguch Station are plotted in Fig. 4.15.a. The

Fig 4.14 Details of FATS measurement sections (Gion and CD Stations)

discharge of the Ota River comprises of the major source of freshwater for the estuary. As it can be seen, there is a significant correlation between the discharge of Oshiba Gate and Yaguchi Station. Fig. 4.15.b shows the relation of the daily-averaged discharge at the Yaguchi Station versus the Gion and Oshina branches. The correlation of the daily averaged discharge between the Yaguchi Station and the Oshiba is greater than the Gion discharge. Also, the variation of the salinity at the FATS Stations and Oshiba Gate are plotted in Fig 4.16.b. The salinity fluctuation at the Gion Station is significantly controlled by the tides. The amounts of the salinity during the spring tides are decreased due to the stronger tidal mixing that damps down the salt intrusion. The salinity variation at the upstream section (CD Station) and Oshiba Gate is strongly modulated by the upstream freshwater discharge. As mentioned before the inflow discharge at the Gion Gate is about 10-20% of the total flow rate of the Ota River on normal days. Therefore, during the flood events the salinity intrusion at the Oshiba Gate is significantly depressed. Unfortunately, in the absence of salinity measurements throughout Old Ota River Branch, it is difficult to discuss about the variability of salinity intrusion length.

Fig 4.17.a shows the ratio between the temporal water discharge at the FATS station and the Yaguchi Station. Also, the relation between the daily averaged discharge at the

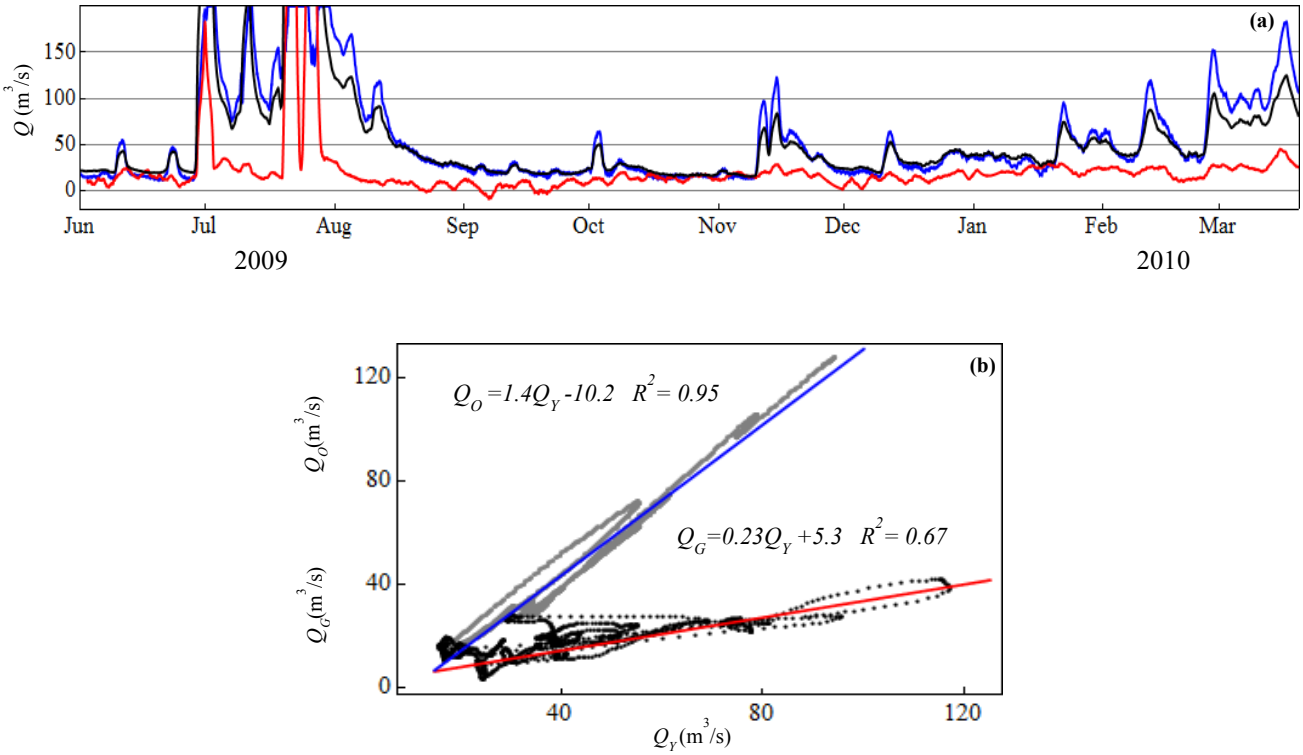

Fig 4.15 (a) Variations of daily averaged discharge at the Yaguchi Station (black line), at the Oshiba (blue line) and at the Gion (red line); (b) Relations between the daily-averaged discharge at the Yaguchi Station and Ota main branches (Oshiba and Gion)

FATS stations and Yaguchi Station are presented in Fig 4.17.b**.** During the low flows, the discharge ratio at the Gion Station varies ranging from -21% to 45% due to the tide effect. However, during the high freshwater discharge at the Yaguchi Station, the discharge ratio is close to 20%.

Fig 4.17.c shows the tidally-averaged salinity variation versus the Yaguchi discharge in the main branches. Generally the salinity variation at both branches can be described as a power-law of upstream freshwater discharge. The exponents -0.53 and -3.86 at the Gion and Oshiba show that the salt intrusion in the Oshiba branch is completely sensitive to change in upstream freshwater discharge (Soltaniasl et al. 2013). These results indicate significant differences between the salt intrusion variations at the Ota main branches. Fig 4.16.(d, e) indicate the variation in the salt fluxes at the FATS stations. During the whole

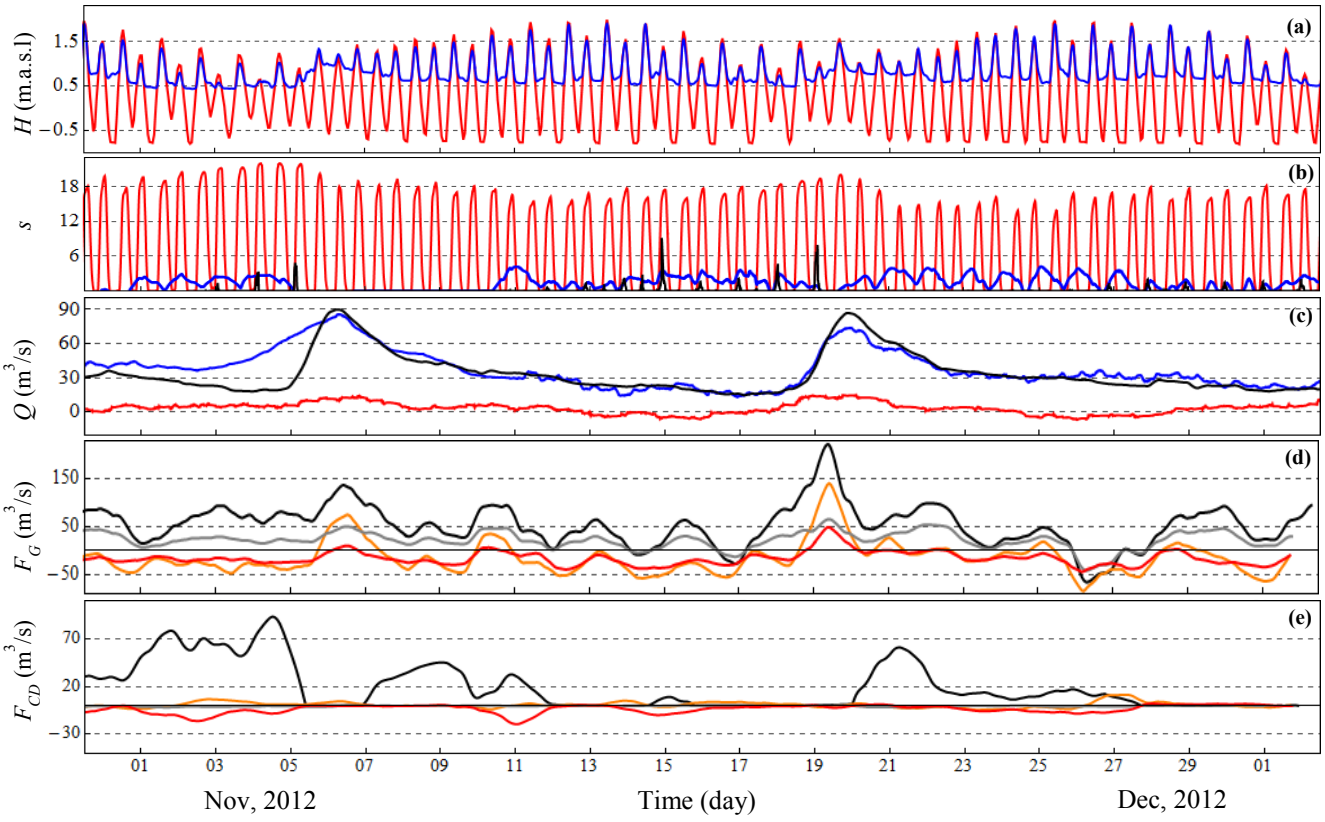

Fig 4.16 Time series of: (a) water level at the Gion Station (red line), at the CD Station (blue line); (b) salinity at the Gion (red line) at the Oshiba Gate (black line), at the CD Station (blue line); (c) water discharge at the Yaguchi Station (black line), at the Gion Station (red line), at the CD Station (blue line); (d)salt fluxes at the Gion Station; (e) salt fluxes at the CD Station, advective term (black line), tidal trapping term (gray line), tidal sloshing term (orange line), tidal pumping term (red line).

observation period the advection components at both stations are mostly seaward and also, are modulated by the variations of the upstream freshwater discharge. The advection flux at the CD Station is mostly due to the river discharge. The salinity variations at the Oshiba Gate and CD Station are sensitive to the upstream freshwater discharge (Fig 4.16.b). However, the advective and dispersive fluxes generally follow the characteristics of spring-neap tidal cycle at the Gion Station.

Tidal sloshing F_2 and tidal pumping F_4 fluxes always act to bring salt into the upstream section. Except the flood events, these fluxes directed landward over the observation period at the Gion Station. However, at the CD Station only the tidal pumping shows the

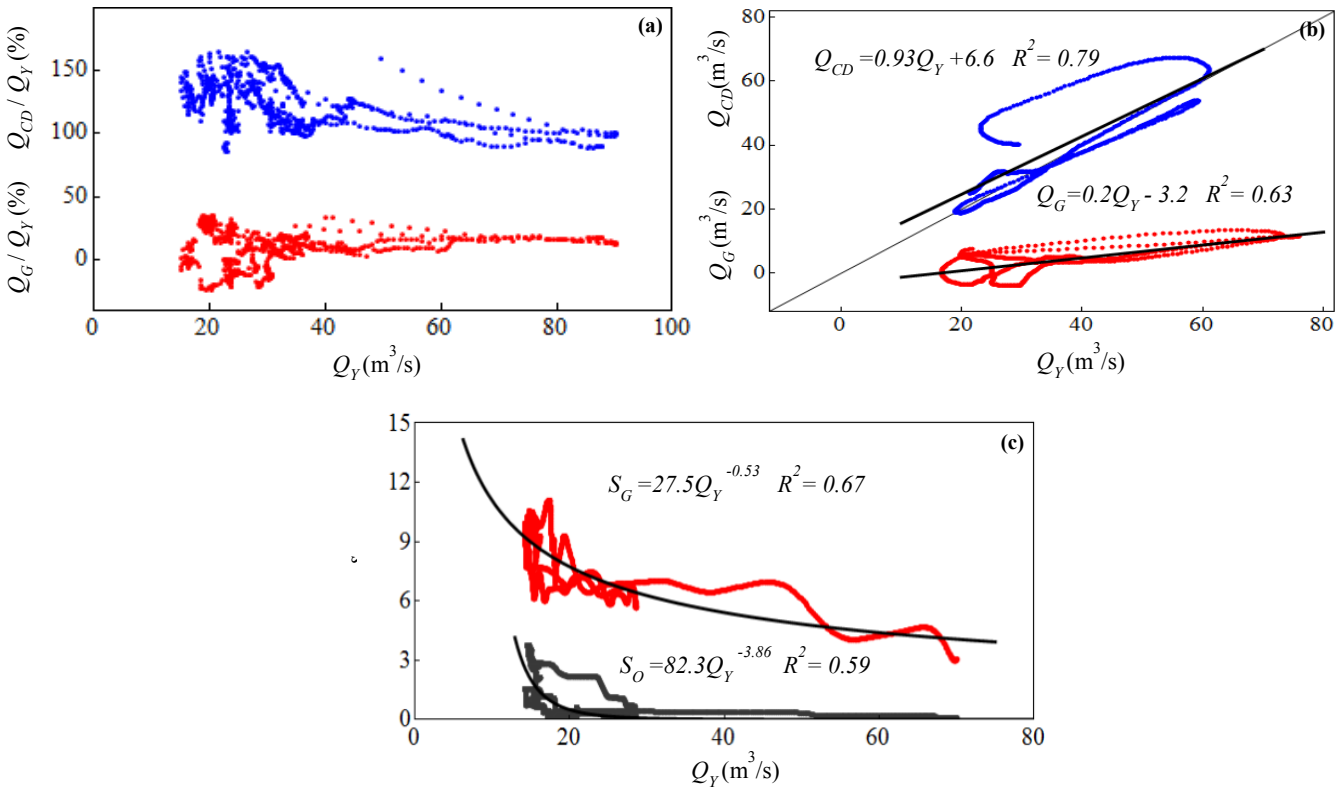

Fig 4.17 (a) The relations between the temporal discharges of FATS and Yaguchi Stations; red disks (Gion station) and blue disks (CD station); (b) Relation between the freshwater discharge at the Yaguchi Station) and FATS discharge at the stations (Gion and CD); (c) Relation between the upstream freshwater discharge (Yaguchi Station) and daily-averaged salinity variations at the Gion and Oshiba Branches

significant contribution to intrude the saltwater beyond the CD station during the spring tides.

The sloshing effect is caused via triple correlation between tidal depth, tidal current, and tidal salinity changes. So the main reasons for the low amounts of the sloshing effect comparing to the tidal pumping at the CD Station is related to the low correlation between the tidal velocities, tidal salinity and tidal water level variations at this station. MacCready, (1999) and Zimmerman, (1986) pointed out that the tidal dispersion tends to increase with tidal velocity, thus pushing more salt upstream at spring tides than at neap tides. As it can be seen the tidal pumping at the CD Station increased during the spring

tides. These results suggest that due to higher correlation between the tidal velocity, salinity and water level at the spring tides the saline water can intrude to the farther distance in the upstream section of the Ota Estuary.

4.5. Conclusions

This chapter presents variability in salinity, flow rate, flushing time and salt flux at the Ota Diversion channel. To evaluate FATS results, section-averaged velocity and salinity, with those acquired from an ADCP and a conductivity sensor, a field observation was conducted. The results indicate that the pattern of bottom and surface salinity indicated a phase lag between the deepest and shallowest regions. The variations of stratification illustrate that the tidal mixing contributes to decreasing the stratification at the whole cross-section. The magnitude of the vertical shear fluxes indicate an important contribution compared with the advection term. Also the results indicate a phase lag between the vertical shear terms at the shallowest and deepest regions which resulted with the correlation between the vertical salinity and velocity variations and the existence of the transversal circulations in velocity.

At the upstream region of the Ota Diversion Channel (Gion Station), the long-term salinity and flow velocity data were measured using an innovative instrument which is called Fluvial Acoustic Tomography System (FATS). FATS data provides novel information about seasonal and annual variability of salinity and flow rate in this region. The long-term salinity and flow rate variations at the Gion Station are analyzed over the period between 2009 and 2013. To quantify the relative effect of main forces on the salinity variations a multiple-regression analysis is employed. The results indicate that the salinity variations have a good correlation with seasonal variations of the mean sea level, winds and freshwater runoff. Furthermore, spring-neap tidal cycles significantly influence

the salinity variations due to differences in tidal mixing. The increasing tidal range during the spring tides constricted the saltwater intrusion.

The flushing time of the Ota Diversion Channel is estimated based on the freshwater fraction method. The flushing time through the Ota Diversion Channel is estimated using a practical method based on the FATS data. The average flushing time is estimated about 1.8 days under mean flow conditions. This result indicates that the flushing time is considerably short. Therefore, the transition time from highly stratified to partially-mixed is a few days. The maximum flushing time in the Ota Diversion Channel is usually occurred during dry seasons when the upstream freshwater discharge is low and the mean sea level is reached the highest levels.

The salinity variations at the main branches of Ota Estuary are investigated. Due to different adjustments of the Gion and Oshiba Gates, the inflow discharge to these branches is significantly different. This difference in the water discharge and topographical features can cause different salt intrusion mechanisms at the Ota main branches. The tidally-averaged salinity variations in the main branches versus the freshwater discharge at Yaguchi Station can be described as a power-law of upstream freshwater discharge. The exponents -0.53 and -3.86 at the Gion and Oshiba show that the salt intrusion in the Oshiba branch is more sensitive to change in upstream freshwater discharge. In contrast, the Gion Gates is not completely open and the freshwater runoff is restricted considerably. Thus the results indicate significant differences between the salinity variations at the Ota main branches.

References

Arnos, B. A., Stommel, H. (1951) A mixing- length theory of tidal flushing, *American Geophysical Union*, Vol. 32, No. 3, pp. 419-421.

Dyer, K.R. (1992) The cross sectional salt balance in a tropical estuary during a lunar tide and a discharge event, *Journal of Estuarine, Coastal and Shelf Science*, 30, 579-591

Fischer, H. B. (1972) Mass transport mechanisms in partially stratified estuaries, *Journal of Fluid Mech*, 53, 671-687

Hughes, F. W., and M. Rattray Jr. (1980) Salt flux and mixing in the Columbia River estuary, *Estuarine, Coastal and Shelf Science*, 10, 479-493

Kawanisi, K., Razaz, M., Soltaniasl, M., Kaneko, A. (2011) Long-term salinity measurement in a tidal estuary by the use of acoustic tomography, Proceeding of UAM, 401-408

Lerczak, J.A., Geyer, W.R., Chant, R.J. (2006) Mechanisms driving the time-dependent salt flux in a partially stratified estuary, *Journal of Physical Oceanography* 36, 2296-2311.

MacCready, P. (1999) Estuarine adjustment to change in river flow and tidal mixing, *Journal of Physical Oceanography*, 29, 708-729

MacCready, P. (2011) Calculating estuarine exchange flow using isohaline coordinates, *Journal of Physical Oceanography*, 41, 1116–1124

MacDonald, D.J., Horner-Devin, A.R. (2008) Temporal and spatial variability of vertical salt flux in a highly stratified estuary, *Journal of Geophisical Research*, 113, C09022, doi:10.1029/2007JC004620

Rattray, M. Jr, & Dworski, J. G. 1980 Comparison of methods for analysis of the transverse and vertical circulation contributions to the longitudinal advective salt flux in estuaries. *Estuarine Coastal Marine Science* 11,515-536.

Simpson, M. R., Oltmann, R. N. (1990) An Acoustic Doppler Discharge Measurement System. *Proceedings of the 1990 National Conference on Hydraulic Engineering*. 2, 903-908.

Simpson, J.H., Brown, J., Matthews, J., and Allen, G. (1990) Tidal straining, density currents, and stirring in the control of estuarine stratification, *Estuaries*, 13,125-132.

Soltaniasl, M., Kawanisi, K., Maghrebi, M. F., Razaz, M. (2011) Estimates of Flushing Time in a Tidal River Using Fluvial Acoustic Tomography, 10th International Conference on Civil and

Environmental Engineering (ICCEE), National Central University Taiwan, on CD-ROM, 364-370

Soltaniasl, M., Kawanisi, K. (2012a) Salt Intrusion and Water Circulation in a Small Multi-channel Estuary", 10th Conference on Hydroscience and Engineering (ICHE), Orlando, USA, on CD-ROM, paper number: 40092313

Soltaniasl, M., Kawanisi, K., Razaz, M. (2012b) Investigation of Salinity Variability in a Small Multi-channel Estuary, *Journal of Japan Society of Civil Engineers, Ser.B1 (Hydraulic Engineering)*, 68, 265-270

Soltaniasl, M., Kawanisi, K, and Razaz, M. (2012c), Salinity Transport Mechanisms in a Small Multi-channel Estuary", 18th Congress of the Asia and Pacific Division of the International Association of Hydro-Environment Engineering and Research (IAHR-APD), Jeju, Korea, on CD-ROM, paper number: S7E-2

Soltaniasl, M., Kawanisi, K., Razaz, M. (2013) Investigation of salinity intrusion variability using acoustic tomography system, *Journal of Japan Society of Civil Engineers, Ser.B1 (Hydraulic Engineering)*, 69, 91-96

Uncles, R.J., Elliott, R.C.A., Weston, S.A. (1985) Observed fluxes of water, salt and suspended sediment in a partially mixed estuary. *Estuarine, Coastal and Shelf Science,* 20, 147-167.

Uncles, R. J., Ong, J. E., & Gong, W. K. 1990 Observations and analysis of a stratification-destratification event in a tropical estuary. *Estuarine, Coastal Shelf Science* 31, 651-665.

Zimmerman, J.T.F. (1986) The tidal whirlpool: A review of horizontal dispersion by tidal and residual currents, *Neth. J. Sea Res.*, 20, 133-154.

CHAPTER 5

Salt Flux, Stratification and Estuarine Circulation

5.1. Introduction

The study of estuarine mechanisms such as salt intrusion and mixing is difficult task because these water systems usually involve complex geometries, hydrodynamics, and transport patterns. The interface between freshwater and saltwater (estuarine circulation) is forced by river discharges, tides and wind in the estuaries. There is a large variability in estuaries depending on the differences in the tides, river discharges and the way these factors interact with topography (Dyer, 1997). The salinity intrusion depends on the balance between freshwater discharges and saltwater flow from the sea. As discussed

earlier, we can distinguish two major approach on variability of the estuarine dynamic and circulation. The dynamics of the estuarine circulation involve a balance between the pressure gradient induced by the out-estuary surface slope, the baroclinic pressure gradient due to the along-estuary salinity gradient, and the stress associated with the estuarine circulation (Pritchard, 1956; Hansen and Rattray, 1965; Chatwin, 1976). However, Jay (1991) introduced the idea of tidal asymmetry, suggesting that the estuarine circulation is not principally driven by the baroclinic pressure gradient but rather by the imbalance of the magnitude of eddy viscosity between flood and ebb. This imbalance results from the weaker stratification, and more intense turbulence, during floods than ebbs. Geyer et al. (1999) estimated eddy viscosity in the Hudson River and found that flood values exceeded ebb values by a factor of 2. Other estuarine field studies have also documented this tidal asymmetry. Stacey and Ralston (2005) suggested that the asymmetry in the flow is due to the strain-induced buoyancy flux, which is stabilizing on ebb tides but destabilizing on flood tides. Simpson et al. (1990) described it as strain-induced periodic stratification (SIPS). Kawanisi (2004) revealed significant asymmetry in stratification over a tidal cycle at the Ota Diversion Channel.

The objective of this chapter is to characterize the salinity distribution, circulation, and salt flux mechanisms in the Ota diversion channel. Different observation datasets were collected and a three-dimensional numerical model (EFDC) was used to examine the temporal and spatial variations of flow rate and salinity at the estuary.

5.2. Numerical Simulation

5.2.1. Model Setup

The EFDC model was used to simulate water level, current, and salinity in the Ota Diversion Channel. The model solves the three- dimensional continuity and free surface equations of motion (Hamrick, 1992). The technical properties of this model are discussed in section 3.3. The model domain covers the Ota Diversion channel from Gion

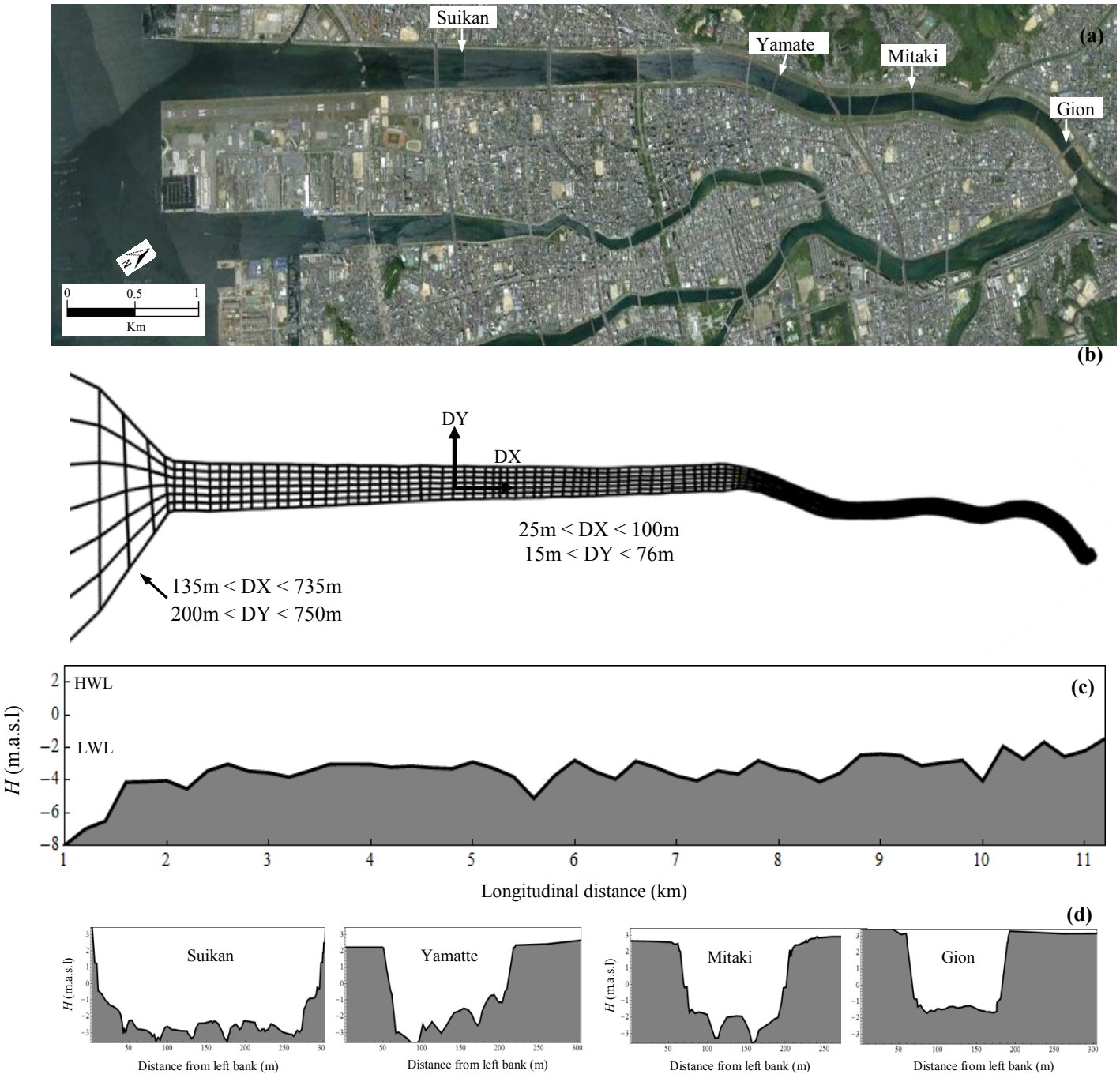

Fig 5.1 (a) Map of Ota Diversion Channel; (b) Model Grid; (c) Bathymetry with distance from the mouth along the channel thalweg (km) ; (d) observation Cross-sections along the Ota Diversion Channel

Gate at the upstream to about 3 km at the offshore. Curvilinear grids are used over the entire domain, and the horizontal spatial resolution ranges from 500 m at offshore to 25 m in the river network (Fig 5.1). Several sensitivity tests were conducted for the vertical

resolution using 5, 10, and 15 sigma layers in the vertical. It was found that using 10 layers improved model results considerably compared to 5 layers, whereas 10 and 15 layers did not improve results further. Thus, use of 10 sigma layers was adopted in the vertical direction. EFDC includes wetting and drying, and the minimum water depth for a cell to be active was set to 0.1 m.

The bottom topography is probably the most important factor that affects the flow properties in environmental modeling. Hence, an accurate representation of bottom topography by the model grid is the most important and fundamental requirement in a successful modeling study. The bottom topography data used in this study were obtained from the Japan Ministry of Lands. Around 50 bathymetry transections along the Ota Diversion Channel (every 200 m intervals) are used for model grid generation.

Boundary conditions included tidal forcing offshore and river discharge at the upstream. For simulations corresponding with the observation periods, the tidal record from Kusatso Station at the mouth of estuary was used to drive the water surface elevation offshore boundary. The offshore salinity boundary condition was fixed on the reference salinity at the Hiroshima Bay which assumed 32.5 for this study. Temperature was not included as a dynamic variable in the model because salinity dominated the density variability in the estuary. Also the river discharge at the Gion Bridge was based on the FATS and ADCP results. For hydrodynamic models, the parameter determining the bottom friction, such as the bottom roughness height, was often adjusted in model calibration.

5.2.2. Model Evaluation

Several field observations have been conducted in the Ota Diversion Channel which were selected for calibration and validation of model. Water salinity and velocity were measured using CTDs and ADCPs at the Gion Bridge from October 18 to end of January 2013 when the average discharge of Yaguchi Station was between 25 and 100 m^3/s. Also

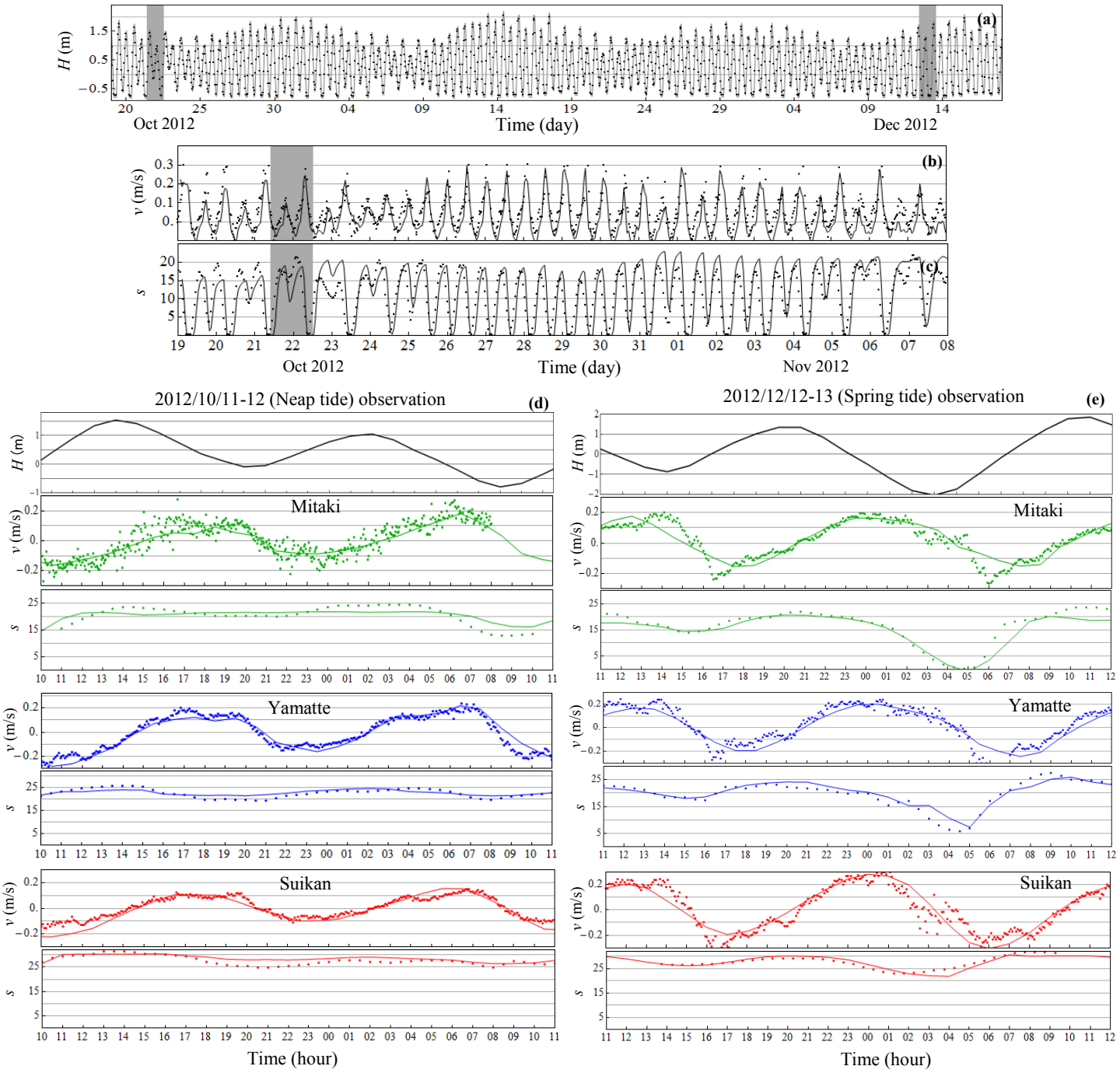

Fig 5.2 (a), (b) and (c) Observation (dots) and model results (solid line) at the Gion Bridge, shaded region indicates the short-time observations periods; (d) and (e) Observation (dots) and model results (solid line) at the three stations during neap and spring tides, respectively.

two short-term observations along the Ota Diversion Channel (three stations) were conducted during the spring and neap tides, respectively (Fig 5.1). Apart from the field

Table 5.1 Skill Scores (SSs) from comparison of model results with observations in 2012

Location	Observation Period	Water level	Salinity	Velocity
Gion	2012/10/19-12/19	0.92	0.81	0.76
Mitaki	2012/10/21-22 Neap tide		0.83	0.81
Yamate			0.91	0.90
Suikan			0.89	0.94
Mitaki	2012/12/12-13 Spring tide		0.91	0.88
Yammate			0.90	0.89
Suikan			0.93	0.90

measurements mentioned above, we used the water level of Kusatsu and Gion Stations for this study. The comparisons of model results and measurements of water level, velocity, and salinity are shown in Fig 5.2. The model skill is evaluated against the measured water level, velocity, and salinity time series using Eq. (3.23). The results indicate that the simulated water level, salinity and velocity at the stations agree well with observation results. The model skill scores are shown in Table 5.1. The model skill score (SS) for the water level at the Gion Bridge is equal to 0.92, showing an excellent skill. The simulated water velocities follow the observation results reasonably. SSs for velocity decreased with distance up-estuary ranging from 0.9 at the Suikan Bridge to 0.76 at the Gion Bridge. The lower skill at the Gion Bridge may be due to effect of freshwater discharge during Low Water Level (LWL) condition or inadequate resolution of the bathymetry at the channel constriction. The model skill scores (SSs) for salinity from comparison between model and observations show an excellent skill. Similar trend for SS variations along the estuary are seen in the salinity skills. The maximum differences between the observed and simulated result occur during neap tides. It seems that the vertical eddy viscosities estimated by the model are larger than the observed values during the neap tides.

5.3. Longitudinal Distribution of Salinity and Velocity

To evaluate the model skill and also to characterize the estuary condition during the spring and neap tides the model and observation results are shown in Figures 5.3-5.7. It should be noted that the discharge of Yaguchi Station during both neap and spring observations was about 25 m^3/s.

Neap tide (Figures 5.3 and 5.4): During the first portion of flood tide (hour 12) the water velocity is directed landward along the channel. However, a weak two-layer flow is dominated at the up-estuary region. The results at the down-estuary sections indicate too much vertical mixing and weak stratification in this region during the floods. However, the model and observation results indicate that the halocline is strong at the up-estuary (Gion). Around high tide (hour 14) the bottom salinity has extended up to Gion Gate, while the surface tidal intrusion becomes stationary near the Mitaki Bridge (around 7 km from the mouth). The channel from the mid to the up-estuary has strong stratification: surface-to-bottom salinity differences are greater than 15. After high tide the barotropic pressure gradient reverses and the water velocity directed seaward. As the ebb progresses the surface flow accelerates and the straining process increases the stratification at the down-estuary sections (Yamatte and Suikan).

Spring tide (Figures 5.5 and 5.6): The model results reveal large landward-directed flow velocity by the values around -0.45 m/s during the first portion of flood tide (hour 17). Similar to the neap tide, the tidal straining enhances the stratification during the ebb tides and diminishes it during the flood tides. Simpson et al., (1990) defined variability in stratification due to tidal straining mechanism as:

$$\phi = \frac{1}{h}\int_{-h}^{0}(\bar{\rho} - \rho)gzdz \tag{5.1a}$$

$$\bar{\rho} = \frac{1}{h}\int_{-h}^{0}\rho dz \tag{5.1a}$$

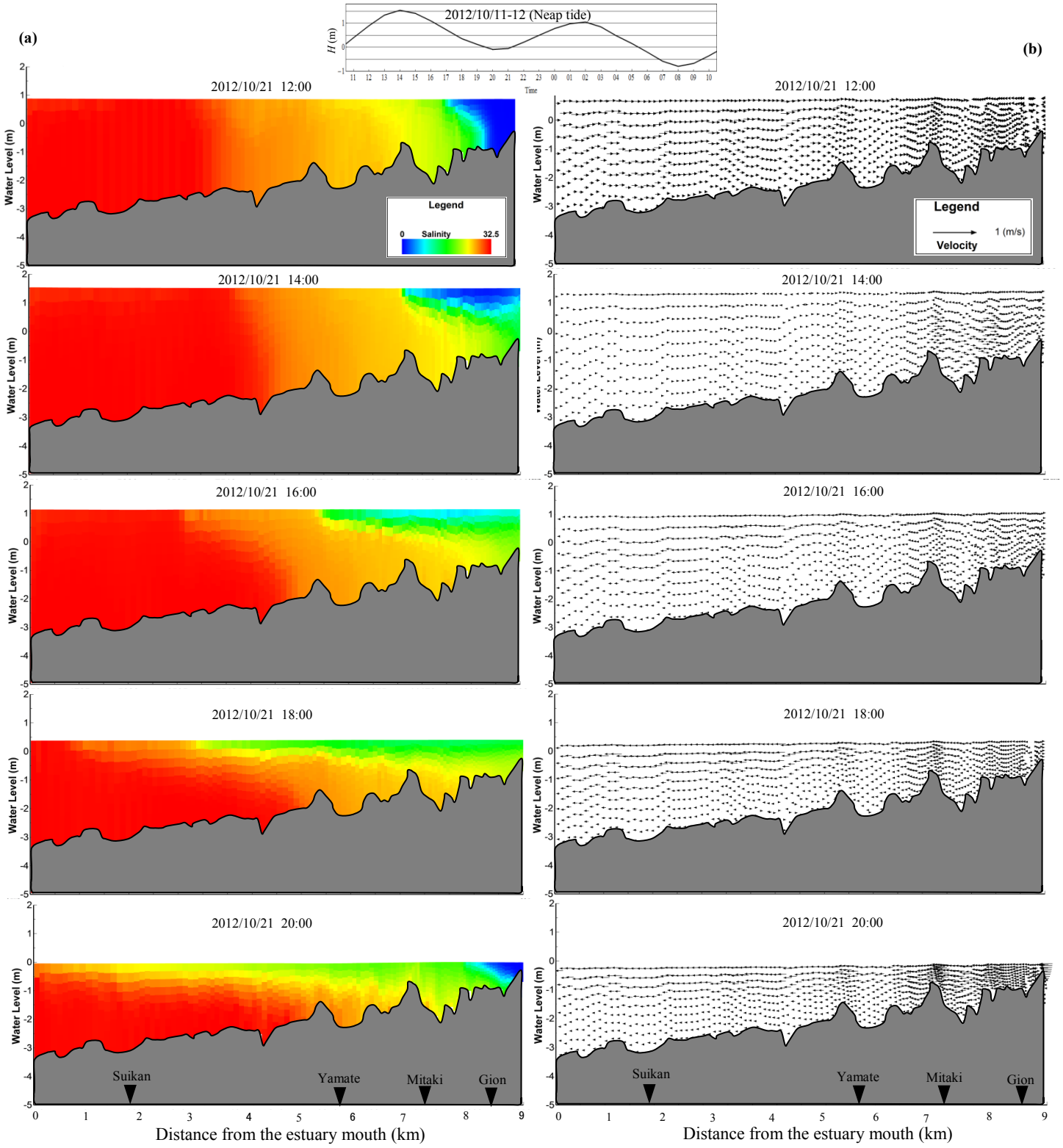

Fig 5.3 Along-channel distribution of (a) simulated salinity, (b) velocity during the neap tide observation

$$\frac{\partial \phi}{\partial t} = 0.031 ghu \frac{\partial \rho}{\partial x} \tag{5.1c}$$

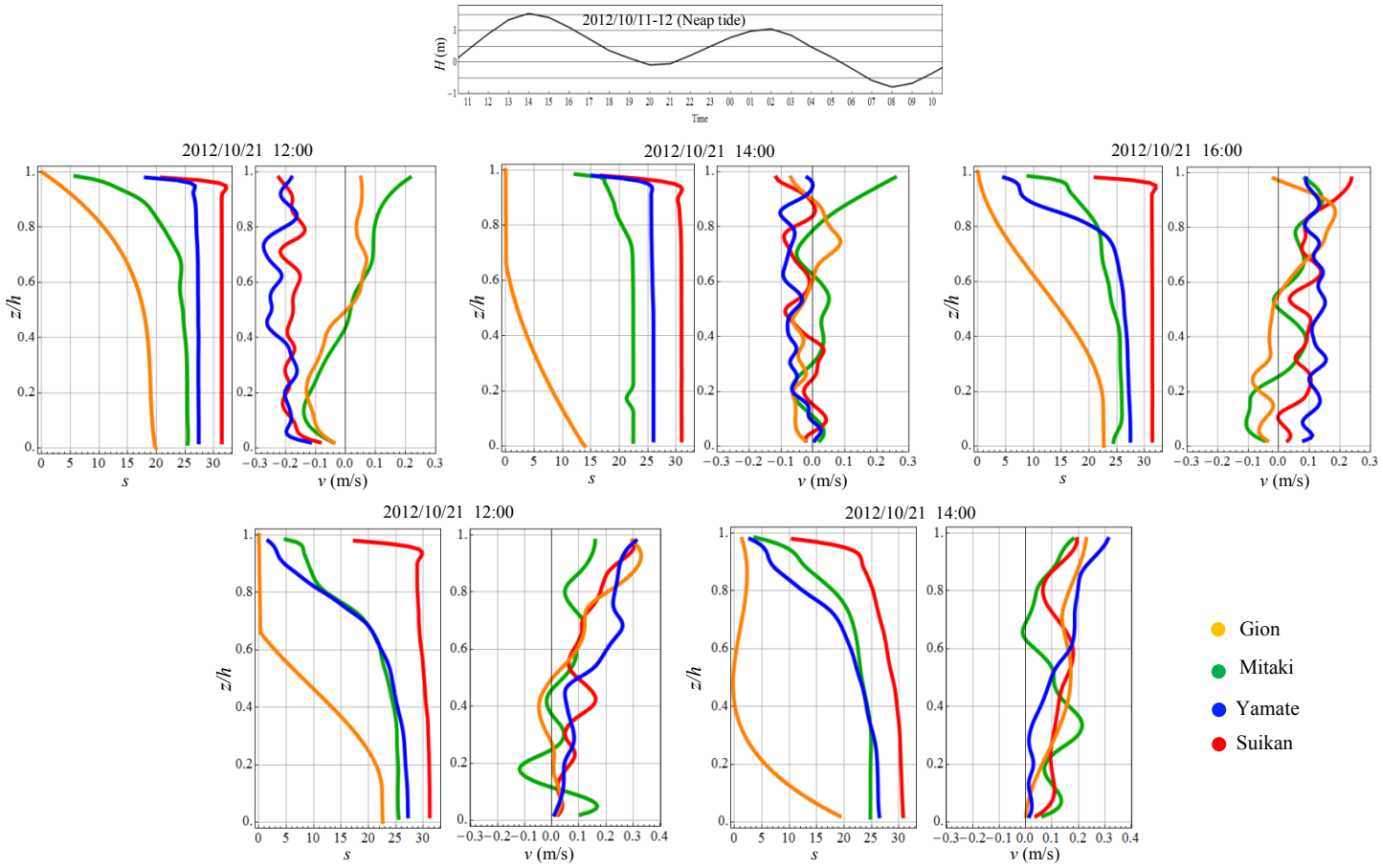

Fig 5.4 Vertical profiles of the salinity and velocity along the channel during the neap tide observation

where, ϕ is stratification, ρ is the density, h is the water depth, and v is the depth-averaged velocity. Knowing the vertical profile of velocity and longitudinal salinity gradient we can estimate the tidal straining as:

$$Tidal\ \ Straining = -\frac{\partial v}{\partial z}\frac{\partial s}{\partial x} \tag{5.2}$$

where, $\partial v/\partial z$ is the velocity shear. Using observation and model data, the tidal straining was estimated at the four stations (Fig 5.8). The velocity shear was estimated as $\Delta v/\Delta z$, where Δv is the differences between surface and bottom velocities. This linear approximation to velocity shear represents an average shear over the water column. The velocity shear and longitudinal salinity gradient both vary through the tidal cycle, as shown in (Figs 5.4, 5.6 and 5.7). The longitudinal salinity gradient had a Dome shape

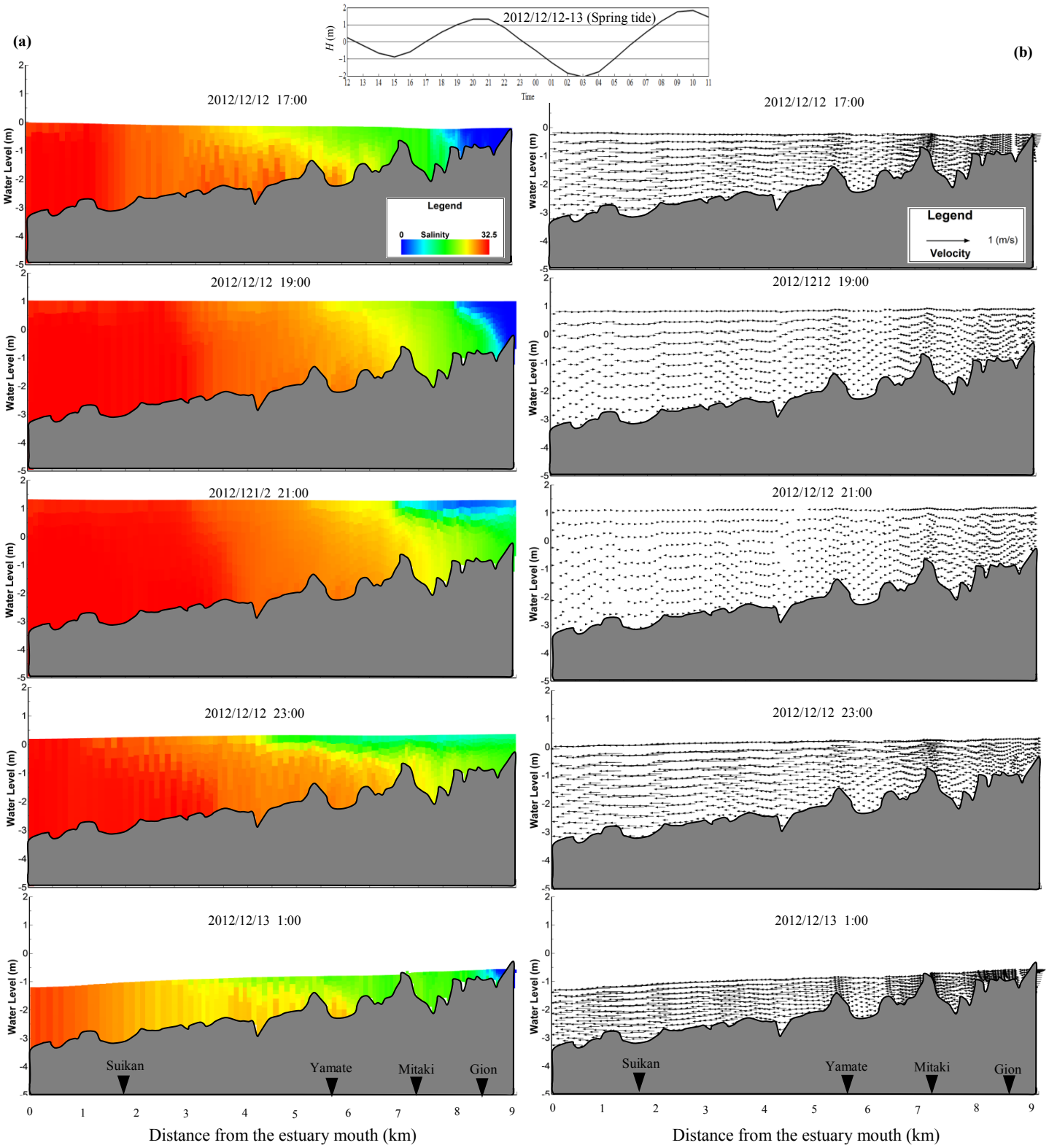

Fig 5.5 Along-channel distribution of (a) simulated salinity, (b) velocity during the spring tide observation

distribution (Fig 2.2); there was the strongest gradient at the upstream section (between

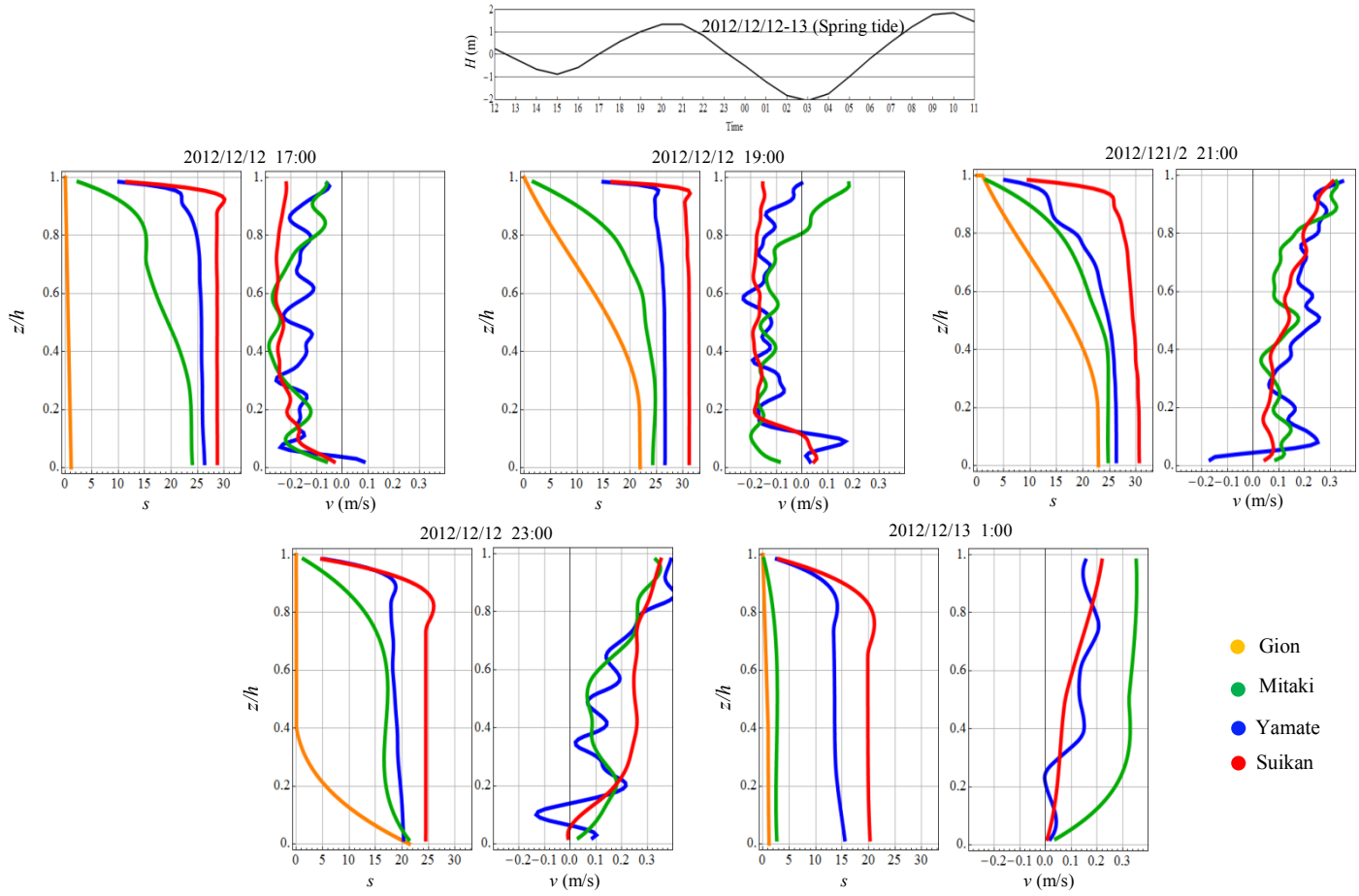

Fig 5.6 Vertical profiles of the salinity and velocity along the channel during the spring tide observation

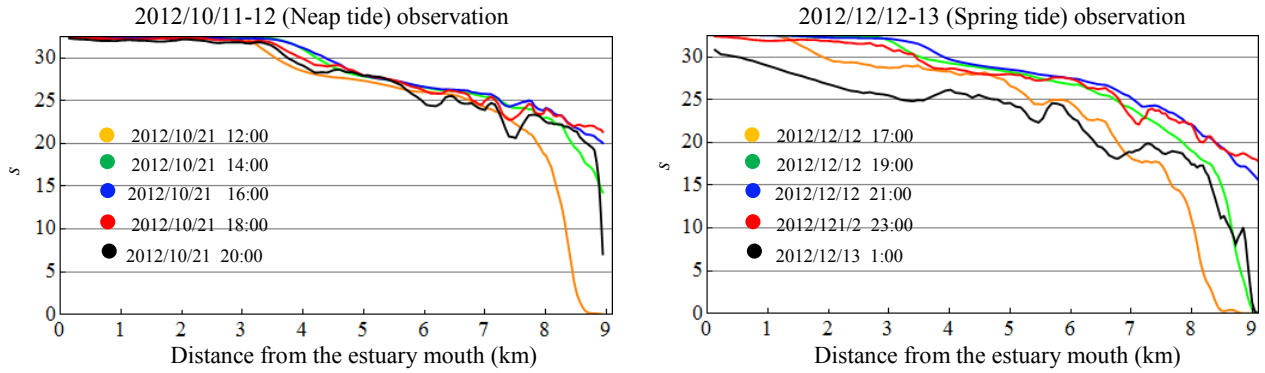

Fig 5.7 Variability in longitudinal salinity distribution during the observation

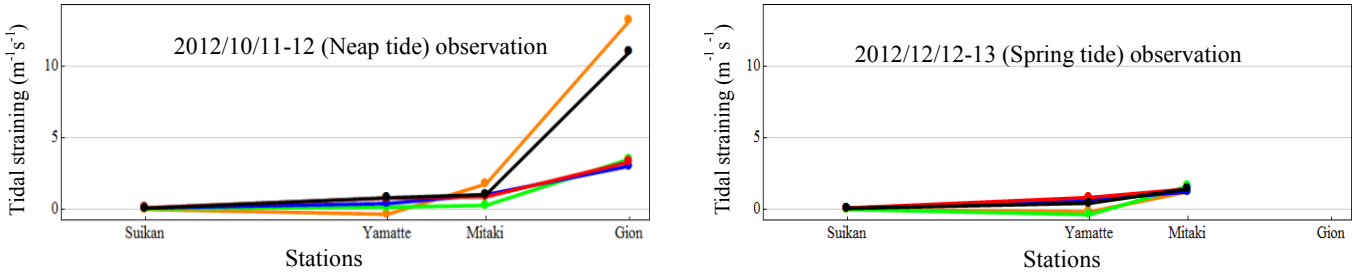

Fig 5.8 Variability in tidal straining during the observation

the Mitaki and Gion Bridges) close to the end of ebb tides. It seems that these variations

are associated to channel convergence and the effect of the upstream freshwater which intensified the horizontal salinity gradient during the ebb tides.

The straining term was estimated using Eq. (5.2) as the product of the vertical shear velocity and longitudinal salinity gradient (Fig 5.8).The longitudinal distributions of tidal straining indicate that tidal straining is significant at the upstream sections due to the high values of the longitudinal salinity gradient.

5.4. The Response of Salt intrusion to Changes in Forces

Simulated scenarios are defined to consider the key estuarine forces on salinity intrusion. Different conditions of upstream freshwater discharge at the Yaguchi Station and water level at the Kusatsu Station are modeled. Adopted water levels reflect the variability of flood and ebb tides. For freshwater discharges six values were adopted (Table 5.2). the minimum one (25 m^3/s) corresponds to the mean discharge during dry season (August to December) with probability of 54% which was considered in section 5.3; the 100 m^3/s value is approximately the mean discharge during the wet season (January to May) with a probability of 40%; the value of 250 m^3/s corresponds to a moderate peak events; the 400 m^3/s, all Gates of Gion are open in this situation; the 1000 m^3/s, 2000 m^3/s and 4000 m^3/s correspond to the typical values for seasonal peak events periods (June and July). The scenarios are summarized in Table 5.3. In each case forcing was held constant until the system reached a tidal equilibrium. The time duration of numerical experiment for S10-S12 is four tidal cycles but up to 10 tidal cycles for lower discharges (S1-S9).

In order to assess the accuracy of model experiments for selected scenarios, the model run for different flood events at the Yaguchi Station ranging between 100 m^3/s and 4000 m^3/s during 2009-2010. For example, the model responses were assessed during Jun and July 2009 (Fig 4.9). Based on model runs, the appropriate boundary conditions for each scenario were estimated.

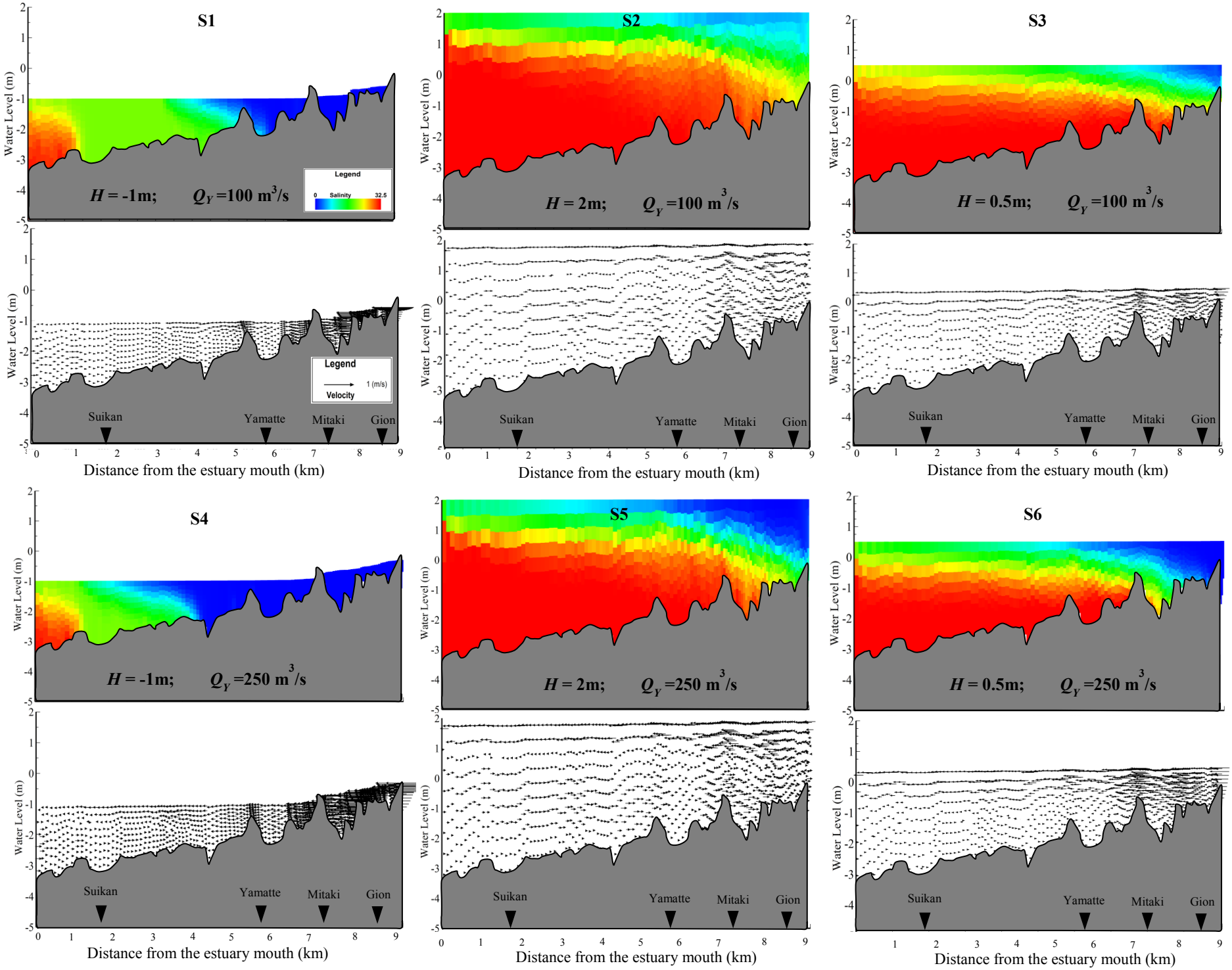

Fig 5.9 Longitudinal distribution of salinity and velocity during flood events

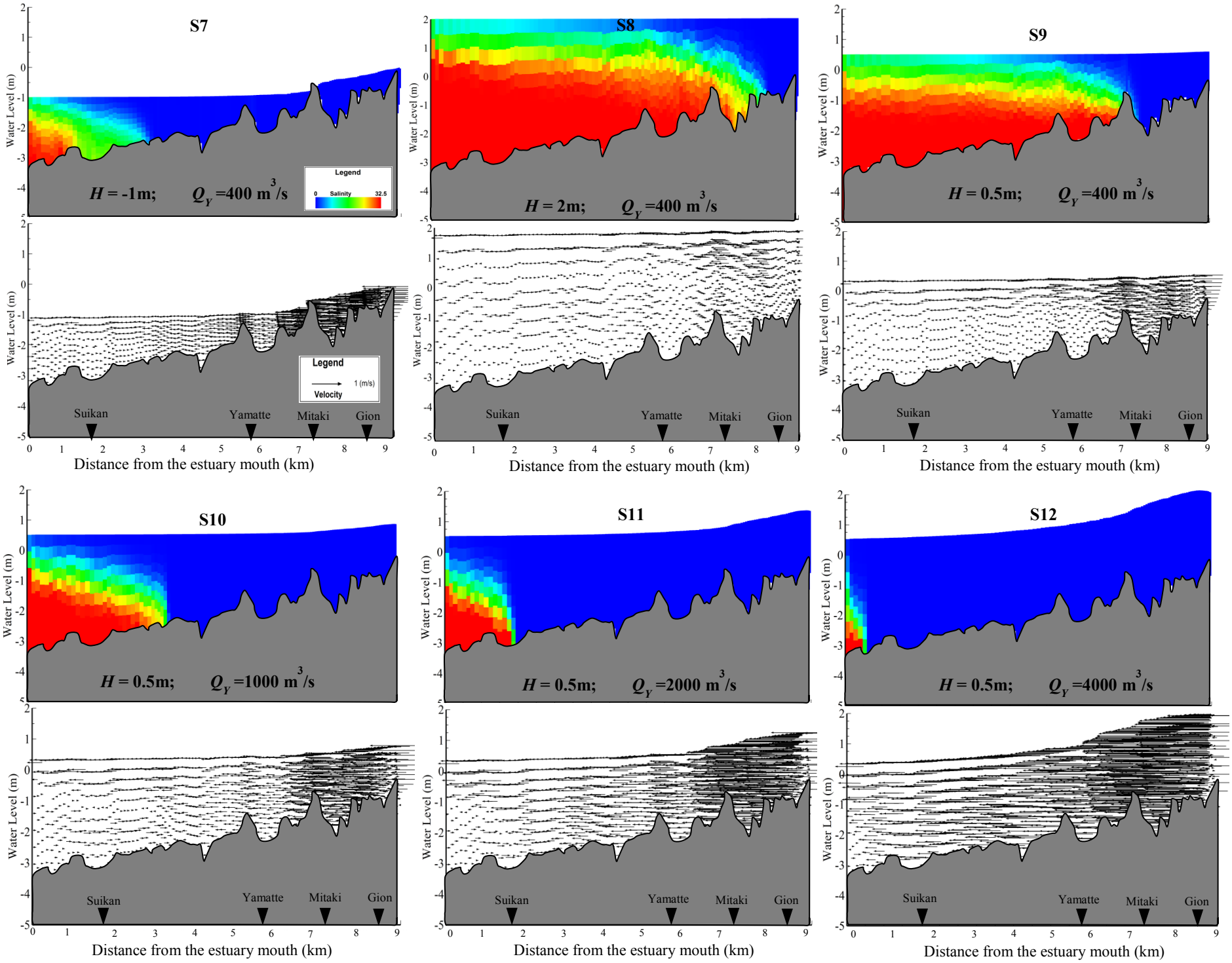

Fig 5.9 (Continued)

Table 5.2 Probability distribution of Yaguchi Discharge (based on four years data)

Yaguchi Discharge	Probability (%)
$Q_Y < 50$ m^3/s	54.1
50 m^3/s $\leq Q_Y < 150$ m^3/s	40.1
150 m^3/s $\leq Q_Y < 350$ m^3/s	3.8
350 m^3/s $\leq Q_Y < 600$ m^3/s	1.15
600 m^3/s $\leq Q_Y < 1200$ m^3/s	0.62
1200 m^3/s $\leq Q_Y < 2500$ m^3/s	0.2
2500 m^3/s $\leq Q_Y$	0.03

Table 5.3 Simulated Scenarios

Yaguchi discharge (m^3/s)	Water level (m)		
	-1 (First portion of flood tide)	0.5 (Last portion of ebb tide)	2 (High tide)
100	S1	S2	S3
250	S4	S5	S6
400	S7	S8	S9
1000	-	S10	-
2000	-	S11	-
4000	-	S12	-

These scenarios represent the most relevant situations for evaluation of the salinity intrusion during the flood events. For each freshwater discharge it is possible to analyses the effect of different tide heights in the salinity intrusion considering scenarios of Table 5.3. Figure 5.9 shows the model results of along-channel salinity and current distribution in the Ota Diversion Channel.

The status of estuary at the downstream sections (e.g., Suikan Station) is well-mixed during the flood tide, and partially mixed during the last half of ebb tides. However, at

the upstream sections (e.g., Mitaki Station) the channel is partially mixed during the flood tides, and stratified during the first portion of ebb tides (Figs 5.3-5.6). During the moderate flood events at the Yaguchi Station ($100 < Q_Y < 400$ m^3/s), the estuary is in the statues of partially to highly stratified (S1-S6). For S1-S9 conditions the stratification is higher around high tides than on ebb tides. This feature may be induced by the higher tidal velocities on ebb tide that increases turbulent mixing which causes a decrease on stratification. Also the results show that the up-estuary region (Gion Bridge) is completely sensitive to discharge of Yaguchi Station and during the discharge larger than 250 m^3/s, the salinity is flushed out of this region. While, at the down-estuary regions the salinity return to the normal values during the flooding (S3, S6 and S9). Under high flow conditions, the model results show that stronger flow pushed salinity down-estuary and the channel is almost entirely freshed out and salinity front is limited to the estuary mouth (S10, S11 and S12). At the downstream region of the Ota Diversion Channel, the flow velocity at the surface layers is strong. The simulated bottom landward flow also completely is depressed, representing a strong salt wedge near the channel mouth.

5.5. Variability in Salt Intrusion Length Due to Changes in River Discharge and Tide

The salt intrusion length generally follows a power law relation to river discharge ($L \approx Q^n$) where the exponent coefficient n varies in a wide range in different estuarine conditions. Abood (1974) found that $n = 1/3$ for low flows in the Hudson River, but $n = -1$ for high-flow conditions. Monismith et al. (2002) calculated $n = -1/7$ in San Francisco Bay. Yang and Khangaonkar (2009) noted that $n = -1/4$ for the Skagit River estuary, a salt-wedge one. Ralston et al. (2010) obtained the coefficient $n = -0.19$ for low flow and $n = -0.57$ for high flow conditions in the Merrimack River estuary. As mentioned before the salinity intrusion length is also varied by the tidal range. To examine the effect of river discharge and tidal velocity on the salt intrusion in the Ota diversion channel, a

numerical experiment was conducted. The semidiurnal tidal component is the dominant in the Ota Estuary, but also mixed with a diurnal component. The tidal ranges are approximately 0.3 and 4 m at the neap and spring tides, respectively. For numerical simulations with 15 days duration which reflects spring-neap variability, and constant freshwater discharges at the Yaguchi Station (25, 50, 100, 250, 400, 1000, 1500, 2000 and 4000 m^3/s) were selected. These discharges span the low flow at the dry seasons to the maximum flood event in July 2009.

Figure 5.10 indicates the longitudinal distribution of salinity along the Ota Diversion Channel and the relation between the salinity intrusion length versus the freshwater discharge for spring and neap tides. Also the variability of discharge exponents during the different situations of river discharge and tides are shown in Table 5.4. The variability of salinity intrusion length versus the freshwater discharge was examined. Statistically, the best fit to the data is obtained with a power-law function during both neap and spring tides. During the moderate peak events (Q_Y < 400 m^3/s), the results indicate the exponents -0.11 and -0.14 for the neap and spring tides, respectively. The dependence of salt intrusion on freshwater discharge is weaker than (-1/3) that predicted by theoretical models for exchange flow dominated estuaries (see Eq. (2.24)). Monismith et al. (2002) calculated $n = -1/7$ in San Francisco. He argued that this weaker dependence of salinity intrusion on flow is due both to geometry of San Francisco Bay and the effects of stratification on vertical mixing. Geyer and Signell, 1992 denoted that for most tidal processes the salt flux is assumed to depend on tidal velocity and not on Q_r (river discharge). In the Ota Diversion Channel for Q_Y < 400 m^3/s, the freshwater discharge is restricted by the Gion Gate. Also the variability in tidal velocity (vertical eddy viscosity) and tidal range (see Eq. (2.24)) can significantly affect the salinity intrusion length. In the Ota Diversion Channel, the larger tidal amplitudes during the spring tides tend to increase the tidal mixing and reduce stratification. The influence of tidal amplitude on the salinity and flow velocity makes the length of salinity intrusion

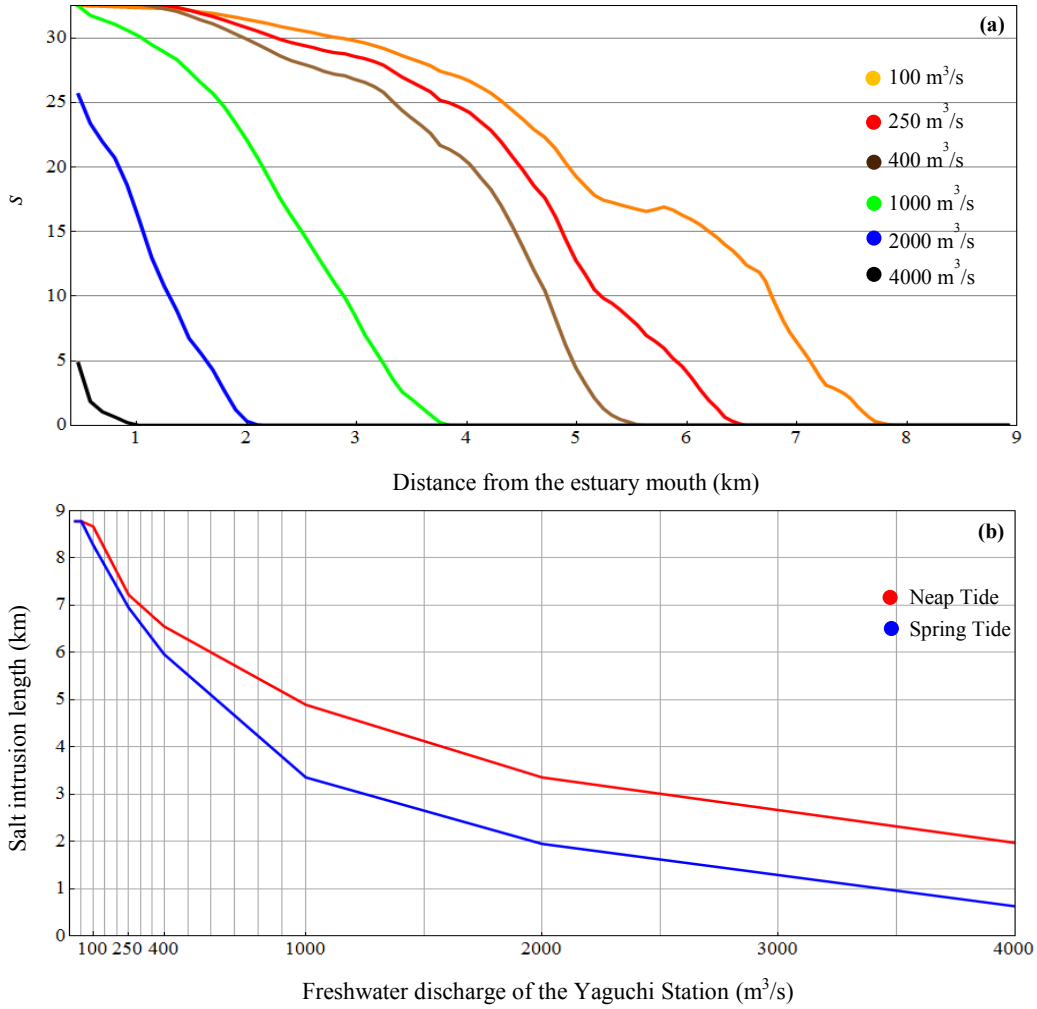

Fig 5.10 (a) Longitudinal distribution of salinity (tidally-averaged) during the peak events (spring tide); Relation between salinity intrusion and freshwater discharge of the Yaguchi Station discharge for spring and neap tides

Table 5.4 Relation between salinity intrusion length and freshwater discharge ($L \approx Q^n$)

n	Neap tide	R^2	Spring tide	R^2
$Q_Y < 400$ m^3/s	-0.11	0.89	-0.14	0.9
400 m^3/s $< Q_Y$	-0.51	0.93	-0.93	0.95

relatively sensitive to tidal amplitude. These results show that the salt intrusion length in

the Ota Diversion Channel is sensitive to spring-neap tidal cycle as well as upstream freshwater discharge at the Yaguchi Station. For high freshwater discharge (Q_Y > 400 m^3/s) the exponents are -0.51 and -0.93 for neap and spring tides, respectively. This result shows that the differences in salt intrusion length between springs and neaps are increased by increasing river discharge. Passone et al. (2003), in a study about effluent discharge policies found that the spring tide with high freshwater inflow was the best situation concerning pollutant distribution in the Upper Milford Haven estuary. Unfortunately, in absence of relation between the salinity intrusion length and tidal velocity, the reason for such a behavior remains unknown and is left for future studies.

5.6. Variability in Salt flux due to Changes in River Flow and Tide

Using the numerical results of the salinity and velocity, the temporal and spatial variability of salt flux was estimated during two sub periods (February 15 to April 1, 2012 and September 15, to November 1, 2012). During these periods, the mean freshwater discharge at the Yaguchi Station was about 100 m^3/s and 25 m^3/s, respectively. To assess the salt flux mechanisms, the salinity and velocity over a tidal cycle are decomposed both spatially and temporally into mean components and deviations from the means based on the method which was described by Lerczak et al. (2006). Similar to Eq. (2.33), the total salt flux per width can be estimated as:

$$F = \left\langle \int_0^h usdz \right\rangle \tag{5.3}$$

where the bracket a 25 hours average, u is the longitudinal velocity, s is the salinity, h is the water depth, and z is vertical coordinate. The velocity and salinity can be decomposed (Lerczak et al., 2006) as:

$$\phi_0 = \frac{1}{h_0}\left\langle \int_0^h \phi(z,t)dz \right\rangle \tag{5.4a}$$

$$\phi_E = \left\langle \frac{h}{h_0}\phi \right\rangle - \phi_0 \tag{5.4b}$$

$$\phi_T = \phi - \phi_0 - \phi_E \tag{5.4c}$$

where ϕ refers to either u or s, and h_0 is the tidally-averaged (25 hours) water depth. The total salt flux is given by (MeacCready, 2011):

$$F = \left\langle \int (u_0 + u_E + u_T)(s_0 + s_E + s_T)dh \right\rangle \approx \left\langle \int (u_0 s_0 + u_E s_E + u_T s_T)dh \right\rangle = Q_f s_0 + F_E + F_T \tag{5.5}$$

where $Q_f s_0$ is the advection transport which is equal to F_1 in Eq. (2.36). Q_f includes both the river discharge and volume transport resulting from correlations between tidal currents and fluctuations in the cross-sectional area. F_E is the salt flux resulting from steady shear dispersion (equal to F_5 in Eq. (2.36)) and F_T is the tidal oscillatory salt flux (F_2, F_3 and F_4). At four cross sections (Gion, Mitaki, Yamate and Suikan Bridges) the salt fluxes were estimated for the mentioned time periods.

During the first period (February 15 to April 1) the freshwater discharge at the Yaguchi Station is larger than 50 m^3/s. The tidally-averaged salinity and flow velocity at the stations are presented in (Figs 5.11.c and 5.11.d). It can be seen that the tidally-averaged salinities at all stations follow the variability of spring-neap tidal cycles. The maximum salinity occurred at the neap tides. Meanwhile, during the flood events (e.g., Oct 4) the salinity was decreased at the Gion Station. The salt flux decompositions at four cross-sections (Gion, Mitaki, Yamate and Suikan) are shown in Figures 5.11.e - 5.11.h. The advection component was predominantly seaward at all stations. It generally followed spring-neap tidal variations. The advection transport at the Gion was more controlled by changes in river flow, while spring-neap variations became more important at the other stations. The landward salt flux was generated by both the steady shear and the tidal oscillatory transports. At all stations, the tidal oscillatory transport were larger

during spring tides and smaller during neap. The relative contribution of the steady and tidal components can be written as the ratio (diffusive fraction)

$$\upsilon = \frac{F_T}{F_E + F_T} \tag{5.6}$$

when υ approaches zero , the estuarine exchange flow dominates the landward salt flux, while when υ approximates unity, the tidal oscillatory dominates the landward salt transport. The values of υ were calculated at the four cross-sections (Figs 5.11- 5.12). The dispersive fraction of upstream transport at the Gion was around 0.2 during neap tides and 0.9 during spring tides at the upstream sections. This results suggest that the tidal oscillatory was dominant during spring tides while the steady shear was more important during neap tides. This ratio is larger than 0.8 at the Suikan Station during both the spring and neap tides, indicating that the tidal oscillatory flux is dominate at the downstream sections. The total salt transport was seaward during spring tides and landward during neap tides. These results suggest that the total salt flux in the Ota Diversion Channel is predominantly balanced by the advective salt flux, and salt leaves the estuary during spring tides and salt enters the estuary during neap tides.

During the second period, the freshwater discharge at Yaguchi Station is less than 50 m^3/s (Fig 5.12.a). With low freshwater discharge, the estuary becomes well-mixed (e.g., Fig 5.3 and 5.4). In this condition, the estuarine circulation diminishes significantly but is still existent at the upstream sections (Fig 5.13). The weak estuarine circulation results in a weak steady shear transport. But the tidal oscillatory transport is significant, especially during the spring tides due to small phase lag between salinity and current velocity. The salt transport is mainly dominated by the advection process, which is landward during neap tides and seaward during spring tides. This finding is consistent with the variability of salt intrusion length in the channel. As mentioned before, the salt intrusion length in the Ota Diversion Channel changes with spring-neap variation under low freshwater discharge (Fig 5.10.b) Maximum salt intrusion occurs at neap tides while minimum salt

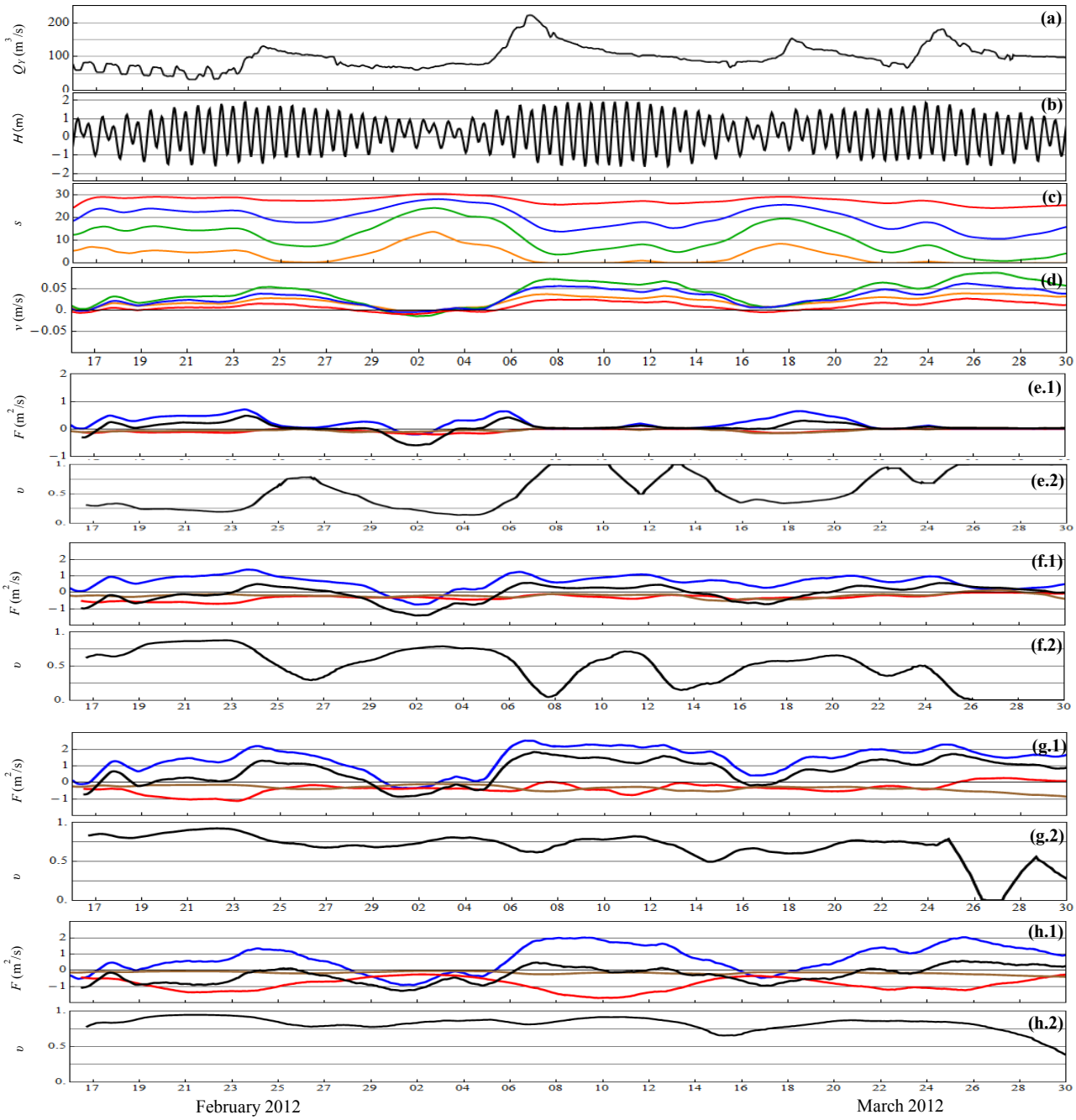

Fig 5.11 Time series of: (a) freshwater discharge at the Yaguchi Station, (b) water level at the Kusatsu Station; (c) and (d) are the tidally-averaged salinity and velocity at the Gion (orange line), Mitaki (Green line), Yamate (Blue line) and, Suikan (red line), respectively; (e)-(h) salt fluxes and diffusive fraction at the Gion, Mitaki, Yamate and Suikan Stations, respectively; in these figures, blue line denotes the advective flux, red line signifies the tidal oscillatory, brown line denotes steady shear flux and black line stand for total salt flux.

intrusion occurs at spring tides. Generally, the diffusive fraction during the second period

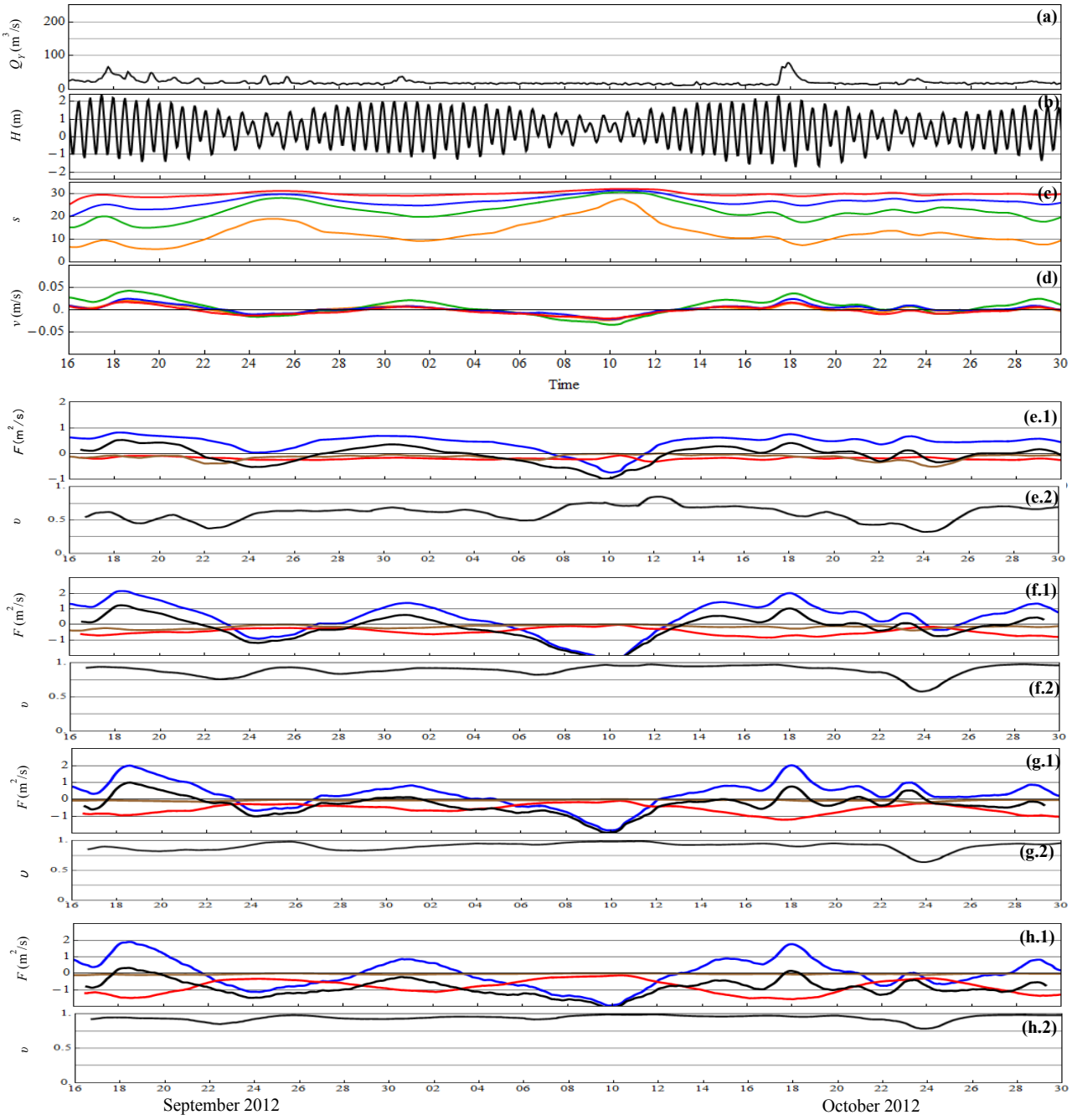

Fig 5.12 Time series of: (a) freshwater discharge at the Yaguchi Station, (b) water level at the Kusatsu Station; (c) and (d) are the tidally-averaged salinity and velocity at the Gion (orange line), Mitaki (Green line), Yamate (Blue line) and, Suikan (red line), respectively; (e)-(h) salt fluxes and diffusive fraction at the Gion, Mitaki, Yamate and Suikan Stations, respectively; in these figures, blue line denotes the advective flux, red line signifies the tidal oscillatory, brown line denotes steady shear flux and black line stand for total salt flux.

(dry season) is larger than that during the first period (wet season). The diffusive fraction

vary around 0.5 at the Gion Bridge, and at the other stations is larger than 0.8. This result indicate that the tidal oscillatory is enhanced due to effect of low freshwater discharge and mean sea level increases. Previous results (Fig 4. 9) show that the tidal velocity and salinity have higher correlation during the highest mean sea level. Then the tidal oscillatory is higher during dry season.

5.7. Variability in Stratification and Estuarine Circulation

Jay and Smith (1990) analysed data collected from the Columbia River estuary and found a flood-ebb asymmetry. Geyer et al. (1999) estimated eddy viscosity in the Hudson River and found that flood values exceeded ebb values by a factor of 2. Other estuarine field studies have also documented this tidal asymmetry and suggested that the asymmetric mixing needs to be considered when calculating tidally averaged vertical fluxes (Stacey et al., 2001; Peters and Bokhorst, 2001). In estuaries that are deep and have moderate river and tidal velocities, the baroclinic pressure gradient provides the dominant mechanism for creating residual circulation, stratification, and up-estuary salt flux (Ralston et al., 2010). Physical processes in baroclinically dominated estuaries have been well documented. For example, James (Pritchard, 1952), Hudson (Lerczak et al., 2006) river estuaries and San Francisco Bay (Monismith et al., 2002). In contrast to the extensive investigations at those estuaries, a few observations of tidal variability have been reported in the shallow tidally dominated estuaries (e.g., Simpson et al., 2001). Previous studies (e.g. Geyer et al., 1999) found that the bottom stress exhibits stronger flood–ebb asymmetry during neap tides than during spring tides. The results of observation at four stations at the Ota Diversion Channel reveal the flood-ebb asymmetry during neap and spring tides as shown in Figure 5.13.

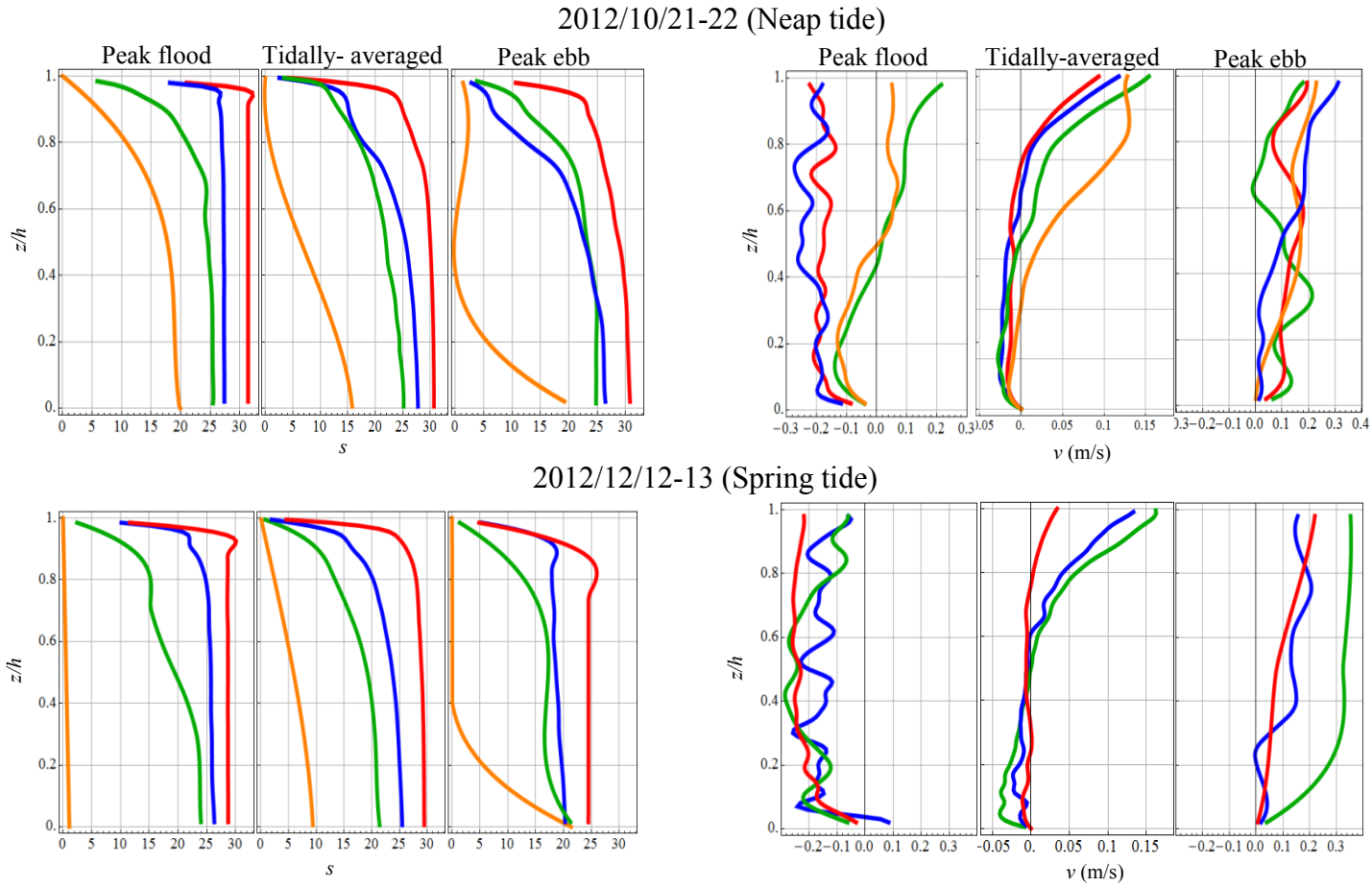

Fig 5.13 Vertical profiles of the salinity and flow velocity at the station at the peak flood, tidally-averaged and peak ebb during neap and spring tides, respectively.

As mentioned before these observations were conducted during the low freshwater discharge ($Q_Y < 50$ m^3/s) at the Yaguchi Station. The longitudinal salinity gradient is about -1.1 km^{-1} between the estuary mouth and Yamate Bridge and, -5 km^{-1} between the Yamate and Gion Bridges. Tidal advection across these salinity gradients generates salinity fluctuations at the stations. Since the flow velocity vary with depth and are different between the flood and ebb tides, vertical salinity profile shows the periodic variation over a tidal cycle (Figs. 5.3, 5.4 and 5.13). During the ebb tides, less saline water from upstream is advected to the stations resulting in stronger freshwater at the upper layer. In contrast, during the flood tides, more saline water is brought to the

stations. This asymmetry in the vertical salinity profile appears to be related to the tidal straining effect (e.g. Simpson et al., 1990; Nepf and Geyer, 1996; Kawanisi, 2004). In addition to the tidal straining effect discussed above, the bed stress may be stronger on flood than on ebb. For example, Geyer et al. (1999) found significant flood–ebb asymmetry in the bed stress in the Hudson River estuary. This asymmetry in the bed stress could also be a cause for the stronger mixing on the flood tide. During the flood tide, the interaction between the barotropic tidal pressure gradient and landward-directed baroclinic pressure gradient in the lower layer of the estuary produces stronger current shear near the bottom boundary and hence larger bed stress (Nepf and Geyer, 1996; Li and Zhong, 2009).

Other important mechanism at the Ota diversion channel is the spring-neap tidal cycles. To analyse the spring–neap variability at the stations the salinity variability at the Suikan and Gion Bridges were selected during the wet and dry seasons (model results). The results are show in Figures 5.14 and 5.15. The amplitude of tidal velocity varies from 0.5 m/s at the strongest spring to 0.16 m/s at the weakest neap. During the wet season (Fig 5.14) the maximum stratification occurred during neap tides at the Gion Bridge. While, at the Suikan Bridge, the maximum stratification accrued during the flood events at the Yaguchi Station (e.g., February 25-27 and March 6-12 in Fig 5.14). By increasing the freshwater runoff the thickness of halocline layer at the downstream regions is increased. So the difference between the bottom and top salinity is increased during flood events. During the dry season (Fig 5.15) the stratification was increased at the Gion Birdge. However, due to well-mixed condition the stratification is low at the Suikan Bridge. These results suggested that seasonal variability in the upstream freshwater discharge affects the estuarine circulation and stratification in a well-mixed estuary such as Ota Diversion Channel. Comparing the longitudinal distributions of salinity and velocity (Figs 5.3-5.6), and the tidally averaged vertical profiles (Fig.5.13) between the spring and neap tides indicate that the salinity distributions in Ota Diversion Channel show

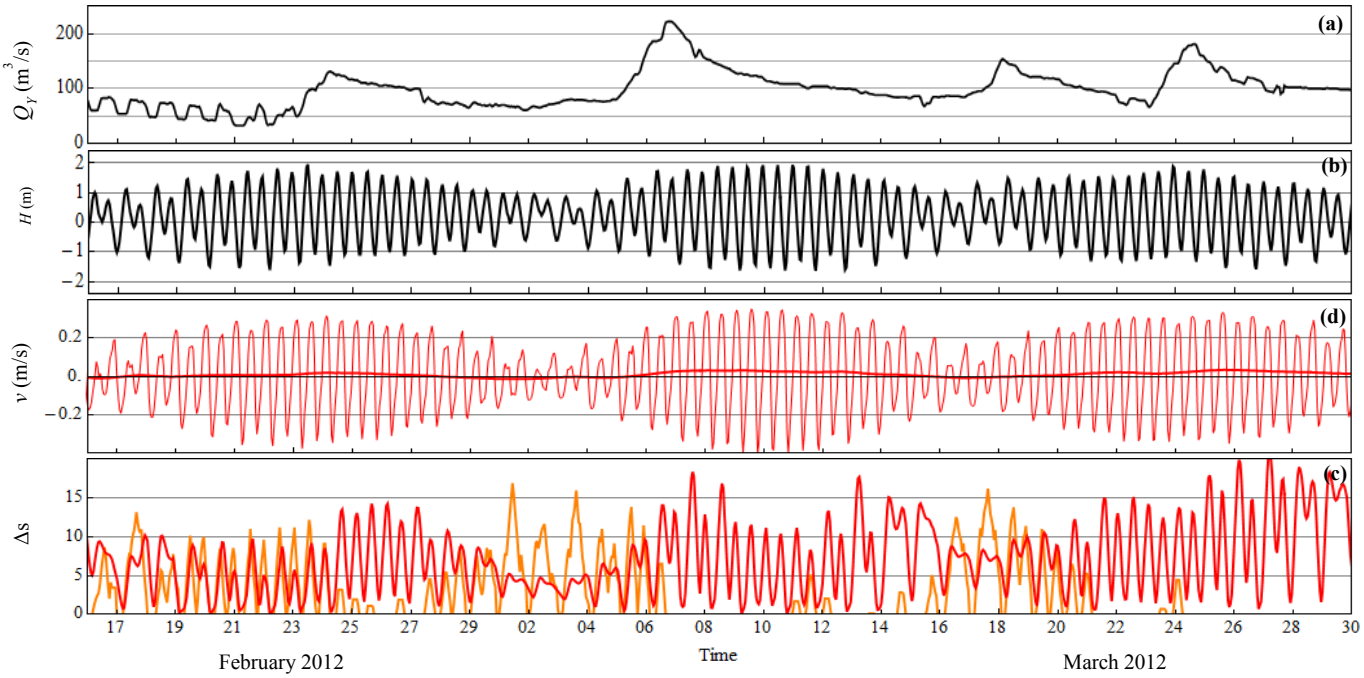

Fig 5.14 Time series of: (a) freshwater discharge at the Yaguchi Station, (b) water level at the Kusatsu Station; (c) tidal velocity, instantaneous (thin line) and tidally averaged (thick line) at the estuary mouth; (d) top-to-bottom salinity difference at the Suikan (red line) and Gion (orange line) Bridges

significant changes between the spring and neap tides (Fig.5.13). As shown in Fig. 5.13, the circulation strength is stronger during the neap tides. The strength of estuarine circulation depends on the competition between the longitudinal density gradient and vertical momentum flux (Eqs. 2.19 and 2.23).

In more turbulent conditions such as during spring tides, due to higher vertical eddy viscosity the estuarine circulation is diminished. When turbulence mixing is reduced during the neap tides, the longitudinal density gradient is able to drive stronger gravitational circulation in the estuary.

Various mechanisms may be responsible for the upstream-directed salt flux in estuaries. Including, tidal pumping at a constriction (Stommel and Farmer, 1952), trapping in side embayments (Okubo, 1973), and lateral stirring (Banas et al., 2004).

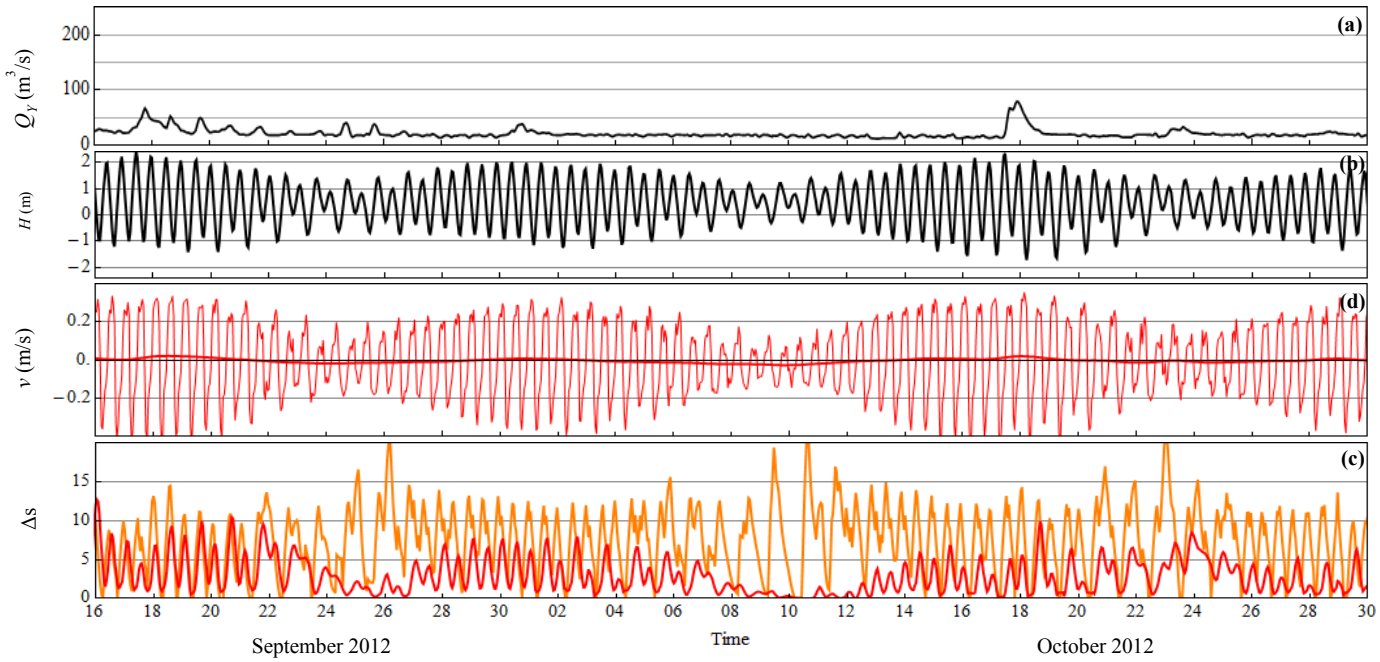

Fig 5.15 Time series of: (a) freshwater discharge at the Yaguchi Station, (b) water level at the Kusatsu Station; (c) tidal velocity, instantaneous (thin line) and tidally averaged (thick line) at the estuary mouth; (d) top-to-bottom salinity difference at the Suikan (red line) and Gion (orange line) Bridges

Tidal Steady shear dispersion flux is induced by gravitational circulation. The Ota Diversion Channel has strong longitudinal salinity gradient in the upstream regions. Thus the steady flux is important in this region. Tidal oscillatory salt flux is resulted from correlations between the tidal current, water level and salinity variability. Lerczak et al. 2006 denoted that three mechanisms drive these temporal correlations: tidal oscillatory shear dispersion, tidal trapping, and tidal pumping. They pointed out that the contribution of tidal oscillatory shear dispersion, compared with other mechanisms is negligible.

The variability of salt flux during the dry and wet periods was estimated using model simulations at the stations (Fig 5.11 and 5.12). The values of diffusion fraction at the down estuary are varied between 0.9 and 1 (Suikan and Yamate). However, at the upstream sections the values of fraction diffusion increase from neap to spring tides. These results show that the tidal oscillation is dominant mechanism between the mouth of estuary and Yamate Bidge. Meanwhile, between the Yamate and Gion Brides due to

higher salinity gradient the steady shear flux is comparable with the tidal oscillation, especially during the neap tides. These results are consistent with the variability of stratification (Figs 5.14 and 5.15) and longitudinal salinity gradient at the Ota diversion channel.

In Ota Diversion Channel, the strong longitudinal salinity gradient at the upstream sections drive baroclinic exchange and steady shear flux, but at the downstream sections the tidal variability in salinity and velocity due to advection component is significantly larger than the tidally averaged circulation. Then during the dry season the estuarine circulation is weak. The results indicate direct relations between salt fluxes and spring-neap tidal variations during both periods. The landward salt flux was dominated by the tidal oscillation at the downstream section during both the neap and spring tides; and at the upstream sections, both tidal oscillatory and steady shear drive the landward salt flux. The estuary was not in a steady state over the spring–neap cycle, because the advective and dispersive salt fluxes did not balance. During spring tides, the time rate of change of total salt flux was predominantly balanced by the seaward advective salt flux, and salt exited from the estuary. During neap tides, both the advective salt flux and the tidal oscillatory dispersion flux were dominant terms in the balance and salt entered the estuary. Steady shear flux was not a dominant term in the salt balance, especially at the downstream sections (e.g., Suikan Station).

5.8. Conclusions

In this chapter a three-dimensional numerical model (EFDC) is used to simulate water level, salinity and flow rate in the Ota Diversion Channel. Several field observations through the Ota Diversion Channel were carried out for validation and calibration purposes. This chapter addresses the variability of salinity flux, the length of the salinity intrusion and estuarine circulation in the Ota Diversion Channel. The results indicate that at low freshwater runoff at the Yaguchi Station, the Ota Diversion Channel is highly

variable at tidal time scales. The results indicate a significant flood-ebb tidal asymmetry in the vertical salinity and velocity profiles due to tidal straining. At moderate to high discharge, the gravitational circulation is enhanced at the downstream sections. However, the up-estuary regions (e.g., Gion Bridge) is completely sensitive to freshwater discharge at the Yaguchi Station and during the discharge larger than 250 m^3/s, the salinity is flushed out of this region. The results indicate that the longitudinal salinity gradient is around -1.1 km^{-1} between the channel mouth and about 7 km upstream from the mouth. However, at the upstream region due to channel convergence and the effect of upstream freshwater the salinity gradient is about -5 km^{-1}.

The relation between the salinity intrusion length and the constant freshwater discharge is examined. The salinity intrusion length responding to the constant freshwater discharge generally follows a power law of -0.11 and -0.14 for the neap and spring tides, respectively. The dependence of salinity intrusion on freshwater discharge is weaker than that predicted by theoretical models for exchange flow dominated estuaries. The first reason for behavior is due to the existence of the Gion Gates. It restricts the freshwater runoff to the channel significantly. Another important characteristic is the influence of tidal amplitude on the salinity and flow velocity which relatively makes the length of salinity intrusion sensitive to tidal amplitude. On the other hand for high freshwater discharge, the exponents are -0.51 and -0.93 for neap and spring tides, respectively. This result shows that the differences in salt intrusion length between springs and neaps increase by increasing river discharge.

To investigate the salinity transport mechanisms, the salinity flux is decomposed into three components: steady shear, advection, and tidal dispersion salt fluxes. The steady shear flux is induced by gravitational circulation and the tidal dispersion generated by temporal correlations between the tidal salinity, water level and velocity. The advection flux is mainly induced by river discharge. The results indicate that the salinity balance is not in a steady balance during spring-neap tidal cycles. During spring tides, the total salt

flux is directed seaward, and the salt exits from the estuary. In contrast, during neap tides, the total salt flux is directed landward, and the salt enters the estuary. During the spring tides, due to larger correlations between the tidal water level, salinity and velocity, the tidal dispersion is maximized. While during the neap tides the steady shear flux is increased due to higher longitudinal salinity gradient and estuarine circulation at the upstream section of Ota Diversion Channel.

Using field observations and numerical simulations, the variability in stratification and estuarine circulation were investigated during dry and wet seasons. The strength of estuarine circulation depends on the competition between the longitudinal density gradient and vertical momentum flux. In more turbulent conditions such as during spring tides, due to higher vertical eddy viscosity the estuarine circulation is diminished. The variability of tidal currents and stratification during wet and dry seasons are simulated. The amplitude of tidal velocity varies from 0.5 m/s at the strongest spring to 0.16 m/s at the weakest neap tides, respectively. During the wet season, the maximum stratification is occurred during neap tides at the upstream region. Meanwhile, at the downstream region, the maximum stratification is accrued during the higher freshwater runoff. By increasing the freshwater runoff the thickness of halocline at the downstream regions is reinforced. Thus the bottom-top salinity difference is increased. During the dry season, the maximum bottom-surface salinity differences at the upstream regions are established during neap tides by the values around 20, when low vertical mixing persists for several days. However, due to well-mixed condition the stratification is low at the downstream sections.

References

Abood, K.A. (1974) Circulation in the Hudson River estuary. In: Roels, O.A. (Ed.), Hudson River Colloquium, 250, New York *Academy of Sciences*, 38-111.

Banas, N.S., Hickey, B.M., MacCready, P., Newton, J.A. (2004) Dynamics of Willapa Bay, Washington: A highly unsteady partially mixed estuary, *Journal of Physical Oceanography*, 34, 2413–2427.

Chatwin, P. C. (1976) Some remarks on the maintenance of the salinity distribution in estuaries, *Estuarine and Coastal Marine Science*, 4, 555-566.

Dyer, K.R. (1997) Estuaries: a physical introduction (new revised issue), *John Wiley & Sons*, Aberdeen, UK.

Geyer, W. R., Trowbridge, J., Bowen, M. (1999) The dynamics of a partially mixed estuary, *Journal of Geophysical Research*, 30, 2035-2048.

Hamrick, J. M. (1992) A Three-dimensional Environmental Fluid Dynamics Computer Code: Theoretical and Computational Aspects, The College of William and Mary, Virginia Institute of Marine Science, Special Report 317, 63 pp.

Hansen, D. V., Rattray, M. Jr. (1965) Gravitational circulation in straits and estuaries, *Journal of Marine Research*, 23, 104-122.

Jay, D. A. (1991) Estuarine salt conservation: A Lagrangian approach. *Estuarine Coastal Shelf Sci,* 32**,** 547-565.

Jay, D.A., Smith, J.D. (1990) Residual circulation in shallow estuaries. II. Weakly stratified and partially mixed, narrow estuaries, *Journal of Geophysical Research* 95, 733-748.

Kawanisi, K. (2004) Structure of Turbulent Flow in a Shallow Tidal Estuary, *J. of Hydraulic Engineering.,* ASCE, 130(4), 360-370.

Lerczak, J.A., Geyer, W.R., Chant, R.J. (2006) Mechanisms driving the time-dependent salt flux in a partially stratified estuary, *Journal of Physical Oceanography* 36, 2296-2311.

Li, M., Zhong, L. (2009) Flood-ebb and spring-neap variations of mixing, stratification and circulation in Chesapeake Bay, *Continental Shelf Research,* 29, 4-14.

MacCready, P. (2011) Calculating estuarine exchange flow using isohaline coordinates, *Journal of Physical Oceanography*, 41, 1116-1124

Monismith, S., Kimmerer, W., Burau, J.R., Stacey, M.T (2002) Structure and flow-induced variability of the subtidal salinity field in Northern San Francisco Bay, *Journal of Physical Oceanography*, 32, 3003-3016

Nepf, H. and W.R. Geyer (1996) Intratidal variations in stratification and mixing in the Hudson Estuary, *J.Geophys. Res.*, 101 (C5), 12079-12086.

Okubo, A. (1973) Effects of shoreline irregularities on streamwise dispersion in estuarine and other embayments. Neth, *J. Sea Res*, 8, 213–224.

Passone, S., Das, D.B., Nassehil, V., Bikangaga, J.H. (2003) Design of discharge policies for multiple effluent sources and returning pollutants scenarios in a branching estuary, *Estuarine, Coastal and Shelf Science*, 56, 227-237.

Peters, H., Bokhorst, R. (2000) Microstructure observations of turbulent mixing in a partially mixed estuary. Part I. Dissipation rate, *Journal of Physical Oceanography*, 30, 1232-1244.

Pritchard, D.W. (1952) Estuarine hydrography, *Adv. Geophys*, 1, 243-280.

Pritchard, D.W. (1956) The dynamic structure of a coastal plain estuary, *Journal of Maine Research*, 15, 33-42.

Ralston, D.K., Geyer, W.R., Lerczak, J.A. (2008) Subtidal salinity and velocity in the Hudson River Estuary: Observations and modeling, *Journal of Physical Oceanography*, 38, 753-770.

Simpson, J.H., Brown, J., Matthews, J., Allen, G. (1990) Tidal straining, density currents, and stirring in the control of estuarine stratification, *Estuaries*, 13, 125-132.

Simpson, J.H., Vennell, R., Matthews, J., Souza, A. J. (2001) The salt fluxes in a tidally-energetic estuary, *Estuarine, Coastal and Shelf Science*, 52**,** 131–142

Stacey, M.T., Ralston, D.K. (2005) The scaling and structure of the estuarine bottom boundary layer, *Journal of Physical Oceanography*, 35, 55-71.

Stommel, H., and H. G. Farmer (1952) On the nature of estuarine circulation, Part I. Woods Hole Oceanographic Institution Tech. Rep 52-88, 131 pp.

Yang, Z.Q., Khangaonkar, T. (2009) Modeling tidal circulation and stratification in Skagit River estuary using an unstructured grid ocean model, *Ocean Modelling*, 28, 34-49.

CHAPTER 6

Conclusions

6.1. Summary

The present study attempts to investigate the salinity intrusion through the Ota Diversion Channel that is a shallow tidally-dominated channel with gates. This thesis addresses the variability of salinity flux, flushing time, salinity intrusion length, stratification and estuarine circulation in the Ota Diversion Channel under the different estuarine forces (freshwater, tides, etc.). This study consists of the field observations and numerical simulations. The characteristics of the field observations can be categorized as:

1. Observations at the Ota Bifurcation and Oshiba Gate from Oct 28, 2011 to February 10, 2012 using FATS and CTDs sensors: In these observations the variability of the salinity at the Ota Bifurcation, Oshiba Gate and Gion Bridge were considered.

2. Observations at the Gion Bridge in January 25-26, 2012 and April 13-14, 2012: In these observations the intertidal variations of salinity and flow velocity at the Gion Bridge were considered. The water velocity and density variations were collected using a Fluvial Acoustic Tomography System (FATS), a moving boat acoustic Doppler current profiler, and a conductivity profiler.

3. Observations at the Gion Bridge between October 18 and November 8, 2012; and between December 29, 2012 and January 29: In this observation the variations of salinity and flow velocity at the Gion Bridge were measured using CTD sensors and ADCP. The results were used for calibration and verification of numerical model.

4. Observations at three stations (Suikan, Yamate and Mitaki Bridges) along the Ota Diversion Channel in Oct 21-22, 2012 (neap tide) and December, 12-13, 2012 (spring tide): The results of these observations were used to investigate the intratidal and residual circulation at the channel. Also were used for validation of numerical simulations.

In addition, a three-dimensional numerical model (EFDC) is used to simulate water level, salinity and flow rate in the Ota Diversion Channel. The numerical experiments are carried out to:

1. To estimate the longitudinal distribution of salinity and flow velocity at the Ota Diversion Channel during the spring and neap tides.

2. To consider the dominated salinity transport mechanisms and salinity balance in the Ota Diversion Channel during spring-neap tidal cycles and wet and dry seasons.

3. To determine the variability in the estuarine circulation and stratification during the wet and dry seasons.

4. To examine the response of the salinity intrusion to changes in the freshwater runoff and tides.

With the results presented in the previous chapters, in the following sections we shall summarize the thesis results as:

6.1.1. Intratidal and Subtidal variability in salinity at the Gion Station

The intratidal variations of salt fluxes at the Gion Station which is located at the upstream section of Ota Diversion Channel are investigated. The intratidal measurement of salinity and flow velocity over three tidal cycles is analyzed. The pattern of bottom and surface salinity indicates a phase lag between the deepest and shallowest regions. The variations of stratification illustrate that the tidal mixing contributes to decreasing the stratification at the whole cross-section. Meanwhile, during the later portion of ebb tides, the stratification is enhanced by the straining process. The magnitude of the vertical shear fluxes indicated an important contribution compared with the advection term. Also the results indicates a phase lag between the vertical shear terms at the shallowest and deepest regions which resulted with the correlation between the vertical salinity and velocity variations and the existence of the transversal circulations in velocity. Also, the long-time variation in the salinity at the Gion Station is investigated over a period of 2009 to 2013. The results indicate an annual cycle in the salinity and water temperature, with maximum values in summer (September and October) and minimum temperatures in winter, respectively. To quantify the relative effect of main

forces on the salinity variations a multiple-regression analysis was employed. The results indicate that the discharge that the freshwater discharge of Yaguchi Station, tidal range and wind depress the salinity. Meanwhile, increasing the mean sea level enhances the salinity intrusion in the estuary. The influence of changes in freshwater discharge is greater than the other variables at the upstream section (Gion) of the estuary.

6.1.2. Variability in Flushing Time at the Ota Diversion Channel

The flushing time of the Ota Diversion Channel is estimated based on the freshwater fraction method. The largest and lowest flushing time occurred during the September and July 2009, respectively. The average flushing time is estimated about 1.8 days under mean flow conditions. Generally, in the tidally-dominated estuaries such as Ota Diversion Channel, tide exerts great influence on the salinity transport. The maximum flushing time in the Ota Diversion Channel was occurred in the September 2009, when the upstream freshwater discharge was low and the mean sea level reached the highest levels. In this condition, the advective flux was directed landward due to higher correlation between the water level, tidal salinity, and velocity. So the flushing time was dramatically increased. This result suggest that the variations in the flushing time at the Ota diversion channel is largely controlled by the advection mechanism contributed by freshwater discharge and the longitudinal dispersion process as a result of tidal forcing.

6.1.3. Salinity Variations in the Main Branches of Ota Estuary

The salinity variations at the main branches of Ota Estuary are investigated. As mentioned before, the correlation of the daily averaged discharge between the Yaguchi Station and the Oshiba is greater than the Gion discharge. This difference in the water discharge and topographical features can cause different salt intrusion mechanisms at the Ota main branches. The tidally-averaged salinity variations in the main branches versus

the freshwater discharge at Yaguchi Station can be described as a power-law of upstream freshwater discharge. The exponents -0.53 and -3.86 at the Gion and Oshiba show that the salt intrusion in the Oshiba branch is more sensitive to change in upstream freshwater discharge. Because all Oshiba Gates are completely open .In contrast, the Gion Gates is not completely open and the freshwater runoff is restricted considerably. Thus the results indicate significant differences between the salinity variations at the Ota main branches.

6.1.4. Response of Salt Intrusion to Changes in Freshwater and Tide

At low freshwater discharge in the Yaguchi Station, the Ota Diversion Channel is highly variable at tidal time scales. The results indicate a significant flood-ebb tidal asymmetry in the vertical salinity and velocity profiles due to tidal straining. At moderate to high discharge, the gravitational circulation is enhanced at the downstream sections. However, the up-estuary regions (e.g., Gion Bridge) is completely sensitive to freshwater discharge at the Yaguchi Station and during the discharge larger than 250 m^3/s, the salinity is flushed out of this region. The relation between the salinity intrusion length and the constant freshwater discharge is examined. The salinity intrusion length responding to the constant freshwater discharge generally follows a power law of -0.11 and -0.14 for the neap and spring tides, respectively. The dependence of salinity intrusion on freshwater discharge is weaker than that predicted by theoretical models for exchange flow dominated estuaries. The first reason for behavior is due to the existence of the Gion Gates. It restricts the freshwater runoff to the channel significantly. The second reason is the influence of tidal amplitude on the salinity and flow velocity variations which relatively makes the length of salinity intrusion sensitive to tidal amplitude.

6.1.5. Variability in Salt Flux

Using the numerical results of the salinity and velocity, the temporal and spatial variability of salt flux was estimated during wet and dry seasons in the Ota Diversion

Channel. To investigate the salinity transport mechanisms, the salinity flux is decomposed into three components: steady shear, advection, and tidal dispersion salt fluxes. The steady shear flux is induced by gravitational circulation and the tidal dispersion generated by temporal correlations between the tidal salinity, water level and velocity. The advection flux is mainly induced by river discharge. The results indicate that the salinity balance is not in a steady balance during spring-neap tidal cycles. During spring tides, the total salt flux is directed seaward, and the salt exits from the estuary. In contrast, during neap tides, the total salt flux is directed landward, and the salt enters the estuary. During the spring tides, due to larger correlations between the tidal water level, salinity and velocity, the tidal dispersion is maximized. While during the neap tides the steady shear flux is increased due to higher longitudinal salinity gradient and estuarine circulation at the upstream section of Ota Diversion Channel.

6.1.6. Stratification and Estuarine Circulation

From field observations and numerical experiments, the variability in stratification and estuarine circulation were investigated during dry and wet seasons. The variability of tidal currents and stratification during wet and dry seasons are simulated. The amplitude of tidal velocity varies from 0.5 m/s at the strongest spring to 0.16 m/s at the weakest neap tides, respectively. During the wet season, the maximum stratification is occurred during neap tides at the upstream region. Meanwhile, at the downstream region, the maximum stratification is accrued during the higher freshwater runoff. By increasing the freshwater runoff the thickness of halocline at the downstream regions is reinforced. Thus the bottom-top salinity difference is increased. During the dry season, the maximum bottom-surface salinity differences at the upstream regions are established during neap tides by the values around 20, when low vertical mixing persists for several days. However, due to well-mixed condition the stratification is low at the downstream sections. The results indicate that the circulation strength is stronger during the neap tides.

The strength of estuarine circulation depends on the competition between the longitudinal density gradient and vertical momentum flux. In more turbulent conditions such as during spring tides, due to higher vertical eddy viscosity the estuarine circulation is diminished. When turbulence mixing is reduced during the neap tides, the longitudinal density gradient is able to drive stronger gravitational circulation in the estuary. In Ota Diversion Channel, the strong longitudinal salinity gradient at the upstream sections drive baroclinic exchange and steady shear flux, but at the downstream sections the tidal variability in salinity and velocity due to advection component is significantly larger than the tidally averaged circulation.

6.2. Future Studies

The thesis has demonstrated several aspects of the variation in salinity intrusion in the Ota Diversin Channel. Additional Future investigations are suggested as:

1- This study focuses on the variability in salt intrusion on the Ota Diversion Channel. As mentioned before due to the different adjustments at the Gion and Oshiba Gates the contribution of freshwater at the main branches is different. Thus analysis of field observation results in Chapter 4 reveals a significant diffrences on the salinity variations at the Gion Station and Oshiba Gate. Additional numerical simulation and field observation at the all branches of the Ota Estuary will help to better understanding of salt intrusion at this estuary.

2-This study addressed salinity variations at the Gion Station using long-term data of FATS. Also the variability of salinity intrusion length to change in the freshwater runoff was eximained using numerical expriments. Low freshwater condition allows

the saltwater from the Hiroshima Bay to propagate upstream and exert a more dominant influence in the higher border of the Ota River. This issue significantly influences water quality and ecosystem at the upstream region of Ota River. Thus, additional future work would be to investigate the salinity intrusion length under low freshwater runoff and high mean sea level to consider the effect of salinity intrusion on the water quality at the upstream region of Ota River.

3-The temporal and spatial variability of the salinity in Ota Estuary is significantly influenced by the gate operation at the main branches. The main objective of constructing the Ota Diversion Channel is flood control in Hiroshima City. However, this channel has extensive tidal flats with habitats for many creatures in the brackish river. The discharge ratio in the Ota bifurcation have been changed by the different river improvement planning. Regarding the changes in the main estuarine forces (e.g., freshwater runoff and sea level) due to global climate change, it is nessessary to investigate the effect of gate operation on the salinity variation in the Ota Estuary to prevent or minimize salinity intrusion to the estuary, specially beyond the Ota bifurcation.

APPENDIX A

A Short Report on Internship Experience

A.1. Introduction

An internship is a training method for professional careers. Generally, an internship consists of an exchange of services for experience between the student and an organization. Students can also use an internship to determine if they have an interest in a particular career and create a network of contacts. The main reason to join internship in Japan for students is to gain a unique experience that is valuable for personal development and career future. This experience helps student to stand out from the crowd of other applicants in today's competitive job market. The Internship in Japan program welcomes motivated students and recent graduates to intern with a wide variety of host organizations. The following report describes the activities carried out during a week (Oct 24-28, 2011) full-time internship at the Keisoku Research Consultant Co

(KRC) in Hiroshima City. This report contains information about the organization and the activities performed throughout the internship period.

Keisoku Research Consultant Corporation was established as a consultant in civil engineering and construction field in 1972. KRC head-quarried in Hiroshima City, with 5 branch offices is administrated with a team of 97 (80 engineers) staffs. Professional engineers, geologists, technologists and managers capable of providing solution to engineering problems. The major engineering activities in KRC are:

- Observational method in civil engineering and construction field.
- Miscellaneous structure deterioration diagnosis.
- Development and sales of miscellaneous measurement system.
- Development and sales of miscellaneous technical software.
- Production of computer graphics.
- Environmental observation and Environmental assessment.

KRC provides wide range of services in transportation network planning, river and hydraulic design and environmental technology (http://www.krcnet.co.jp).

A.2. Personal Experiences

Table. A.1 shows the targets and experiences that I introduced during my internship period in KRC. In the next sections I explain these activities in more details.

A.2.1 3D Laser Scanning System

First of all there was a friendly and warm welcome from managers and employees of KRC. Then I have guided to work with 3D Laser Scanning and Monitoring Systems. Nowadays, maintenance and management of infrastructures, such as, road and bridge, have been a serious problem. The era has been shifted from “Build and Scrape” to “Stock and Maintenance”. From such background, KRC supports rational and reliable

Table A.1 The schedule of the internship

Date	Targets
2011/10/24	▪ Orientation ▪ Responsibilities, duties, and Targets ▪ 3D Laser Scanning system
2011/10/25	▪ Introduced by Maptek Software ▪ Merging the scans
2011/10/26	▪ Image Measurement System ▪ Scanning technology for the Shinkansen tunnels
2011/10/27	▪ Portable scanner ▪ 3D scan
2011/10/28	▪ Final merging the scans ▪ Edit the AutoCAD files ▪ Get the information

information for adjusting repair design through inspection, measurement, evaluation and structural health assessment. Examples for application of 3D Laser Monitoring technology are:

- ✓ Displacement monitoring of bridges and embankment.
- ✓ Subsidence monitoring of railway track.
- ✓ Monitoring underground structures.
- ✓ Deformation measurements such as displacement of the river port and airport.
- ✓ Subsidence measurements such as cultural heritage building.

KRC has different projects in this field. I learned about the applications of this technology to make more accurate maps for engineering projects. Also I was introduced with Maptek Software and the merging technics for 3D maps. Fig A.1 shows examples for this advanced method of surveying. I worked on the data from a 3D monitoring at the Asahi Bridge (in Hiroshima City). I merged the data in Maptek. I did not have enough time to read the manual of Maptek carefully. However, my adviser gave general

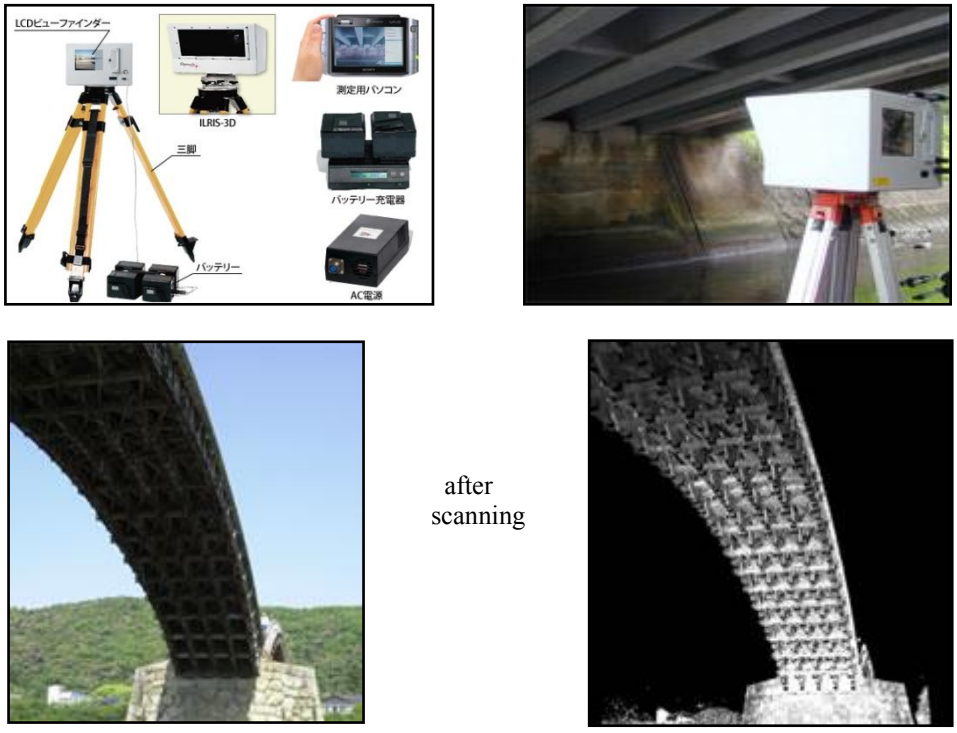

Fig A.1 3D Laser Scanning System

information about that. The results are depicted in Fig A.2. In addition I worked on the 3D monitoring results in a big Gas reservoir. Also I studied about 3D Laser Scanning system. Generally, I understood that many different technologies can be used to build these 3D scanning devices; each technology comes with its own limitations, advantages and costs. Many limitations in the kind of objects that can be digitized are still present, for example, optical technologies encounter many difficulties with shiny, mirroring or transparent objects. 3D Laser Scanning System is useful for a wide variety of applications include industrial design, orthotics and prosthetics, reverse engineering and prototyping, quality control/inspection and documentation of cultural artifacts.

A.2.2 Image Measurement System

The safety of transportations in Japan is concerning issue for managers. One of the important projects in KRC was related to the safety of tunnels in subways and Shinkansen train tracks. For this project they have developed innovative method using

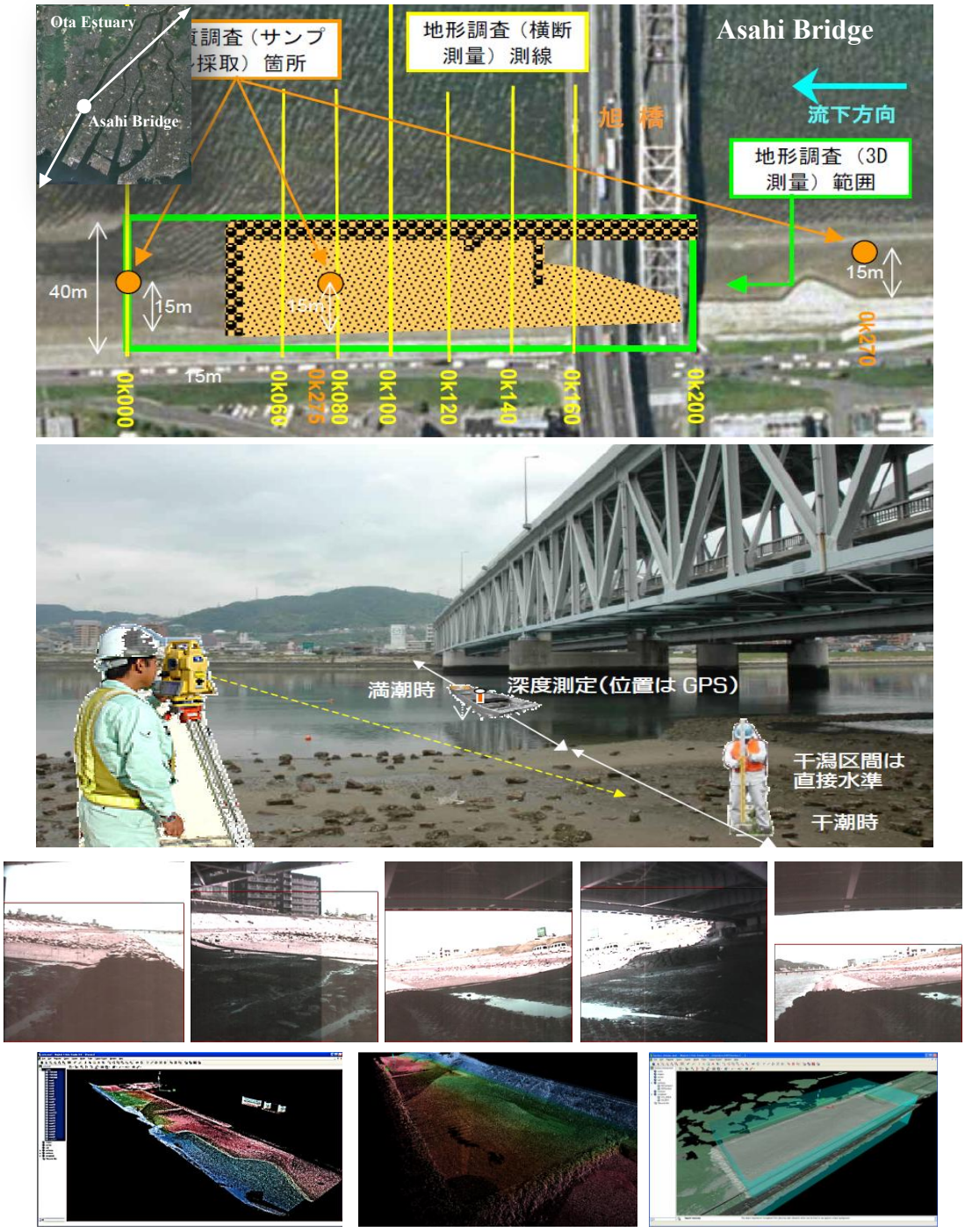

Fig A.2 3D Scanning results at the Asahi Bridge in Hiroshima City

multiple cameras to take high resolution and synchronized images from the internal surface of the Shinkansen tunnels. To clarify the characteristics of the camera, "Image

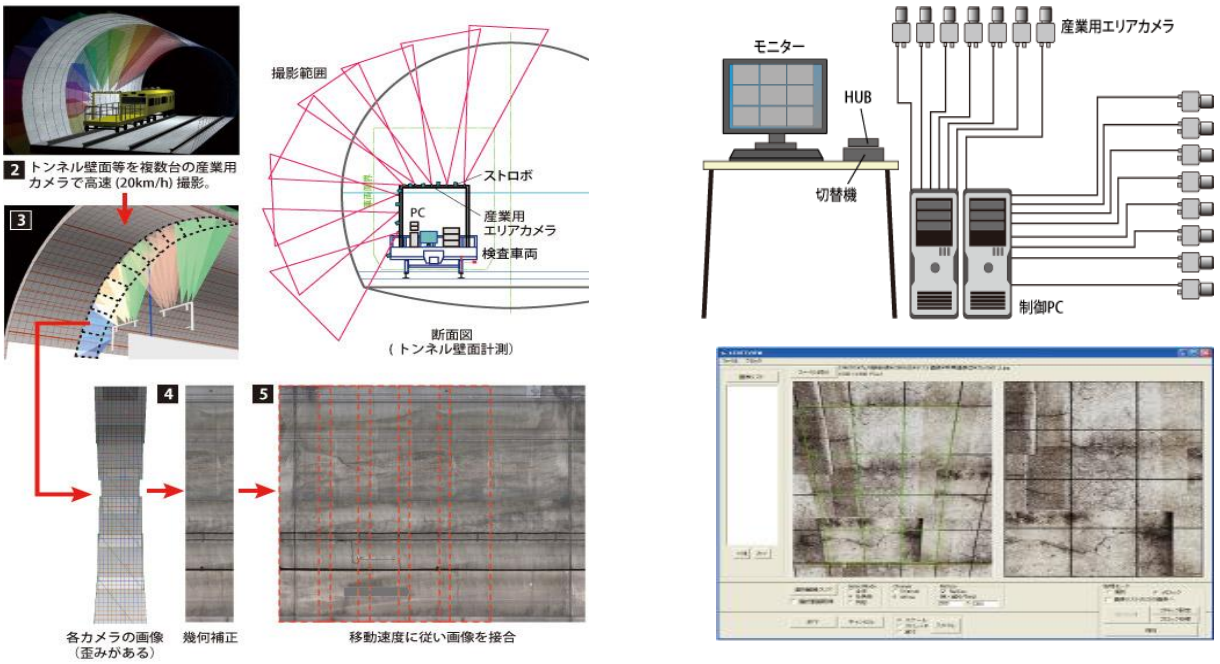

Fig A.3 Image Measurement System

Measurement System with continuous driving" has been developed. By using this system it is possible to recognize the cracks along the tunnel surface. For more information please see http://www.krcnet.co.jp. During the second day I checked more than 100 photo frames. I found some cracks on the walls. We discussed about the important features of vertical and horizontal cracks and the effect of the cracks on the tunnel structure during the time. Fig A.3 shows some examples of this project.

A.2.3 Portable Laser Scanning System

There are a variety of technologies for digitally acquiring the shape of a 3D object. The handheld scanners stand out as the most accurate portable 3D scanners on the market today. My advisor taught me how to use the equipment and I was trained with the technical procedure for applying the instrument. The handheld laser scanner can be used to digitize the surface of objects for animation, rapid prototyping, 3D measurement,

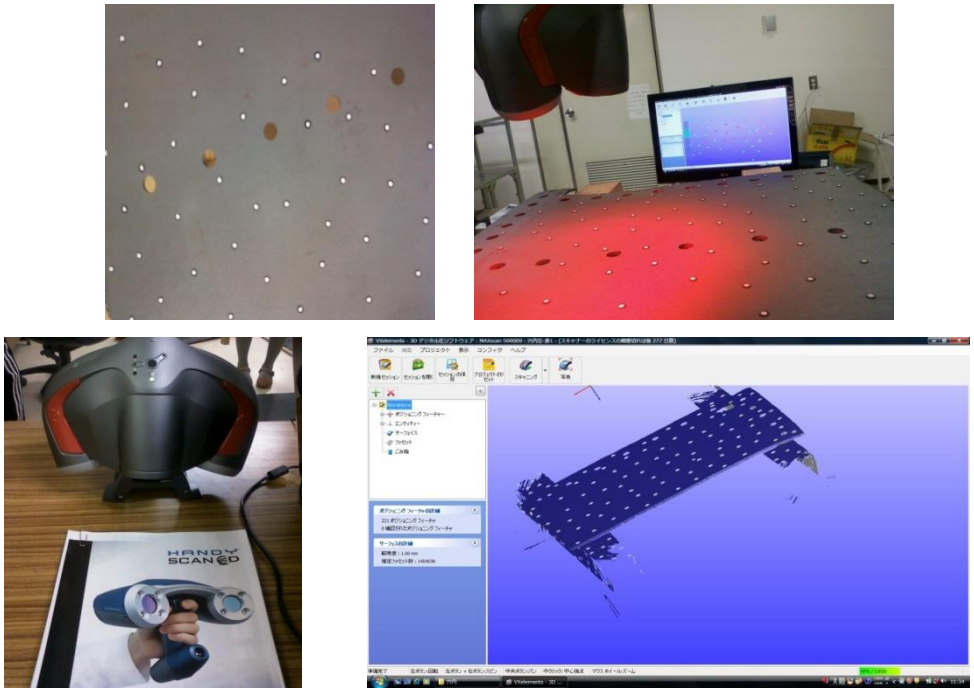

Fig A.4 Portable Laser Scanning System

archiving, etc. The following example demonstrates the scanner's ability to do two things: rapidly digitize the complete 3D surface of an object and save the data in industry standard formats to be used by other programs. I did a 3D scan using REV portable scanner. Fig A.4 indicates the scanning procedure.

A.2.4 3D Printing System

Additive manufacturing or 3D printing is a process of making a three-dimensional solid object of virtually any shape from a digital model. 3D printing is achieved using an additive process, where successive layers of material are laid down in different shapes. 3D printing is considered distinct from traditional machining techniques, which mostly rely on the removal of material by methods such as cutting or drilling (subtractive processes). A materials printer usually performs 3D printing processes using digital technology. Form the beginning of the 21st century there has been a large growth in the sales of these machines, and their price has dropped substantially. The 3D printing

Fig A.5 3D Printing System

technology is used for both prototyping and distributed manufacturing with applications in architecture, construction, industrial design, civil engineering and etc.

The KRC Company has been started developing of this technology for engineering projects. They explained that the construction of a 3D model with contemporary methods can take anywhere from several hours to several days, depending on the method used, the size and the complexity of the model. Fig A.5 shows a small size 3D print from an Old building in a non-resident Island (Gunkanjima-Nagasaki) which was printed in KRC.

A.3. Discussion

The technology transfer is the process of transferring discoveries and innovations resulting from university research to the commercial sector and typically comprises several steps. Technology transfer is an area of interest not just to business and economists but also to other disciplines such as engineering. Developing a relationship with relevant research experts in universities may begin by establishing personal contacts in universities during related technical conferences, or by building a longer history of

interaction with faculty by industry sponsorship through research grants and contracts. Graduate students or university alumni who have completed their degrees and have taken positions in industry are another major source of researchers. The internship was an excellent opportunity for me because I learned a great deal about how to conduct an advanced technology in the engineering fields. My internship at KRC was a great chance to get exposure to technologies I would rarely get to see or work with anywhere else, I work with KRC because their technology was so interesting and it has a real chance to revolutionize that space. I understood that implementing change at organizations takes time. Also I knew for using the high advanced technologies the international relationship between companies is very important. Language barrier is the most common problem among students who experienced internship course in a Japanese company.